UNIVERSITAT DE BARCELONA

Assessment of the lipidomic effects of environmental pollutants on exposed organisms using chemometric and analytical methods

Eva Gorrochategui Matas

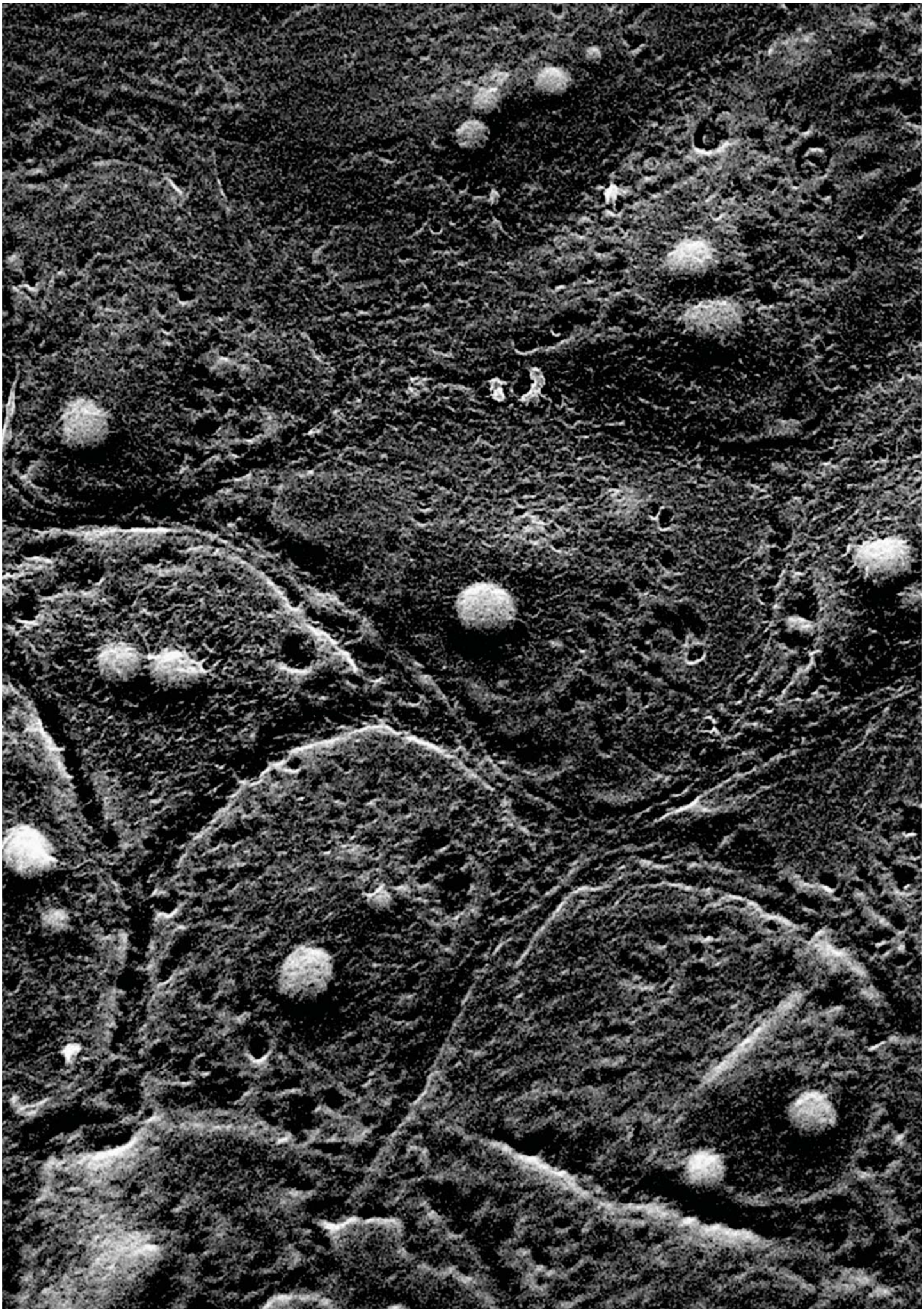

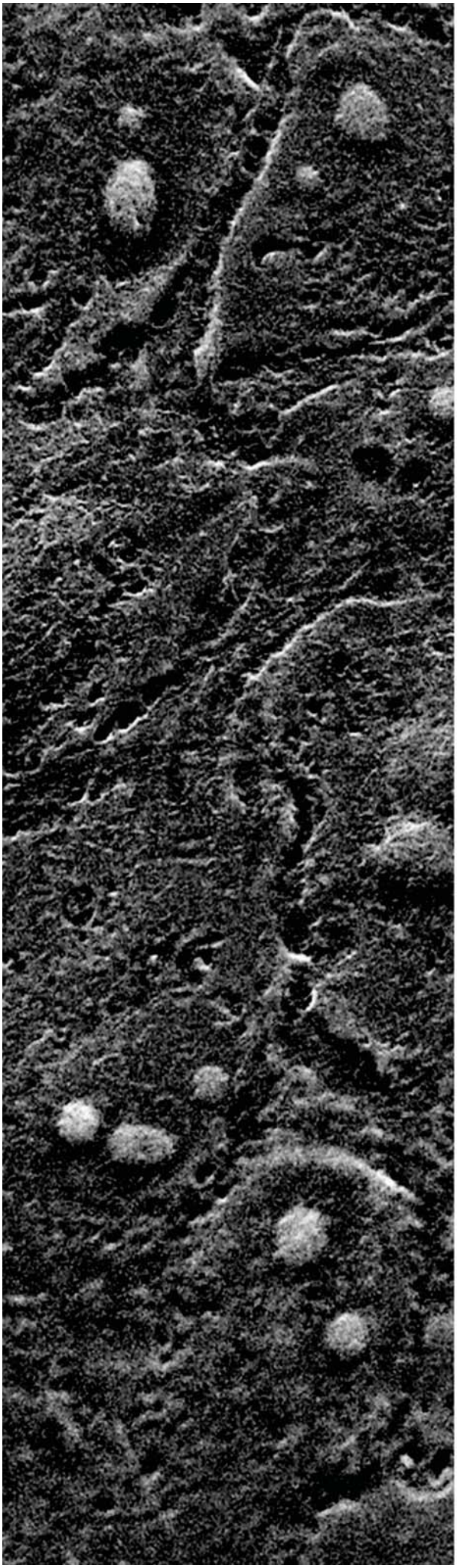

CHAPTER 3

LC-MS lipidomic studies using human cell lines

CHAPTER 3

The study of the effects of pollutants on humans is a matter of concern within the scientific community. In order to evaluate the effects of these contaminants on humans, human model-biosystems, relatively simple to manipulate and relatively accessible to researchers are used. Among them, human cell line models are one of the most used in omics research, as an alternative to animal models and human subjects. In this Thesis, two human cell lines were used to assess the effects of a mixture of eight PFASs (*i.e.*, PFBS, PFBA, PFOS, PFOA, PFHxS, PFHxA, PFNA and PFDoA) and of five proautophagic drugs (i.e., CCX, PXD, RV, GTE and XM462). PFASs effects were assessed on the human placental choriocarcinoma JEG-3 cell line whereas the effects of proautophagic drugs were evaluated on a human glioblastoma T98G cell line.

This Chapter of the Thesis is structured in the following manner: an introduction section, a scientific research section including the scientific articles containing *lipidomic data obtained from experiments performed with human cell lines exposed to environmental pollutants*, a discussion section and some specific conclusions.

3.1. INTRODUCTION

Cell culture is a complex process by which cells are grown under controlled conditions of temperature, humidity and gaseous atmosphere, generally in an artificial environment composed of nutrient solutions. In other words, cell culture is the art of maintaining live cell lines separated from their original tissue source. The applications of cell culture are very diverse: i) to investigate the normal physiology or biochemistry of cells (*e.g.* studies of cell metabolism)[430], ii) to test the effects of various chemical compounds or drugs on specific cell types (normal or cancerous cells),[431] iii) to study the sequential or parallel combination of different cell types to generate artificial tissues (*e.g.* artificial skin in tissue engineering)[432] and iv) to synthesize valuable biological products (*e.g.* therapeutic proteins like monoclonal antibodies) from large scale cell cultures.[433] In each of these applications cells act as independent units, so they are capable of dividing, they increase in size and, in batch culture; they can grow until limited by some culture variable (*e.g.*, nutrient depletion). In such conditions, consistent and reproducible results can be obtained. Also, in vitro assays represent a quick and cost-effective alternative to in vivo assays.[434,435] However, the inconvenient of cell culture is that, after a period of continuous growth, cell characteristics can be different from the ones of the original population. This adds an uncontrollable source of variability which can affect the results negatively. The acquisition of cell lines can be from either the scientific community or from culture collections. There is a general list of worldwide culture collections (http://wdcm.nig.ac.jp/hpcc.html) where the national organizations for culture collection are named. One of the resource centers who provide standard reference microorganisms, cell lines and other materials for research life sciences is the ATCC.

Cell culture maintenance and environmental toxicity assessment

To ensure the proper maintenance of cells, some specific conditions must be under control in the incubator where cells are placed such as the temperature, the gas mixture (*e.g.*, 37 ºC and 5% CO_2) and the growth media. Depending on the cell type, culture conditions can vary widely, and the variation of conditions for a specific cell type can result in different phenotypes being expressed. Related with the growth mode, cells are divided in two types:

suspension and adherent cells. The first ones grow floating in culture medium so they survive and proliferate without attaching to culture container. Generally these cells come from blood, spleen or bone marrow. Contrarily, adherent cells, the ones used in this Thesis, grow as a monolayer attached to the surface of culture container, normally a bottle or a plate. In this case, cells require the surface most of the time. This is the case of cells derived from ectodermal and endodermal embryonic layers, fibroblasts, epithelial cells and neurons. In order to assess environmental toxicity, cell lines may undergo different tests. In this Thesis, two determinations are performed including endocrine disruption evaluation and cytotoxicity assays.

Endocrine disruption evaluation, cytotoxicity tests and factors influencing EC_{50}-values

The study of the capacity of chemicals to act as endocrine disruptive chemicals by producing inhibition of CYP19 activity is of vital importance. The P450 aromatase activity can be measured using radioisotope labelled substrates. In this Thesis, a method based on the detection of titrated water resulting from the reaction catalysed by aromatase enzyme has been used. This reaction aromatises a substrate labelled with tritium (^{3}H-androstenediona) releasing a molecule of water that ^{3}H has incorporated, which can be further measured. The capacity of chemicals to inhibit aromatase activity is expressed with IC_{50}-values, *i.e.* concentrations which induce a 50% loss of enzyme activity. Another important determination in the study of the effects of chemicals on cell cultures is the evaluation of their cytotoxicity.

Two different approaches for the toxicity study in cell lines exist: the first one is based on the estimation of the basal functions of cells and the second one is based on testing specialized cell functions. In vitro cell line studies generally measure "basal cytotoxicity", a concept that supports the idea that the majority of chemicals exert their acute toxicity through interference with basal cellular functions resulting in similar effect levels in all cell types. In basal cytotoxicity studies, such as the ones performed in this Thesis, a large number of test compounds can be exposed to cells and analyzed in a high throughput system using multi-well plate readers. No animals are used, little test substance is needed and little toxic waste is produced. Furthermore, in vitro studies can address aspects of toxic mechanisms underlying a general toxic response.[436,437] There are various cytotoxicity tests available which can be

classified into three different types based on the cellular processes being targeted: *cell membrane integrity*, *metabolic impairment* and *lysosomal damage*. In this Thesis the first two were performed. Assessing *cell membrane integrity* is one of the most usual ways to measure cell viability and cytotoxic effects, and can be performed following different procedures. In this Thesis, membrane integrity assay was based on monitoring the passage of substances that are normally sequestered inside cells to the outside. In particular, the substance used was esterase 5-carboxyfluorescein diacetate acetoxymethyl ester (CFDA-AM). This compound is taken up by viable cells and converted to a fluorescent product called carboxyfluorescein (FIGURE 3.1). Damaged cells lose the esterase enzyme and do not present fluorescence.[438]

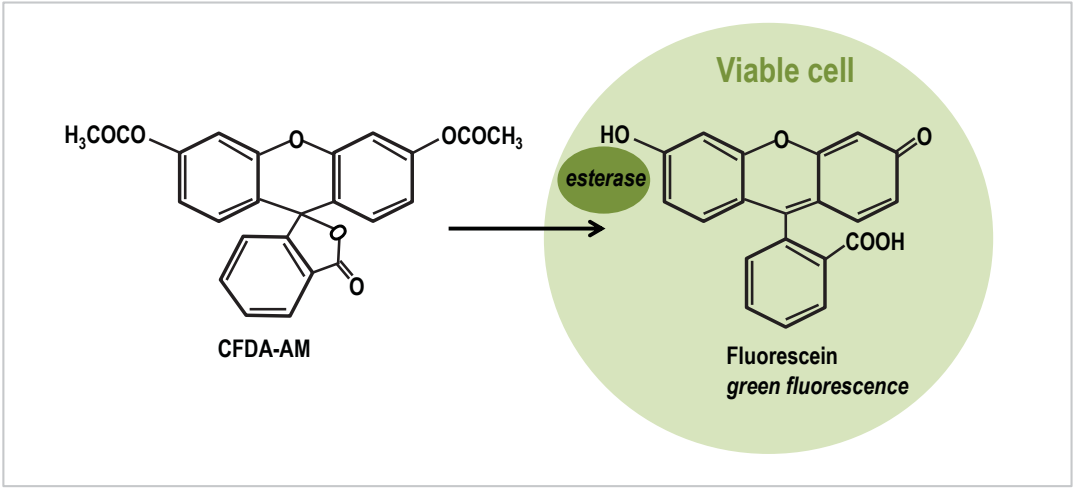

FIGURE 3.1

Basic principle of the cytotoxicity assay, based on membrane integrity, performed with CFDA-AM. The esterase species of the membranes transform CFDA into fluorescein, which emits fluorescence.

On the other hand, the *metabolic capability* of cell cultures can be monitored by measuring their ATP content or their ability to reduce either 3-(4,5-dimethylthizol-2-yl)-2,5 diphenil tetrazolium bromide (MTT), 3-(4,5-dimethylthizol-2-yl)-5-(3-carboxymethoxyphenyl)-2-(4-sulfophenyl)-2H-tetrazolium (MTS) or resazurin, purchased as a commercial solution called Alamar Blue (AB), the latter used in this Thesis. Enzymes, such as diaphoreses, with both cytoplasmic and mitochondrial locations are responsible of AB reduction. Thus, a decline in AB reaction indicates an impairment of cellular metabolism rather than specific mitochondrial dysfunction (FIGURE 3.2).

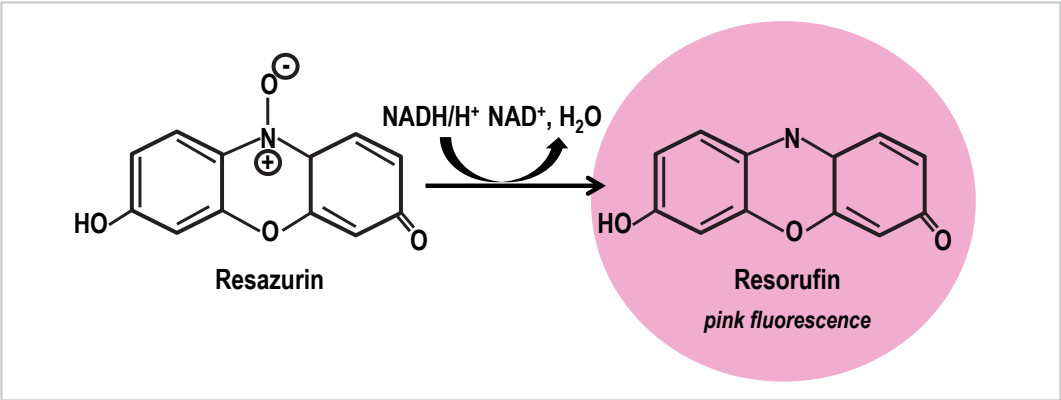

FIGURE 3.2

Basic principle of the cytotoxicity assay, based on metabolic capability, performed with Alamar Blue. Resazurin (blue, not fluorescent) is reduced by viable cells (in this example by NADH) to resorufin, a pink compound that emits fluorescence.

The results of the cytotoxicity tests (*i.e.*, cell membrane integrity and metabolic impairment assays) are expressed by EC_{50}-values, *i.e.* concentrations which induce a 50% loss of *viable* cells. In EC_{50} assays, cells are exposed to chemicals from higher to lower concentrations. The results are plotted into a graph and EC_{50}-values are obtained after adjusting them into a regression model. The experimental EC_{50}-values are nominal concentrations, calculated from the amount of substance added to the in vitro system.[439] However, substantial fractions of the total concentration of chemicals may bind to cellular and extracellular components of the in vitro systems. Only the aqueous concentration of the freely available unbound compound is considered to be related to the intensity of the pharmacological or toxic effect. Thus, in vitro potency data based on nominal effective concentrations (EC_{50}-values) not only reflects the sensitivity of the cells studied or the activity of the compounds tested but, to an unknown degree, the availability of a chemical compound in the in vitro system. This complicates the comparison of potency data obtained with different in vitro systems as well as the extrapolation of data from one system to another.[440] As a consequence, to obtain reliable information about the toxicity of a group of chemicals, their bioavailability in cells should be studied in order to obtain free cytotoxic concentration. However, in most of the toxicological studies, it is an uncommon practice to find out the relationship between the unbound and the total concentration. Another unresolved question when interpreting EC_{50}-values is the relation

between the average of compounds that have entered into cells and the toxic effects observed. In this way, the nature of the compound would not be the only cause of cell's damage but also the capacity of such compound to cross the membranes of cells. A new method used in this Thesis to carry out this investigation is the combination of uptake and cytotoxic evaluations.

Screening of PFASs in biological samples to perform uptake studies

As recently stated, the analysis of the fraction of chemicals that can enter into cells is of crucial importance to know the real dose of exposure. In this Thesis, the ratio of PFASs incorporated into JEG-3 cells, as well as the remaining fraction of PFASs in the culture medium was determined. To perform such determination some considerations regarding the analysis of PFASs were taken into account.

The general properties of PFASs (*i.e.,* compounds with low volatility and considerably high solubility in water) make them suitable to be analyzed by LC-MS or LC-MS/MS. Thus, only the most volatile fluorine chemicals, PFSAs and PFTOHs, are analyzed by gas chromatography-mass spectrometry (GC-MS)[441]. Among the different types of liquid chromatography, reversed-phase liquid chromatography has been the most popular, employing either octadecyl or octyl carbon chain (C_{18} and C_8)-bonded silica columns. In addition, a C_8 column is used as mobile phase residue trap to remove any PFASs traces from the mobile phases and tubing and a C_{18} pre-column for the final purification of samples. Typical mobile phases are mixtures of methanol-water or acetonitrile-water often modified with ammonium acetate to improve chromatographic separation and MS sensitivity[442].

Analysis of PFASs via LC-MS/MS has generally been conducted using electrospray ionization (ESI)[442,443] instead of APCI. The normal mode of operation is negative ESI since carboxylic and sulfonic groups of PFASs can be easily deprotonated. Even more, short-chain PFAs are present in the environment in the predominant anionic form, due to their low pKa values. In all cases, the frequent operation mode is selected reaction monitoring (SRM) since it allows multiple transitions to be monitored simultaneously. Quantization is generally based on the most abundant precursor > product transition[442]. Precursor > product transitions commonly monitored during the analysis of ionic PFASs are summarized in **TABLE 3.1**.

TABLE 3.1. Precursor > product transitions used in the LC-MS/MS analysis of PFASs. Transitions commonly used for quantization are indicated in bold.

Class	Analyte	Precursor > product	Product ion
PFSAs	PFBS	299 > 219	$(M\text{-}SO_3)^-$
		299 > 99	FSO_3^-
		299 > 80	SO_3^-
	PFHxS	399 > 319	$(M\text{-}SO_3)^-$
		399 > 99	FSO_3^-
		399 > 80	SO_3^-
	PFOS	499 > 419	$(M\text{-}SO_3)^-$
		499 > 99	FSO_3^-
		499 > 80	$SO3^-$
	PFDS	599 > 519	$(M\text{-}SO_3)^-$
		599 > 99	FSO_3^-
		599 > 80	$SO3^-$
PFCAs	PFHxA	**313 > 269**	$(M\text{-}COOH)^-$
		313 > 119	$C_2F_5^-$
	PFHpA	**363 > 319**	$(M\text{-}COOH)^-$
		363 > 169	$C_3F_7^-$
	PFOA	**413 > 369**	$(M\text{-}COOH)^-$
		413 > 119	$C_2F_5^-$
	PFNA	**463 > 419**	$(M\text{-}COOH)^-$
		463 > 169	$C_3F_7^-$
	PFDA	**513 > 469**	$(M\text{-}COOH)^-$
		513 >119	$C_2F_5^-$
	PFUA	**563 > 519**	$(M\text{-}COOH)^-$
		563 > 169	$C_3F_7^-$
	PFDoA	**613 > 569**	$(M\text{-}COOH)^-$
		613 > 119	$C_2F_5^-$
	PFTriA	**663 > 619**	$(M\text{-}COOH)^-$
		663 > 169	$C_3F_7^-$
	PFTetA	**713 > 669**	$(M\text{-}COOH)^-$
		713 > 119	$C_2F_5^-$
	PFPA	**763 > 719**	$(M\text{-}COOH)^-$
		763 > 169	$C_3F_7^-$
	PFHxDA	**813 > 769**	$(M\text{-}COOH)^-$
		813 > 119	$C_2F_5^-$

* Data obtained from the Persistent Organic Pollutants' book [63]

Among all the transitions, the most used for the quantitative analysis of PFOS (and other PFSAs) in biological samples is 499 > 99 since the most abundant product ion, *m/z*= 80, is interfered with taurodeoxycholate. Typical detection limits obtained using LC-MS/MS for the analysis of ionic PFASs range from pg/L for water samples, ng/g wet weight for biota and from

pg/g to ng/g for soils and sediments. The major limitation of LC-MS/MS methodology is that compounds in the sample extract, typically lipids, can affect the ionization of the analyte. This is referred to matrix effects and can either enhance or suppress the electrospray ionization, leading to considerable inaccuracies in both qualitative and quantitative analyses. As such, the clean-up methodology employed, especially working with biological samples, is of the utmost importance. In addition, the use of mass-labeled internal standards and matrix-matched standards can minimize matrix effects.

Cell line applications in metabolomic and lipidomic studies

The development of *cell culture metabolomics*[73] has provided a powerful alternative to the analysis of whole systems. Some extremely difficult problems facing other metabolomic applications –such as individual variations across different subjects and time points, difficulty in population control, and various confounding factors such as age, gender, overall health, environmental exposures and contributions from different tissues- are not issues when using cell culture models. Moreover, the analysis of cell cultures does not require the same level of ethics consideration as is needed with animals and human subjects. However, the performance of metabolomic experiments using cell cultures has also some associated challenges. Some of the major issues associated to cell culture metabolomics include[74–78]: 'quenching' of cell cultures –halting cellular metabolism, harvesting and processing of samples to prevent alterations in metabolic profiles during the extraction procedures; variability of growth medium formulation and additives; differential rates of proliferation for cell lines based on growth conditions and age (passage number) of the culture and possible downstream effects on metabolite concentrations; addition of foreign molecules during metabolite extraction procedure and their possible effects on metabolic profiles; time-consuming metabolite extraction procedures that can lead to degradation of labile metabolites, as well as long hands-on-time, making high-throughput screening and experimentation problematic; and complications in obtaining sufficiently large numbers of cultured cells for analysis.

Nowadays, the number of lipidomic (and metabolomic) studies that use cell lines is increasing, due to the valuable information that they can generate, essential for system level analysis and modelling of biological systems. A large variety of cell lines have been used to

perform lipidomic studies including epithelial[79], mammalian, colon adenocarcinoma[82], glioblastoma[81], melanoma[83], breast cancer[84], placental choriocarcinoma cell lines, among others. Nowadays, the number of cell lines in existence is vast. The ATCC currently holds over 4,000 cell lines from over 150 different species, and significantly more probably exist in Patent Repositories throughout the world.

Target cell lines of this Thesis

The proper selection of cell lines is a vital early step in a lipidomic study. In this Thesis, two human cell lines were selected, according to their characteristics, to properly assess the effects of some chemicals in an in vitro approach. The JEG-3 cell line (**FIGURE 3.3**), derived from human placental carcinoma obtained from ATCC (HTB-36), was specifically chosen to evaluate the effects of PFASs.

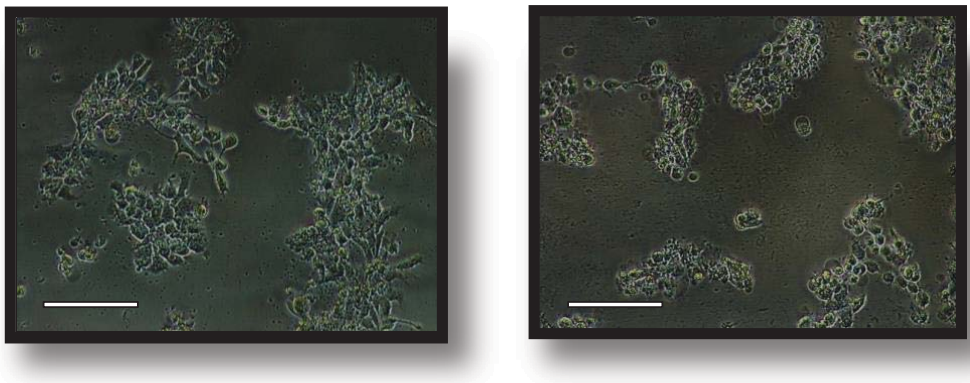

FIGURE 3.3

Phase-contrast images of JEG-3 cells. ATCC Number: HTB-36. (Scale bars = 150 µm).

In this Thesis, the human placental JEG-3 cell line was selected to assess the effects of PFASs, mainly for two reasons. First reason is the reported capacity of PFASs to affect steroidogenesis through decrease Bzrp and increased cytocrome P450 aromatase (CYP19) gene expression leading to lower androgen and higher estrogen levels. In humans, CYP19 activity has been reported in gonads, brain, ovaries, testis, placenta, adipose tissue, fetal liver, intestine, skin and brain[444]. In particular, JEG-3 cells have been recently reported to allow the

detection of changes in aromatase gene expression, making these cells a suitable model to assess PFASs endocrine disruption effects[445].

In TABLE 3.2 some studies performed with JEG-3 cells to assess the capacity of environmental pollutants to inhibit CYP19 activity are mentioned, together with the reported IC_{50}-values.

TABLE 3.2. Compilation of some studies performed on the JEG-3 cell line to assess the capacity of distinct chemicals to inhibit CYP19 aromatase activity.

Type of chemicals	Chemical	IC_{50}-values (μM)	Reference
Fungicides	Tebuconazole (TEB)	56.84 ± 0.13 μM	446
	Triadimeton (TRI)	58.73 ± 0.14 μM	
	Vinclozolin (VCZ)	57.42 ± 0.171 μM	
	Tributyltin (TBT)	4.58 ± 0.048 μM	
	Tetrabutyltin (TTBT)	n.d.	
Plasticizers	Bisphenol A (BPA)	71 ± 7 μM	447
	Nonylphenol (NP)	n.d.	
	Octylphenol (OP)	166 ± 31 μM	
	Benzyl butyl phthalate (BBP)	104 ± 9 μM	
	Dibutyl phthalate (DBP)	n.d.	
	Di(2-ethylexyl)phtalate (DEHP)	n.d.	
Insecticides	Methoxychlor (MXC)	n.d.	448
	Hydroxychlor (HPTE)	97.16 ± 0.10 μM	
Drugs	Triptolide (CAS 38748-32-2)	~ 17 nM	449

n.d.: not detected.

Apart from being useful to assess the endocrine disruptive effects of PFASs, the JEG-3 cell line is an excellent model to evaluate the reported capacity of PFASs to alter lipid species, mainly corresponding to membrane lipids. In mammals, the cellular membrane has special importance in placental cells, because it is the organ responsible of the transference of nutrients and other biomolecules (*e.g.*, lipids and hormones) to the fetal compartment. The human placenta shows lipoprotein lipase activity, an enzyme that is in charge of the release of fatty

acids from the triacylglycerols found in the maternal blood, and also of the transference of these fatty acids to the fetus by diffusion or by active transport[450]. The long chain and unsaturated fatty acids are more apt to cross the placental barrier, making that the fetal compartment has a high amount of these lipid species[451]. Placental cells are capable of synthetizing some of these fatty acids, including the oleic, palmitic and palmitoleic and in less degree, stearic, myristic and lauric[452,453]. From these fatty acids, other fatty acids are synthetized through combinations of elongation and unsaturation processes, and are transferred to the fetus or are used in the synthesis of glycerophospholipids or glycerolipids. The elongation processes are catalysed by enzymes placed in the cytoplasmic side of the smooth endoplasmic reticulum that use the energy of CoA. The unsaturation processes, or addition of double bounds, take place through oxidation reactions catalysed by the enzymatic complex of cytochrome P450 desaturase, consuming O_2 and NADH. Moreover, placenta has an active role under a toxicological point of view. Due to the fact that the fetal liver is immature, the placenta presents numerous characteristic components of the adult hepatic tissue, including enzymes and transport proteins involved in the metabolism of pigments, bile acids and xenobiotics[451]. Furthermore, due to ethic reasons, the information of the effects that xenobiotics can pose on the lipidic composition of plasmatic membranes of human placental cells is scarce. In this sense, the human placenta JEG-3 cell line offers high possibilities of study.

The other human cell line selected in this Thesis was the human glioblastoma T98G cell line; in this case, this cell line was chosen to assess the effects of five proautophagic drugs. This glioblastoma cell line has been reported to be useful to assess the effects of some dihydroceramide desaturase (Des1) inhibitors that also induce autophagy[127,449]. In particular this is the case of the drugs resveratrol (RV)[454–457] and celecoxib (CCX)[458–461] and the synthetic Des1 inhibitor XM462, which have been reported to induce autophagy simultaneously to Des1 inhibition. Moreover, ɣ-tocotrienol (ɣ-TE)[462,463] has been reported to produce increased levels of dihydrosphingosine and dihydroceramides in prostate cancer cells, and this increase appears to contribute to the autophagic response elicited by the compound. Also, phenoxodiol (PXD) is a synthetic analogue of genistein, a natural isoflavone reported to induce autophagy[464,465], so it is also a potential candidate to induce autophagic effects on cells.

3.2. SCIENTIFIC RESEARCH

In order to assess the effects of the mixture of the eight PFASs on human placental JEG-3 cells, the cytotoxicity of these compounds in these cells, their capacity to inhibit aromatase activity and their capacity to disrupt lipids was evaluated. The research of this study is included in the scientific article entitled "*Perfluorinated chemicals: Differential toxicity, inhibition of aromatase activity and alteration of cellular lipids in human placental cells*" (Section 3.2.1). In addition, in order to characterize the lipidome of JEG-3 cells, an UHPLC-MS methodology was developed and tested for two mass spectrometers (*i.e.*, TOF and Orbitrap). The results of the targeted lipidomic characterization of JEG-3 cells were included in the scientific article entitled "*Characterization of complex lipid mixtures in contaminant exposed JEG-3 cells using liquid chromatography and high-resolution mass spectrometry*" (Section 3.2.2). Furthermore, a chemometric methodology to perform untargeted lipidomic evaluation of the effects of the mixture of PFASs as well as of TBT on JEG-3 cells was developed. The elaborated chemometric strategy for untargeted lipidomics was enclosed in the scientific article entitled "*Chemometric strategy for untargeted lipidomics: Biomarker detection and identification in stressed human placental cells*" (Section 3.2.3). Finally, the effects of five proautophagic drugs were assessed in the lipidome of human glioblastoma T98G cells. This evaluation was included in the scientific article entitled "*Chemometric evaluation of glioma cell lipidome in response to proautophagic drugs*" (Section 3.2.4).

3.2.1. SCIENTIFIC ARTICLE IV

Perfluorinated chemicals: Differential toxicity, inhibition of aromatase activity and alteration of cellular lípids in human placental cells

E. Gorrochategui, E. Pérez-Albaladejo, J. Casas, S. Lacorte, C. Porte

Toxicology and Applied Pharmacology (2014) **277**, 124-130

Toxicology and Applied Pharmacology 277 (2014) 124–130

Contents lists available at ScienceDirect

Toxicology and Applied Pharmacology

journal homepage: www.elsevier.com/locate/ytaap

Perfluorinated chemicals: Differential toxicity, inhibition of aromatase activity and alteration of cellular lipids in human placental cells

Eva Gorrochategui [a], Elisabet Pérez-Albaladejo [a], Josefina Casas [b], Sílvia Lacorte [a,*], Cinta Porte [a,**]

[a] Department of Environmental Chemistry, IDAEA–CSIC, 08034 Barcelona, Catalonia, Spain
[b] Department of Biomedicinal Chemistry, IQAC–CSIC, 08034 Barcelona, Catalonia, Spain

ARTICLE INFO

Article history:
Received 17 January 2014
Revised 12 March 2014
Accepted 16 March 2014
Available online 26 March 2014

Keywords:
Perfluorinated chemicals
JEG-3
Cytotoxicity
CYP19
Phosphatidylcholines
PFBS

ABSTRACT

The cytotoxicity of eight perfluorinated chemicals (PFCs), namely, perfluorobutanoic acid (PFBA), perfluorohexanoic acid (PFHxA), perfluorooctanoic acid (PFOA), perfluorononanoic acid (PFNA), perfluorododecanoic acid (PFDoA), perfluorobutanesulfonate (PFBS), perfluorohexanesulfonate (PFHxS) and perfluorooctanesulfonate (PFOS) was assessed in the human placental choriocarcinoma cell line JEG-3. Only the long chain PFCs – PFOS, PFDoA, PFNA, PFOA – showed significant cytotoxicity in JEG-3 cells with EC50 values in the range of 107 to 647 μM. The observed cytotoxicity was to some extent related to a higher uptake of the longer chain PFCs by cells (PFDoA > PFOS ≫ PFNA > PFOA > PFHxA). Moreover, this work evidences a high potential of PFOS, PFOA and PFBS to act as aromatase inhibitors in placental cells with IC50s in the range of 57–80 μM, the inhibitory effect of PFBS being particularly important despite the rather low uptake of the compound by cells. Finally, exposure of JEG-3 cells to a mixture of the eight PFCs (0.6 μM each) led to a relative increase (up to 3.4-fold) of several lipid classes, including phosphatidylcholines (PCs), plasmalogen PC and lyso plasmalogen PC, which suggests an interference of PFCs with membrane lipids. Overall, this work highlights the ability of the PFC mixture to alter cellular lipid pattern at concentrations well below those that generate toxicity, and the potential of the short chain PFBS, often considered a safe substitute of PFOS, to significantly inhibit aromatase activity in placental cells.

Introduction

Perfluorinated chemicals (PFCs) represent a large group of compounds characterized by a hydrophobic fluorinated carbon tail attached to a polar hydrophilic head. PFCs are classified as perfluorinated sulfonic acids (PFSAs), perfluorinated carboxylic acids (PFCAs), fluorotelomer alcohols (PFTOHs), high-molecular weight fluoropolymers and low-molecular weight perfluoroalkanamides. They are used in a variety of consumer products and have emerged as global environmental pollutants (Stahl et al., 2011). They are resistant to degradation and have a high accumulation potential; thus, once released in the environment, PFCs persist in aquatic organisms (Giesy and Kannan, 2002; Kannan et al., 2002). PFSAs and PFCAs are the most ubiquitous compounds and they have been detected in human blood (Ericson et al., 2007). Typical serum levels of PFOS and PFOA are in the range of 1 to 50 ng/mL, although concentrations up to 300 and 2000 ng/mL have been detected in occupationally exposed workers (Olsen et al., 1998).

Concerns about PFC toxicity have risen due not only to its widespread distribution and persistence in humans and the environment, but also to its toxicity and ability to act as endocrine disrupters and obesogens (Du et al., 2013; Hines et al., 2009). However, while the toxicity of PFOS and PFOA has been deeply investigated in the last decades, other PFC homologs have been rarely studied. PFCs of shorter chain length are expected to have similar functions to PFOS and be less bioaccumulative and less toxic. Thus, Buhrke et al. (2013) showed a positive correlation between carbon chain length of PFCAs and its toxicity in the human hepatocarcinoma cell line HepG2: the short chain length PFBA and PFHxA were less toxic than PFOA. Nonetheless, both PFOS and PFBS promoted expression of the estrogen and the androgen receptor at environmentally relevant concentrations and caused adverse hepato-histological effects in the amphibian *Xenopus laevis* at high concentrations (100–1000 μg/L), which opens the question of whether short chain PFCs are safe substitutes of PFOS (Lou et al., 2013).

Moreover, long chain PFCs can modulate the biosynthesis of gender-specific steroid hormones. Olsen et al. (1998) reported a 10% increase in estradiol levels among occupationally exposed workers who had the highest levels of serum PFOA (>30 ng/mL), although this association was confounded by body mass index. Decreased gene expression of key enzymes and transporters involved in steroidogenesis was observed in male rats exposed to PFDoA and male mice exposed to PFOS (Shi et al., 2007, 2009; Wan et al., 2011). Also, Zhao et al. (2010) showed a decrease in testosterone levels in isolated rat Leydig cells exposed to PFOA. All these studies seem to indicate that long chain PFCAs can act as endocrine disruptors, but their mechanisms of action are still unknown. A recent

* Corresponding author.
** Corresponding author. Fax: +34 932045904.
E-mail addresses: slbqam@cid.csic.es (S. Lacorte), cinta.porte@cid.csic.es (C. Porte).

http://dx.doi.org/10.1016/j.taap.2014.03.012
0041-008X/

work by Rosenmai et al. (2013) revealed that fluorochemicals present in food packaging materials can affect steroidogenesis through decreased Bzrp and increased CYP19 gene expression leading to lower androgen and higher estrogen levels. CYP19 aromatase plays a key role in catalyzing the irreversible conversion of androgens to estrogens and maintaining the androgen/estrogen hormonal balance. Thus, any interaction of chemicals with the expression of this enzyme or its catalytic activity is very likely to disrupt the internal hormonal balance between androgens and estrogens. In humans, aromatase activity has been reported in gonads, brain, ovaries, testis, placenta, adipose tissue, fetal liver, intestine, skin and brain. Numerous assays have been developed to evaluate the potential effects of chemicals on CYP19 aromatase, among them, the human recombinant microsomal aromatase assay that measures the direct effect of chemicals on aromatase catalytic activity in vitro (Vinggaard et al., 2000). Currently, the human placental choriocarcinoma JEG-3 cell line is also frequently used to assess CYP19 aromatase, since it allows the detection of changes in aromatase gene expression (Huang and Leung, 2009).

The structural resemblance of PFCs to fatty acids and the discovery that they bind to peroxisome proliferator-activated receptors (PPARs), nuclear receptors that play a key role in lipid metabolism and adipogenesis, have recently raised the concern that PFCs may disrupt lipid and weight regulation. Indeed, several studies suggest that exposure to PFOS and PFOA may be associated with increased cholesterol levels in humans (Nelson et al., 2010). Also, developmental exposure to low-doses of PFOA lead to increased weight in adult rats, with increased serum insulin and leptin, an effect not seen in animals exposed to high doses of PFOA (Hines et al., 2009). Interestingly, other environmental chemicals, termed obesogens, have been shown to induce obesity in adulthood after low-dose developmental exposure, while inducing weight loss at higher doses (Grün et al., 2006). In addition, PFOS has been shown to affect membrane properties (e.g. membrane fluidity, mitochondrial membrane potential) at concentrations below those associated with other adverse effects (Hu et al., 2003). Despite these evidences, more in-depth studies on the effects of PFCs on cellular lipidome and the physiological consequences for the cell, are still lacking.

Within this context, the aim of this study was to comparatively determine the cytotoxicity and ability to disrupt CYP19 aromatase activity of five perfluorinated carboxylic acids and three perfluorosulfonates of different chain lengths in the human placental choriocarcinoma cell line JEG-3. Special emphasis was placed on the analysis of cellular lipids by ultra-high performance liquid chromatography/mass spectrometry (UPLC/MS) in an attempt to roughly characterize major alterations of cellular lipids following exposure to a mixture of PFCs. This was designed as an exploratory analysis to be more fully investigated in future experiments with individual PFCs. The PFCs selected for the study were: perfluorobutanoic acid (PFBA), perfluorohexanoic acid (PFHxA), perfluorooctanoic acid (PFOA), perfluorononanoic acid (PFNA), perfluorododecanoic acid (PFDoA), perfluorobutanesulfonate (PFBS), perfluorohexanesulfonate (PFHxS) and perfluorooctanesulfonate (PFOS).

Materials and methods

Chemicals and reagents. Minimum Essential Medium, fetal bovine serum, L-glutamine, sodium pyruvate, nonessential amino acids, penicillin G, streptomycin, PBS and trypsin–EDTA were from Gibco BRL Life Technologies (Paisley, Scotland, UK). PFBA, PFHxA, PFOA, PFNA, PFDoA and PFHxS were purchased from Sigma-Aldrich (Steinheim, Germany), except PFBS and PFOS which were obtained from Fluka (Austria). Stock standard solutions and serially diluted test solutions were prepared in ethanol, except for PFOS which was prepared in dimethyl sulfoxide (DMSO). These compounds were added to the complete growth medium so that the final solvent concentration never exceeded 0.4% (v/v), which was not cytotoxic. Perfluoro-n-(1,2,3,4-$^{13}C_4$)octanoic acid (m-PFOA) and sodium perfluoro-1-(1,2,3,4-$^{13}C_4$)octanesulfonate (m-PFOS) from Wellington Laboratories (Ontario, Canada) were used as surrogate standards. HPLC grade water, ethanol (>99.8%) and acetonitrile (>99.8%) were purchased from Merck (Darmstadt, Germany).

Cell culture. JEG-3 cells derived from human placental carcinoma were obtained from American Type Culture Collection (ATCC HTB-36). They were grown in Eagle's Minimum Essential Medium supplemented with 5% fetal bovine serum, 2 mM L-glutamine, 1 mM sodium pyruvate, 0.1 mM nonessential amino acids, 1.5 g/L sodium bicarbonate and 50 U/mL penicillin G/50 μg/mL streptomycin in a humidified incubator with 5% CO_2 at 37 °C. Cells were routinely cultured in 75 cm^2 polystyrene flasks. When 90% confluence was reached, cells were dissociated with 0.25% (w/v) trypsin and 0.9 mM EDTA for subculturing and experiments. Experiments were carried out on confluent cell monolayers.

Cell viability. Two fluorescent dyes were used to monitor cell viability on JEG-3 cells (Schirmer et al., 1997). Metabolic activity was monitored with Alamar Blue (AB™, resazurin) and membrane integrity was evaluated with 5-carboxyfluorescein diacetate (CFDA-AM). Cells were seeded at a rate of 25,000 cells per well (96-well plate) and allowed to attach overnight at 37 °C, 5% CO_2. After 24-hour exposure to PFCs, the medium was replaced by 100 μL of a solution of AB™/CFDA-AM, incubated for 1 h, and cell viability was measured using a fluorescence plate reader (Varioskan, Thermo Electron Corporation) at the excitation/emission wavelengths of 530/590 nm for AB™ and 485/530 nm for CFDA-AM. Results were recorded as relative fluorescence units.

Three independent sets of experiments were performed for each PFC. PFBA, PFBS, PFHxA and PFHxS were tested at 500 μM whereas PFOA, PFNA, PFDoA and PFOS were also tested at lower concentrations to obtain concentration–response curves. Within each experiment, addition of the test compound was done in septuplicate.

Uptake of PFCs. Cells were seeded at a rate of 100,000 cells per well (24-well plate) and allowed to attach overnight in an incubator at 37 °C, 5% CO_2. Cells were then dosed in triplicate with a mixture of eight PFCs at a concentration of 6.0 μM for each compound, and control cells were exposed to the carrier (0.4% ethanol). Given the intensive analytical work required to test eight PFCs individually at different concentrations, we decided to carry out an exploratory assay with a mixture of PFCs at a single non-toxic concentration, high enough to allow the detection of the fraction of PFCs absorbed by the cells. Right after dosing (time zero), and after 1, 3, 5, 8 and 24 h of incubation, the medium was aspirated, and the cells were rinsed with PBS, trypsinized and centrifuged at 3600 rpm for 10 min. The supernatant was aspirated and the cells were stored at −80 °C until analysis. Two independent sets of experiments were performed.

PFCs were extracted from JEG-3 cells following the method of Fernández-Sanjuan et al. (2010), with some modifications. A surrogate standard solution containing m-PFOA and m-PFOS was added to the cell pellets followed by 1 mL of acetonitrile. Samples were shaken and extracted in an ultrasonic bath for 10 min (×3); the supernatant was transferred to a new vial and purified by adding 25 mg of activated carbon and 50 μL of glacial acetic acid. The obtained supernatant was evaporated to dryness and reconstituted in 15% methanol/acetonitrile (60:40) and 85% water.

PFCs were analyzed using an Acquity Ultra Performance Liquid Chromatography (UPLC) system (Waters, USA) connected to a Triple Quadrupole Detector. An XBridge™ C_{18} column (3.5 μm particle size, 50 mm × 4.6 mm, Waters, Ireland) was used as mobile phase residue trap to remove any PFC traces from the mobile phases and tubing. The analysis was performed on an Acquity UPLC BEH C_{18} column (1.7 μm particle size, 50 mm × 2.1 mm, Waters, Ireland) connected to an Acquity UPLC BEH C_{18} (1.7 μm particle size, 5 mm × 2.1 mm, Waters, Ireland) VanGuard™ pre-column at a flow rate of 0.4 mL/min at a column temperature of 40 °C. The mobile phase was 20 mM NH_4OAc/

acetonitrile (90:10) (A)/methanol/acetonitrile (60:40) (B). Gradient elution started at 15% of B and continued to 95% of B in 8 min. Initial conditions were attained in 2 min and the system was stabilized for 3 min. PFCs were measured under negative electrospray ionization (ESI) and acquisition was performed in Multiple Reaction Monitoring (MRM) using one or two transitions from parent to product ion to identify each compound. The elution times, transitions used as well as the dwell times, cone voltages and collision energies are given in Table 1. m-PFOA was used as an internal standard to quantify PFBA, PFHxA, PFOA, PFNA and PFHxS, while m-PFOS was used to quantify PFDoA, PFBS and PFOS. Samples were extracted and analyzed in batches together with a procedural blank in order to control any external contamination during the analytical process. Instrument detection limits (LOD_{inst}) were calculated with a standard solution at a concentration of 0.001 ng/μL of each compound by using three times the signal-to-noise ratio value. Method detection limits (LOD_{method}) were calculated in the same way, using spiked cells at a concentration of 0.6 μM (Table 1). No traces of PFCs were detected in procedural blanks.

Cellular P450 aromatase (CYP19) activity. The assay was adapted from the method of Lephart and Simpson (1991) that measures the amount of ^3H_2O formed during the aromatization of [1β-^{3}H] androstenedione (^{3}H-AD) by JEG-3 cells. PFC test solutions ranged from 3 nM to 500 μM; the most cytotoxic PFCs (PFOS, PFDoA, PFNA and PFOA) were tested at an upper concentration of 100 μM, while PFBA, PFHxA, PFBS and PFHxS were tested at 500 μM and below.

Cells were seeded at a rate of 100,000 cells per well (24-well plate) and allowed to attach overnight in an incubator at 37 °C, 5% CO_2. After 24-hour exposure to the different PFCs, the cells were washed with PBS and incubated for 1 h in the presence of 39.5 nM of ^{3}H-AD in DPBS–Glucose. Under these conditions, titrated water production was linear over time. The reaction was stopped by placing the plate on ice and aspirating 1 mL of medium that was extracted with 3 mL of dichloromethane (×3). The amount of titrated water formed was counted in an aliquot of the aqueous phase (Tri-Carb 2100TR, Packard). Aromatase activity was expressed in pmol/min/mg protein.

Analysis of lipids in JEG-3 cells. Cells were seeded at a rate of 100,000 cells per well (24-well plate) and allowed to attach overnight. The medium was then replaced with a medium containing a mixture of the eight PFCs at a concentration of 0.6 and 6 μM each, or the solvent (0.4% ethanol). After 24 h incubation, the medium was aspirated; the cells were rinsed with PBS and trypsinized.

Lipids were extracted by a modification of the method of Christie (1985). A solution of methanol: chloroform (1:2) containing 0.01% of butylated hydroxytoluene (BHT) was added to the cell pellets, vortexed and extracted in an ultrasonic bath for 5 min (×2). The extracts were evaporated to dryness and stored at −20 °C in an argon atmosphere. Lipids were measured using an Acquity UPLC system (Waters, USA) connected to a Time of Flight (LCT Premier XE) Detector with an Acquity UPLC BEH C_8 column (1.7 μm particle size, 100 mm × 2.1 mm, Waters, Ireland) at a flow rate of 0.3 mL/min and column temperature of 30 °C. The mobile phase was methanol with 1 mM ammonium formiate and 0.2% formic acid (A)/water with 2 mM ammonium formiate and 0.2% formic acid (B). Gradient elution started at 80% of A, increased to 90% A in 3 min, held for 3 min, increased to 99% A in 9 min and held for 3 min. Initial conditions were attained in 2 min and the system was stabilized for 3 min. Phosphatidylcholine (PC), plasmalogen PC, lyso plasmalogen PC, diacylglycerol (DAG), triacylglycerol (TAG) and cholesterol ester (CE) were analyzed under positive ESI. Positive identification of the lipids was based on the accurate mass measurement with an error < 5 ppm and its LC relative retention time, compared to that of the standard (±2%) (Garanto et al., 2013). Glycerophospholipids, diacylglycerol, triacylglycerol and cholesteryl esters were annotated as <lipid subclass> <total fatty acyl chain length>:<total number of unsaturated bonds>.

Curve fitting and statistical analysis. Statistical significance was assessed with non-parametric Mann–Whitney U and Kruskal–Wallis tests by using Stata 12. $P < 0.05$ was considered statistically significant. The concentrations which caused a 50% decline on cell viability (EC50) and on enzyme activity (IC50) were calculated using SigmaPlot 11.0.

Results

Cytotoxicity

No significant cytotoxicity was observed for the shortest chain length PFCs (PFBA, PFHxA, PFBS and PFHxS) after 24 h incubation with the human placental choriocarcinoma cell line JEG-3. In contrast, cell viability decreased to 55–59% following exposure to 500 μM PFOA, while PFOS, PFDoA and PFNA caused a decline in cell viability higher than 90% (Fig. 1). Both, CFDA-AM and Alamar Blue gave a similar response. PFOA, PFOS, PFDoA and PFNA were tested at lower concentrations to obtain the corresponding EC_{50}-values (Table 2). PFOS was the most cytotoxic compound for JEG-3 cells, with EC_{50} in the range of

Table 1
Elution times, MRM transitions monitored, optimized cone voltages, collision energies and quality parameters for the analyzed PFCs.

PFCs	Elution time (min)	Transition (m/z)	Cone voltage (V)	Collision energy (eV)	LOD_{instr} (pg)	LOD_{met} (pg)	Recoveries[a] (±SD)
PFBA	0.99	213 > 169	16	10	3.57	4.74	87 ± 8
PFBS	3.38	299 > 80	50	29	4.05	3.19	146 ± 15
		299 > 99		26			
PFHxA	3.77	313 > 119	15	8	3.33	3.84	98 ± 13
		313 > 269		22			
PFHxS	5.20	399 > 80	45	40	8.82	28.1	106 ± 7
		399 > 99		40			
PFOA	5.52	413 > 169	19	11	1.90	5.34	98 ± 1
		413 > 369		20			
m-PFOA	5.52	417 > 372	17	11	n.a.	n.a.	n.a.
PFNA	6.12	463 > 419	16	8	1.58	4.04	87 ± 7
PFOS	6.40	499 > 80	50	42	5.77	17.1	101 ± 11
		499 > 99		42			
m-PFOS	6.40	503 > 80	52	39	n.a.	n.a.	n.a.
		503 > 99		39			
PFDoA	7.53	613 > 169	20	10	5.73	9.21	70 ± 9
		613 > 569		28			

*In all cases the dwell time is 0.07 s.
n.d.: not determined.
[a] Values obtained in culture medium spiked with the mixture of PFCs at 6 μM.

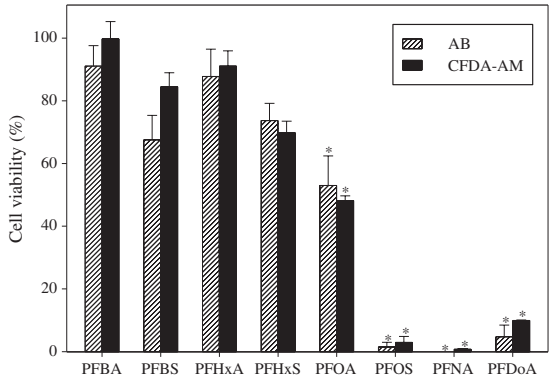

Fig. 1. Cytotoxicity of PFCs tested at a concentration of 500 μM in JEG-3 cells. Cell viability expressed as percentage of viable cells referred to control cells (exposed to the solvent). Values are mean ± SEM (n = 3). *Statistical significant differences with respect to the control ($P < 0.05$).

107–125 μM, followed by PFDoA and PFNA (181–220 μM) and PFOA (594–647 μM) (Table 2).

Uptake of PFCs

The differential bioavailability of PFCs in the in-vitro system was assessed by measuring the fraction retained in the cells right after exposure (time 0) to the eight PFC mixture (6 μM), and 1, 3, 5, 8 and 24 h later. Under the assay conditions, PFDoA and PFOS exhibited the highest concentration in JEG-3 cells. Right after dosing, a concentration of 149 pmol/mg cell protein was detected for PFDoA, which reached the maximum cellular concentration 5 h later (1000–1200 pmol/mg cell protein); no significant increase was detected thereafter (Fig. 2A). Similarly, a high concentration of PFOS was detected in the cells right after exposure (127 pmol/mg cell protein), and the maximum cellular concentration was reached after 5 h of exposure (340–470 pmol/mg cell protein). Comparatively, lower concentrations were detected for PFNA, PFOA and PFHxA at time 0 (3–10 pmol/mg cell protein) and 24 h later (10–39 pmol/mg cell protein) (Fig. 2B). Interestingly, maximal cellular concentration of PFHxA was reached after 1 h of exposure, while PFOA reached equilibrium after 3 h of exposure, and the long chain PFNA after 5 h. The concentration of PFBA, PFBS and PFHxS in the cells was below detection limit under our assay conditions.

P450 aromatase (CYP19) activity

CYP19 activity in JEG-3 cells following 24 h exposure to a wide range of PFC concentrations (3 nM–500 μM) is presented in Figs. 3 & 4. Fig. 3 summarizes the data obtained for the shorter chain PFCs (PFBA,

Table 2
Estimated EC_{50} of PFCs in the Alamar Blue and CFDA-AM cytotoxicity assays, and estimated IC_{50} for CYP19 activity. Values are mean ± SD (n = 3).

Compound	EC_{50} (μM)		IC_{50} (μM) CYP19
	Alamar Blue	CFDA-AM	
PFBA	–	–	n.d.
PFBS	–	–	68 ± 11
PFHxA	–	–	n.d.
PFHxS	–	–	298 ± 29
PFOA	594 ± 19	647 ± 22	80 ± 4
PFNA	213 ± 3	220 ± 3	132 ± 51
PFDoA	181 ± 10	219 ± 16	518 ± 562
PFOS	107 ± 9	125 ± 6	57 ± 4

–: No significant cytotoxicity at the highest concentration tested (500 μM).
n.d.: Not determined, low potential to inhibit CYP19 aromatase.

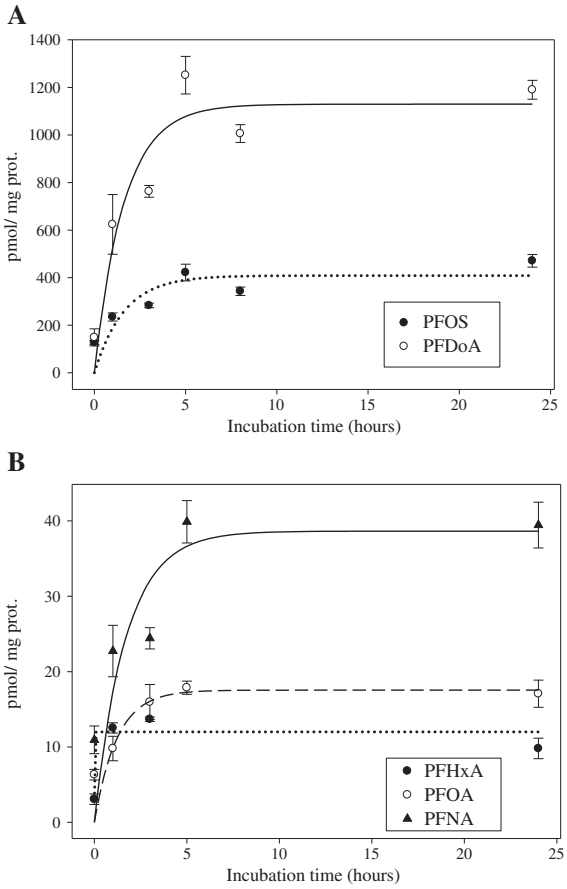

Fig. 2. Time-dependent concentration of (A) PFOS and PFDoA, and (B) PFHxS, PFOA and PFNA in JEG-3 cells exposed to a mixture of eight PFCs at a nominal concentration of 6 μM. Values are mean ± SEM (n = 3). Concentrations of PFBA, PFBS and PFHxS were below detection limit.

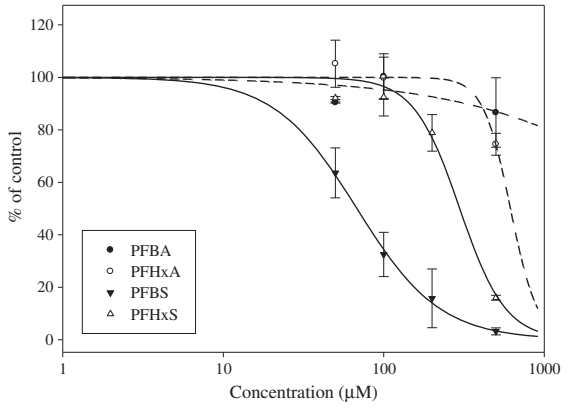

Fig. 3. Aromatase activity after exposure to PFBA, PFHxA, PFBS and PFHxS in the range of 1 μM to 500 μM. Values are relative to control cells (set to 100%) as mean ± SEM (n = 3). CYP19 aromatase activity in control cells was 0.252 ± 0.02 pmol/min/mg protein.

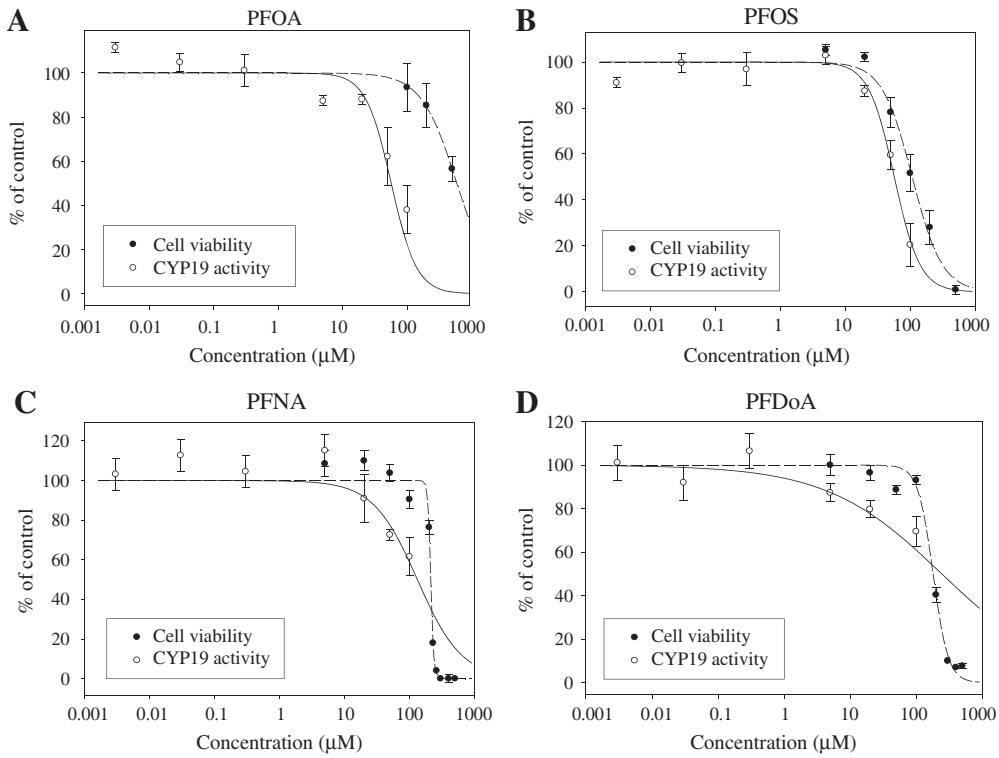

Fig. 4. Aromatase activity and percentage of cell viability in JEG-3 cells following 24 h exposure to different concentrations of PFOA (A), PFOS (B), PFNA (C) and PFDoA (D). Values are relative to control cells (set to 100%) as mean ± SEM (n = 3). CYP19 aromatase activity in control cells was 0.252 ± 0.02 pmol/min/mg protein.

PFHxA, PFBS and PFHxS) which were not cytotoxic for the cells. The sulfonates PFBS and PFHxS were stronger inhibitors of aromatase activity (97 and 84% inhibition when tested at 500 μM) than the corresponding acidic compounds (PFBA and PFHxA: 13 and 26% inhibition). Exposure of JEG-3 cells to the shorter chain PFCs resulted in a concentration dependent inhibition of aromatase activity, with an IC_{50} of 298 ± 29 μM for PFHxS and 68 ± 11 μM for PFBS (Table 2).

Conversely, the potential of longer chain PFCs (PFOA, PFOS, PFNA and PFDoA) to act as CYP19 inhibitors was to some extent affected by their toxicity, particularly for PFOS, as both toxicity and CYP19 inhibition curves were closely related (Fig. 4). Thus, 48% cell death and 80% inhibition of aromatase activity were observed for 100 μM PFOS, and IC_{50} (57 ± 4 μM) and EC_{50} (107–125 μM) differed only by a factor of 2. In contrast, PFOA was not cytotoxic but acted as a strong inhibitor of CYP19 activity (62% inhibition) when tested at 100 μM, with an IC_{50} of 80 ± 4 μM, comparable to the ones obtained for PFOS and PFBS. PFNA and PFDoA were weaker inhibitors of CYP19 aromatase: a 39% inhibition and a 31% inhibition were detected at 100 μM, when the toxicity of these compounds was very low (Fig. 4).

Changes in cell lipidome

A total of 45 lipids belonging to the classes of PC (16), plasmalogen PC (10), lyso-plasmalogen PC (1), DAG (6), TAG (10) and CE (2) were detected by UPLC-TOF ESI positive mode. Relative changes in lipid content of JEG-3 cells exposed for 24 h to the mixture of PFCs at 0.6 and 6 μM are indicated in Fig. 5. A statistically significant increase (2- to 3-fold) of PC, plasmalogen PC and lyso plasmalogen PC was detected together with a minor increase of TAG (30%), and no significant changes in the relative abundance of DAG and CE. The effects were more evident in cells exposed to 0.6 μM PFC mixture than in those exposed to 6 μM PFC.

The identified compounds were the following: lyso plasmalogen PC 18:1; plasmalogen PC (34:3, 34:2, 34:1, 34:0, 36:4, 36:3, 36:2, 36:1, 36:0, 38:4); PC (32:2, 32:0, 34:4, 34:3, 34:2, 34:1, 36:6, 36:3, 36:1,

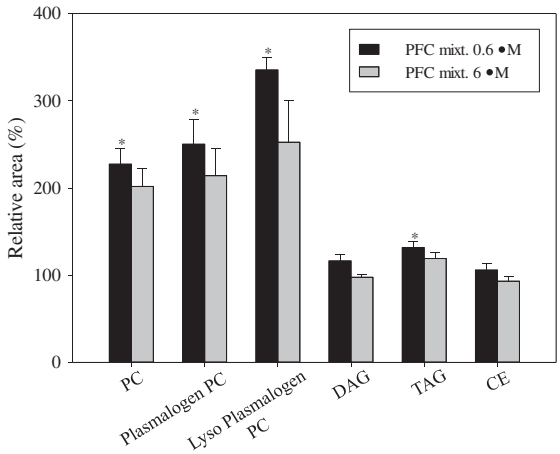

Fig. 5. Relative changes in lipid content of JEG-3 cells exposed to the mixture of PFCs at 0.6 and 6 μM. Lipids are grouped in families of PCs (16), PC-plasmalogens (10), LPC-plasmalogens (1), DGs (6), TGs (10) and ChEs (2). Values are relative to controls (set to 100%) and are mean ± SEM (n = 3). *Statistical significant differences with respect to the control ($P < 0.05$).

38:8, 38:7, 38:6, 38:4, 38:3, 38:2, 38:0); TAG (48:2, 48:1, 50:3, 50:1, 52:3, 52:2, 52:1, 54:3, 54:2, 54:1); CE (22:6, 18:1), and DAG (32:1, 32:0, 34:2, 34:0, 36:2, 36:1).

Discussion

PFCs with long fluorinated carbon chains, namely PFDoA, PFNA, PFOA and PFOS, were cytotoxic to JEG-3 cells, while the short chain ones (PFBA, PFBS, PFHxA and PFHxS) showed no cytotoxicity at the highest concentration tested (500 μM). Similarly, Kleszczyński et al. (2007) measured EC_{50}-values of different PFCAs in human colon carcinoma HCT116 cells showing that cytotoxicity increased with the elongation of the fluorocarbon chain; EC_{50}-values ranged from 124 for perfluorotetradecanoic acid (PFTeA) to 4154 μM for PFHxA. Also, Buhrke et al. (2013), by using the human hepatocarcinoma cell line HepG2 as an in vitro model for human hepatocytes, showed a positive correlation between the carbon chain length of the respective PFCA and its cytotoxicity. The EC_{50}-values obtained in JEG-3 cells are in agreement with those reported by Kleszczyński et al. (2007), but 9- to 25-fold higher than those reported in HepG2, which suggests a higher sensitivity of the latter to PFCs exposure in comparison to JEG-3 or HCT116 cells. Our work also evidenced a comparatively higher toxicity of the perfluorosulfonates than PFCAs of the same chain length, which is particularly evident for PFOS with an EC_{50} 5-fold lower than PFOA (Table 2).

Interestingly, length of the fluorocarbon chain was not the only factor affecting PFC absorption by JEG-3 cells. Among the eight analytes, PFDoA and PFOS showed the highest intracellular concentration (1190 and 470 pmol/mg protein after 24 h exposure), while the concentration of the long chain PFNA was 10- to 30-fold lower (Fig. 2). PFC residues detected in JEG-3 cells after 24 h exposure were as follows: PFDoA > PFOS ≫ PFNA > PFOA ~ PFHxA, being shorter chain PFCs (PFBA, PFBS, PFHxS) below detection limit. The cytotoxic effect of PFCs, although to some extent affected by the absorption of the compounds, did not follow the same pattern: PFOS > PFDoA ~ PFNA > PFOA > PFHxA. Interestingly, the non cytotoxic compounds (PFBA, PFHxA, PFBS and PFHxS) were the ones that were not detected in JEG-3 cells or that showed the lowest cell residue after 24 h exposure (Figs. 1 & 2).

Moreover, this work evidences a high potential of PFOS, PFOA and PFBS to act as aromatase inhibitors in placental cells. It is important to stress that not only PFBS, but also PFHxS significantly inhibited CYP19 aromatase activity despite the fact that the measured uptake of the compounds by cells was below detection limit. Therefore, both PFBS and PFHxS may exert the inhibitory effect on CYP19 aromatase activity at rather low endogenous cellular concentrations. These findings are of particular relevance since at present, producers of fluorochemicals are replacing long-chain for short-chain PFCs, which are expected to have a lower impact on environment and human health.

Reproductive toxicity following exposure to long chain PFCs has often been reported in animals and human cells. Thus, PFOA alters female pubertal timing in multiple strains of mice (Yang et al., 2009), and both PFOA and PFOS have been reported to delay pubertal timing in girls, but not in boys (Lopez-Espinosa et al., 2011). Exposure to PFOS (3×10^{-8}–3×10^{-7} M) increased estradiol concentration in H295R cell medium and increased CYP19 expression; however, exposure to 500 mg/L PFOS, decreased expression of CYP19a and CYP19b and changed the expression pattern of estrogen receptor in zebrafish embryos (Du et al., 2013). Similarly, Ankley et al. (2005) and Shi et al. (2008) found that PFOS exposure reduced aromatase activity in fathead minnow and gene expression zebrafish embryos, which is consistent with our findings, although in the present study, the inhibitory effect of PFOS is very closely related to its cytotoxic effect (Fig. 4B).

Concerning effects on JEG-3 cell lipidome, exposure to the mixture of PFCs produced a high increase in lyso plasmalogen PC, plasmalogen PC and PC, the major components of cell membranes, and a relatively low increase in TAG. The strongest alteration in cell lipids was registered at the lowest concentration tested (0.6 μM). These results suggest the ability of PFCs to interact with cellular membranes, possibly inducing the synthesis of PCs and plasmenyl-PCs as a defense mechanism of cells. Xie et al (2010a) reported that PFOS may cause adverse biological effects by altering the fluidity of lipid assemblies. Also PFOA has a high tendency to partition into phosphatidylcholine bilayers and to alter their phase behavior (Xie et al., 2010b). Furthermore, PFOA and PFOS exposures in PPARα knock-out mice have shown changes in gene expression indicative of lipotoxicity and altered fatty acid metabolism (Rosen et al., 2008, 2010).

Levels of PFOS and PFOA in human serum are in the range of 1 to 50 ng/mL, which corresponds to concentrations of 2 and 100 nM, respectively. However, the concentrations in occupationally exposed workers rise to 0.6 and 4.8 μM, respectively (Olsen et al., 1998). Thus, although we report significant alterations in JEG-3 cell lipidome at concentrations about two orders of magnitude above the PFC levels reported in human serum, the observed alterations are very likely to occur in occupationally exposed workers. Moreover, future studies are needed to investigate the ability of individual components of the PFC mixture to alter lipid profiles, as well as to determine the lowest concentration of individual and combined PFCs that leads to a significant alteration of cellular lipids.

Overall, this work contributes to the better knowledge of the effects of PFCs in human cells indicating an interference with cellular lipids at concentrations well below those associated with other adverse effects, such as cytotoxicity or endocrine disruption. The work also highlights: (a) the ability of PFOS and PFOA, particularly the shorter chain PFBS and PFHxS, to inhibit CYP19 aromatase activity in human placental cells, and (b) the importance of measuring the uptake of xenobiotics by cells in further in-vitro studies in order to establish a more realistic concentration–effect scenario.

Acknowledgments

This study was financed by the Ministry of Education, Science and Innovation in Spain, with the project INNPACTO [IPT-2011-0709-060000] and the Agència de Gestió d'Ajuts Universitaris i de Recerca de la Generalitat de Catalunya Grant 2009SGR1072. Dr. R. Chaler, D. Fanjul and M. Comesaña are acknowledged for MS support.

Conflict of interest

The authors declare that there are no conflicts of interest.

References

Ankley, G.T., Kuehl, D.W., Kahl, M.D., Jensen, K.M., Linnum, A., Leino, R.L., Villeneuve, D.A., 2005. Reproductive and developmental toxicity and bioconcentration of perfluorooctanesulfonate in a partial life-cycle test with the fathead minnow (*Pimephales promelas*). Environ. Toxicol. Chem. 24, 2316–2324.

Buhrke, T., Kibellus, A., Lampen, A., 2013. In vitro toxicological characterization of perfluorinated carboxylic acids with different carbon chain lengths. Toxicol. Lett. 218, 97–104.

Christie, W.W., 1985. Rapid separation and quantification of lipid classes by high performance liquid chromatography and mass (light-scattering) detection. J. Lipid Res. 26, 507–512.

Du, G., Hu, J., Huang, H., Qin, Y., Han, X., Wu, D., Song, L., Xia, Y., Wang, X., 2013. Perfluorooctane sulfonate (PFOS) affects hormone receptor activity, steroidogenesis, and expression of endocrine-related genes in vitro and in vivo. Environ. Toxicol. Chem. 32, 353–360.

Ericson, I., Gómez, M., Nadal, M., van Bavel, B., Lindström, G., Domingo, J.L., 2007. Perfluorinated chemicals in blood of residents in Catalonia (Spain) in relation to age and gender: a pilot study. Environ. Int. 33, 616–623.

Fernández-Sanjuan, M., Meyer, J., Damásio, J., Faria, M., Barata, C., Lacorte, S., 2010. Screening of perfluorinated chemicals (PFCs) in various aquatic organisms. Anal. Bioanal. Chem. 398, 1447–1456.

Garanto, A., Mandal, N.A., Egido-Gabás, M., Marfany, G., Fabriàs, G., Anderson, R.E., Casas, J., Gonzàlez-Duarte, R., 2013. Specific sphingolipid content decrease in *Cerkl* knockdown mouse retinas. Exp. Eye Res. 110, 96–106.

Giesy, J.P., Kannan, K., 2002. Perfluorochemical surfactants in the environment. Environ. Sci. Technol. 36, 146A–152A.

Grün, F., Watanabe, H., Zamanian, Z., Maeda, L., Arima, K., Cubacha, R., Gardiner, D.M., Kanno, J., Iguchi, T., Blumberg, B., 2006. Endocrine-disrupting organotin

compounds are potent inducers of adipogenesis in vertebrates. Mol. Endocrinol. 20, 2141–2155.
Hines, E.P., White, S.S., Stanko, J.P., Gibbs-Flournoy, E.A., Lau, C., Fenton, S.E., 2009. Phenotypic dichotomy following developmental exposure to perfluorooctanoic acid (PFOA) in female CD-1 mice: low doses induce elevated serum leptin and insulin, and overweight in mid-life. Mol. Cell. Endocrinol. 304, 97–105.
Hu, W.Y., Jones, P.D., DeCoen, W., King, L., Fraker, P., Newsted, J., Giesy, J.P., 2003. Alterations in cell membrane properties caused by perfluorinated compounds. Comp. Biochem. Physiol. C Toxicol. Pharmacol. 135, 77–88.
Huang, H., Leung, L.K., 2009. Bisphenol A downregulates CYP19 transcription in JEG-3 cells. Toxicol. Lett. 189, 248–252.
Kannan, K., Corsolini, S., Falandysz, J., Oehme, G., Focardi, S., Giesy, J.P., 2002. Perfluorooctanesulfonate and related fluorinated hydrocarbons in marine mammals, fishes, and birds from coasts of the Baltic and the Mediterranean Seas. Environ. Sci. Technol. 36, 3210–3216.
Kleszczyński, K., Gardzielewski, P., Mulkiewicz, E., Stepnowski, P., Składanowski, A.C., 2007. Analysis of structure–cytotoxicity in vitro relationship (SAR) for perfluorinated carboxylic acids. Toxicol. in Vitro 21, 1206–1211.
Lephart, E.D., Simpson, E.R., 1991. Assay of aromatase activity. Methods Enzymol. 206, 477–483.
Lopez-Espinosa, M.J., Fletcher, T., Armstrong, B., Genser, B., Dhatariya, K., Mondal, D., Ducatman, A., Leonardi, G., 2011. Association of perfluorooctanoic acid (PFOA) and perfluorooctane sulfonate (PFOS) with age of puberty among children living near a chemical plant. Environ. Sci. Technol. 45, 8160–8166.
Lou, Q.Q., Zhang, Y.F., Zhou, Z., Shi, Y.L., Ge, Y.N., Ren, D.K., Xu, H.M., Zhao, Y.X., Wei, W.J., Qin, Z.F., 2013. Effects of perfluorooctanesulfonate and perfluorobutanesulfonate on the growth and sexual development of *Xenopus laevis*. Ecotoxicology 22, 1133–1144.
Nelson, J.W., Hatch, E.E., Webster, T.F., 2010. Exposure to polyfluoroalkyl chemicals and cholesterol, body weight, and insulin resistance in the general U.S. population. Environ. Health Perspect. 118, 197–202.
Olsen, G.W., Gilliland, F.D., Burlew, M.M., Burris, J.M., Mandel, J.S., Mandel, J.H., 1998. An epidemiologic investigation of reproductive hormones in men with occupational exposure to perfluorooctanoic acid. J. Occup. Environ. Med. 40, 614–622.
Rosen, M.B., Abbott, B.D., Wolf, D.C., Corton, J.C., Wood, C.R., Schmid, J.E., Das, K.P., Zehr, R. D., Blair, E.T., Lau, C., 2008. Gene profiling in the livers of wild-type and PPARalpha-null mice exposed to perfluorooctanoic acid. Toxicol. Pathol. 36, 592–607.
Rosen, M.B., Schmid, J.R., Corton, J.C., Zehr, R.D., Das, K.P., Abbott, B.D., Lau, C., 2010. Gene expression profiling in wild-type and PPARalpha-null mice exposed to perfluorooctane sulfonate reveals PPARalpha-independent effects. PPAR Res. 2010. http://dx.doi.org/10.1155/2010/794739.
Rosenmai, A.K., Nielsen, F.K., Pedersen, M., Hadrup, N., Trier, X., Christensen, J.H., Vinggaard, A.M., 2013. Fluorochemicals used in food packaging inhibit male sex hormone synthesis. Toxicol. Appl. Pharmacol. 266, 132–142.
Schirmer, K., Chan, A.G.J., Greenberg, B.M., Dixon, D.G., Bols, N.C., 1997. Methodology for demonstrating and measuring the photocytotoxicity of fluoranthene to fish cells in culture. Toxicol. in Vitro 11, 107–119.
Shi, Z., Zhang, H., Liu, Y., Xu, M., Dai, J., 2007. Alterations in gene expression and testosterone synthesis in the testes of male rats exposed to perfluorododecanoic acid. Toxicol. Sci. 98, 206–215.
Shi, X., Du, Y., Lam, P.K., Wu, R.S., Zhou, B., 2008. Developmental toxicity and alteration of gene expression in zebrafish embryos exposed to PFOS. Toxicol. Appl. Pharmacol. 230, 23–32.
Shi, Z., Ding, L., Zhang, H., Feng, Y., Xu, M., Dai, J., 2009. Chronic exposure to perfluorododecanoic acid disrupts testicular steroidogenesis and the expression of related genes in male rats. Toxicol. Lett. 188, 192–200.
Stahl, T., Mattern, D., Brunn, H., 2011. Toxicology of perfluorinated compounds. Environ. Sci. Eur. 23–38, 1–52.
Vinggaard, A.M., Hnida, C., Breinholt, V., Larsen, J.C., 2000. Screening of selected pesticides for inhibition of CYP19 aromatase activity in vitro. Toxicol. in Vitro 14, 227–234.
Wan, H.T., Zhao, Y., Wong, M.H., Giesy, J.P., Wong, C.K.C., 2011. Testicular signaling is the potential target of perfluorooctanesulfonate-mediated subfertility in male mice. Biol. Reprod. 84, 1016–1023.
Xie, W., Ludewig, G., Wang, K., Lehmler, H.J., 2010a. Model and cell membrane partitioning of perfluorooctanesulfonate is independent of the lipid chain length. Colloids Surf. B: Biointerfaces 76, 128–136.
Xie, W., Bothun, G.D., Lehmler, H.J., 2010b. Partitioning of perfluorooctanoate into phosphatidylcholine bilayers is chain length-independent. Chem. Phys. Lipids 163, 300–308.
Yang, C., Tan, Y.S., Harkema, J.R., Haslam, S.Z., 2009. Differential effects of peripubertal exposure to perfluorooctanoic acid on mammary gland development in C57Bl/6 and Balb/c mouse strains. Reprod. Toxicol. 27, 299–306.
Zhao, B., Chu, Y., Hardy, D.O., Li, X.k, Ge, R.S., 2010. Inhibition of 3β- and 17β-hydroxysteroid dehydrogenase activities in rat Leydig cells by perfluorooctane acid. J. Steroid Biochem. Mol. Biol. 118, 13–17.

3.2.2. SCIENTIFIC ARTICLE V

Characterization of complex lípid mixtures in contaminant exposed JEG-3 cells using líquid chromatography and high-resolution mass spectrometry

E. Gorrochategui, J. Casas, E. Pérez-Albaladejo, O. Jáuregui, C. Porte, S. Lacorte

Environmental Science and Pollution Research (2014) **21 (20)**, 11907-11916

Environ Sci Pollut Res
DOI 10.1007/s11356-014-3172-5

14TH EUCHEMS INTERNATIONAL CONFERENCE ON CHEMISTRY AND THE ENVIRONMENT (ICCE 2013, BARCELONA, JUNE 25 - 28, 2013)

Characterization of complex lipid mixtures in contaminant exposed JEG-3 cells using liquid chromatography and high-resolution mass spectrometry

Eva Gorrochategui · Josefina Casas · Elisabet Pérez-Albaladejo · Olga Jáuregui · Cinta Porte · Sílvia Lacorte

Received: 4 October 2013 / Accepted: 6 June 2014

Abstract The aim of this study was to develop a method based on ultra high performance liquid chromatography coupled with mass spectrometry (UHPLC-MS) for lipid profiling in human placental choriocarcinoma (JEG-3) cells. Lipids were solid–liquid extracted from JEG-3 cells using a solution of chloroform/methanol (2:1, v/v) in a simple procedure requiring minimal sample alteration. Simultaneous separation of complex lipid mixtures in their major classes was achieved with a reversed-phase (C_8) UHPLC column and a mobile phase containing methanol with 1 mM ammonium formate and 0.2 % formic acid (A)/water with 2 mM ammonium formate and 0.2 % formic acid (B). Lipids were characterized using time-of-flight (TOF) and Orbitrap under full scan and positive electrospray ionization mode with both analyzers. A total of 178 species of lipids, including 37 phosphatidylcholines (PC), 32 plasmalogen PC, 9 lyso PC, 4 lyso plasmalogen PC, 30 triacylglycerols, 22 diacylglycerols, 7 cholesterol esters, 25 phosphatidylethanolamines, and 12 sphingomyelins, were identified using TOF and Orbitrap. The identification of all lipid classes was based on exact mass characterization with an error < 5 ppm. The developed methodology was applied to study lipid alterations in human placental cells against the exposure to perfluorinated chemicals (PFCs) and tributyltin (TBT).

Keywords Lipidomics · JEG-3 cells · Mass spectrometry · Time-of-flight and orbitrap analyzers · Perfluorinated chemicals (PFCs) · Tributyltin (TBT)

Responsible editor: Philippe Garrigues

Electronic supplementary material The online version of this article (doi:10.1007/s11356-014-3172-5) contains supplementary material, which is available to authorized users.

E. Gorrochategui · E. Pérez-Albaladejo · C. Porte · S. Lacorte (✉)
Department of Environmental Chemistry, Institute of Environmental Assessment and Water Research (IDAEA), Consejo Superior de Investigaciones Científicas (CSIC), Jordi Girona 18-26, Barcelona 08034, Catalonia, Spain
e-mail: slbqam@cid.csic.es

J. Casas
Department of Biomedicinal Chemistry, Institute of Advanced Chemistry of Catalonia (IQAC), Jordi Girona 18-26, Barcelona 08034, Catalonia, Spain

O. Jáuregui
Scientific and Technological Centers, University of Barcelona, Baldiri Reixac, 10-12, Barcelona 08028, Catalonia, Spain

Introduction

Lipidomics, a ramification of metabolomics, is the end point of omics cascade and can be described as the system wide study of lipids and their interaction with other biochemicals. In fact, the term lipidome can be defined as the comprehensive and nonexhaustive quantitative description of a group of lipid classes that may constitute a cell or bio-organism (Castro-Perez et al. 2010). Lipids and their interaction with cells play a crucial role in living organisms. Among the multiple biological functions of lipids, they contribute in compartmentalization, energy production and storage, cell-signaling processes, protein trafficking, and membrane organizing tasks (Oresic et al. 2008; Van Meer 2005). Moreover, several diseases, including obesity (Shi and Burn 2004), cardiovascular dysfunctions, diabetes, cancer, and neurodegenerative alterations, are associated with abnormalities in lipid functions and physiological levels (Shui et al. 2007). Lipid alterations have been attributed to the possible involvement of environmental obesogens, xenobiotics that can disrupt the normal developmental and homeostatic control over adipogenesis and energy balance (Grün and Blumberg 2006). Among others, tributyltin (TBT) has raised a lot of

Published online: 28 June 2014

attention since it is an environmental endocrine disrupter with the capacity to promote adipogenesis (Grün et al. 2006). In addition to TBT, perfluorinated chemicals (PFCs) have been reported to alter lipid levels in some animal species and humans (Gilliland and Mandel 1996; Nelson et al. 2010). Both TBT and PFCs share bioaccumulative properties; they are widely distributed environmental pollutants and are the target analytes of the present study.

According to all that, the importance of lipidomics lays not only on its contribution toward the enhanced understanding of the pathogenesis of multiple disease states related to lipids but also on the study of the impact of some emerging chemicals such as obesogen compounds in the environment and humans.

Lipids are exceptionally diverse in their structural, chemical, and physical properties. According to the latest version of the Comprehensive Classification System for Lipids firstly established on 2005 by the International Lipid Classification and Nomenclature Committee (ILCNC), lipids are divided into eight main distinctive classes: (1) fatty acids (FA), (2) glycerolipids (GL), (3) glycerophospholipids (GP), (4) sphingolipids (SP), (5) sterol lipids (ST), (6) prenol lipids (PR), (7) saccharolipids (SL), and (8) polyketides (PK) (Fahy et al. 2009). The characterized lipids in the present study include some GL (diacylglycerols and triacylglycerols), various GP (phosphatidylcholines and its lyso forms and derivatives with plasmalogens and phosphatidylethanolamines), sphingomyelins in the group of SP, and cholesterol esters as ST.

Lipid extraction is the first step toward lipidomic analysis. Due to the water-insoluble nature of lipid molecules, most of the described procedures in literature use organic solvents as the preferred extractive agents. Among the organic solvents, the most common for lipid extraction in biological tissues are chloroform and methanol combined in a mixture (2:1, v/v; Bligh and Dyer 1959; Folch et al. 1957). However, nontraditional extractive methods have used other organic solvents, such as isopropanol or hexane, in order to maximize the selective collection of particular lipid classes of interest (Hughes and Brash 1991).

Separation of the extracted lipid species in their major classes is a complicated procedure due to the highly complex biological matrices in which they are contained. One of the earliest techniques developed was thin layer chromatography (TLC) for routine analysis of lipids (Bennett and Heftmann 1962; Ruggieri 1962). However, in most recent applications, this technique is only used as a fast and extensive screening tool prior to the exhaustive analysis with more sensitive and selective techniques such as liquid chromatography (LC; Watson 2006).

Lipidomic analysis by LC can follow either normal-phase or reverse-phase strategies. While fatty acids are commonly separated on reverse-phase columns (Watson 2006), separation of phospholipids (PL) can be achieved by both approaches. Normal-phase LC effectively separates PL according to their different polar heads and not considering their sn-1 and sn-2 fatty acid substituent. In contrast, reversed-phase strategy separates PL on the basis of their fatty acid residues (Castro-Perez et al. 2010). However, for a complete separation of lipids, two-dimensional LC has reported to be the ideal method since it allows the combination of normal- and reversed-phase approaches (Pulfer and Murphy 2003, Wang et al. 2013).

Various classic detection methods, such as spectrophotometric analysis in the ultraviolet (UV) range and evaporative light scattering, have reported to be adequate for detecting lipids (Watson 2006). However, in recent years, mass spectrometry (MS) has evolved as a superior detection method for identifying lipids in biological matrices due to its high sensitivity and the additional information it provides (Sommer et al. 2006). Moreover, the recent ability of high-resolution mass spectrometers to obtain accurate mass measurements has emplaced them at the top of MS analyzers in lipidomic research. In fact, analyzers, such as Orbitraps, Fourier transform ion cyclotron resonance (FTICR), time-of-flight (TOF), and hybrid quadrupole orthogonal TOF (Q-TOF), have replaced the conventional low-resolution quadrupoles and linear ion traps, as they can resolve isomeric and isobaric species and elucidate elemental composition.

Thus, the aim of this study was to characterize the lipidomic composition of JEG-3 cells using high-resolution mass spectrometry (HRMS). Moreover, the effects of PFCs and TBT on the lipidome of the human placental choriocarcinoma cell line JEG-3 were investigated.

Materials and methods

Chemicals and reagents

Minimum essential medium, fetal bovine serum, L-glutamine, sodium pyruvate, nonessential amino acids, penicillin G, streptomycin, phosphate buffered saline (PBS), and trypsin-ethylenediaminetetraacetic acid (EDTA) were supplied by Gibco BRL Life Technologies (Paisley, Scotland, UK). Tributyltin (TBT), perfluorobutanoic acid (PFBA), perfluorohexanoic acid (PFHxA), perfluorooctanoic acid (PFOA), perfluorononanoic acid (PFNA), perfluorododecanoic acid (PFDoA), and perfluorohexanesulfonate (PFHxS) were purchased from Sigma-Aldrich (Steinheim, Germany), and perfluorobutanesulfonate (PFBS) and perfluorooctanesulfonate (PFOS) were obtained from Fluka (Austria). Stock standard solutions containing the mixture of the eight PFCs were prepared in ethanol at concentrations of 0.1 and 1 mM, and the stock solution of TBT was prepared in dimethyl sulfoxide (DMSO) at a concentration of 0.02 mM. These solutions were stored at −20 °C. High-performance liquid chromatography (HPLC)-

grade water, methanol (>99.8 %), and acetonitrile (>99.8 %) were purchased from Merck (Darmstadt, Germany). Chloroform was supplied by Carlo-Erba (Peypin, France) and butylated hydroxytoluene (BHT) by Sigma-Aldrich (St. Louis, MO, USA).

Cell culture

JEG-3 cells derived from a human placental carcinoma were obtained from American Type Culture Collection (ATCC HTB-36). They were grown in Eagle's minimum essential medium supplemented with 5 % fetal bovine serum, 2 mML-glutamine, 1 mM sodium pyruvate, 0.1 mM nonessential amino acids, 1.5 g/l sodium bicarbonate, and 50 U/ml penicillin and 50 μg/ml streptomycin in a humidified incubator with 5 % CO_2 at 37 °C. Cells were routinely cultured in 75 cm^2 polystyrene flasks (Corning; NY, USA). When 90 % confluence was reached, cells were dissociated with 0.25 % (w/v) trypsin and 0.9 mM EDTA (trypsin-EDTA) for subculturing and experiments. Experiments were carried out on confluent cell monolayers.

Sample preparation

Cell exposure to PFCs and TBT

Cells were seeded at a rate of 0.67×10^6 cells per well (six-well plate) and allowed to attach overnight in an incubator at 37 °C, 5 % CO_2. Then, 6 μl of the 0.02 mM stock solution of TBT or 6 μl of the 0.1 and 1 mM stock solutions containing the eight PFCs of study (PFBA, PFHxA, PFOA, PFNA, PFDoA, PFBS, PFHxS, and PFOS) were directly added to the wells. The final concentration of DMSO and ethanol in culture wells was 0.4 % (v/v), and final concentrations of PFCs were 0.6 and 6.0 μM and 0.1 μM for TBT. After 24 h of exposure, the medium was aspirated and cells were washed with PBS, trypsinized, and centrifuged at 5,400×*g* for 10 min. The supernatant was aspirated and cells were stored at −80 °C until analysis. In all cases, addition of the tested compound was done in triplicate, and controls were performed by adding the corresponding solvent to cells.

Lipid extraction

Lipids were extracted from JEG-3 cells with similar extraction conditions of a previous study (Christie 1985). To the cell pellets, 540 μl of a methanol:chloroform (1:2, v/v) solution containing 0.01 % of BHT, acting as an antioxidant, were added. Samples were shaken with a vortex mixer (1 min), were settled for 30 min, and extracted in an ultrasonic bath for 5 min at room temperature (two times). Between each period of 5 min, samples were thoroughly mixed. Afterwards, samples were centrifuged at 13,000×*g* for 5 min. The supernatant was transferred to a new micro vial, evaporated to dryness, reconstituted with 160 μl of acetonitrile, and stored at −20 °C in an argon atmosphere.

Instrumental analysis

UHPLC conditions

All analyses were performed with an ultra high performance liquid chromatography (UHPLC) system using an octyl carbon chain (C_8)-bonded silica column. Chromatographic parameters, such as column temperature, injection volume, flow rate, mobile phases, and gradient elution programs, are summarized in Table 1.

MS conditions

Analyses were performed with an UHPLC system coupled to two distinct mass analyzers. The analytical instrumentation used were an UHPLC system coupled to a Waters/LCT Premier XE TOF analyzer controlled with Waters/Micromass MassLynx 4.1 software and an UHPLC system (Accela) coupled to a Thermo Fischer Scientific LTQ Orbitrap Velos controlled with Thermo Fischer Scientific/Xcalibur software. The MS parameters, such as the ionization mode (positive electrospray), the mass acquisition range used in each mass analyzer along with other parameters, are summarized in Table 1.

Identification and relative quantification of lipids

Positive identification of lipids was based on the accurate mass measurement with an error < 5 ppm using both high-resolution TOF and Orbitrap. Relative retention times in UHPLC, compared to that of some standards (±2) used in a previous study, analyzed under the same chromatographic conditions (Garanto et al. 2013), were also considered as identification criteria. An inventory of a total of 225 lipids, containing 45 phosphatidylcholines (PC), 36 plasmalogen PC, 18 lyso PC, 4 lyso plasmalogen PC, 39 triacylglycerols (TAG), 26 diacylglycerols (DAG), 7 cholesterol esters (CE), 35 phosphatidylethanolamines (PE), and 15 sphingomyelins (SM), based on reported identified species (Garanto et al. 2013), was first generated. Their theoretical exact masses were determined using a spectrum simulation tool of Xcalibur software, and the obtained list was further used as a home-made referential database. Individual chromatographic peaks of distinct lipid species were isolated from full-scan MS spectra when selecting their theoretical exact masses, extracted from the database. Then, a list of possible candidates fitting the specific exact mass was generated using formula determination tools (elemental composition search) of both Micromass MassLynx and Thermo Fischer Scientific Xcalibur softwares. The elemental number was restricted to include C, H, O, N, and P. The formula constraints were C, H,

Table 1 UHPLC and MS conditions tested for the analysis of lipids in JEG-3 cells

Conditions	A	B
UHPLC		
LC system	Waters ACQUITY UHPLC system	Thermo Fischer Scientific Accela UHPLC system
Column	ACQUITY UPLC BEH (Waters, Ireland)	Then a list of possible candidates fitting
	C_8 column (100×2.1 mm) 1.7 μm	
Column T	30 °C	30 °C
Injection volumen	10 μl	5 μl
Flow rate	0.3 ml/min	
Mobile phase	A: Methanol with 1 mM ammonium formiate and 0.2 % formic acid	B: Water with 2 mM ammonium formiate and 0.2 % formic acid
Gradient elution	80–90 % of A/3 min, held for 3 min, increase to 99 % A/9 min, held for 3 min, return to initial conditions in 2 min and stabilization for 3 min	85 % of A/1 min, increase to 90 % A/9 min, held for 2 min, increase to 99 % A in 6 min, held for 2 min, return to initial conditions in 2 min and stabilization for 3 min
MS		
MS system	Waters/ LCT Premier XE time-of-flight (TOF) analyzer	Thermo Fischer Scientific Orbitrap analyzer
Ionization mode	ESI (+)	ESI (+)
Acquisition range	50–1,800 *m/z*	395–1,000 *m/z*
Capillary voltage	3.0 kV	Source voltage 3.5 kV
	Desolvatation temperature 350 °C	Capillary temperature 300 °C
	Desolvatation gas flow 600 l/h	Sheath gas flow 50 l/h
		Auxiliar gas flow 20 l/h
		Sweep gas flow 2 l/h

O≥1, P≥0, and N≥1, following the nitrogen rule. The number of double-bond equivalents (DBEs) was set between −0.5 and 15.0. The search was based on single mass analysis and only considered the *m/z* value of the monoisotopic peak.

Annotation of lipid species: GL, GP SP, and ST are annotated as < lipid subclass > <total fatty acyl chain length>:<total number of unsaturated bonds > and SM < total fatty acyl chain length>:<total number of unsaturated bonds in the acyl chain>. Relative quantification was done by comparison of peak areas in extracted ion chromatograms between exposed cells and controls.

Data processing and statistical analysis

Significant differences among controls and TBT/PFC-exposure treatment mean values (n=3) were determined by an ANOVA of one factor, considering statistical significance of P<0.05. All graphics were computed in Excel 2007.

Results and discussion

Chromatographic separation

Successful UHPLC separation of lipids in their major classes was achieved using a C_8-bonded silica column of 100-mm length. With TOF, 10 μl of the sample extract provided good resolution and sensitivity. However, with the Orbitrap, improved chromatographic peak shape was obtained when injecting 5 μl instead of 10 μl into the system and optimum column temperature was set to 30 °C. Concerning mobile phases, the optimum conditions were the use of methanol with 1 mM ammonium formate and 0.2 % formic acid (A) combined with water with 2 mM ammonium formate and 0.2 % formic acid (B). The addition of ammonium formate to the solvents has reported to be advantageous due to the formation of adduct ions $[M+NH_4]^+$ in positive mode, which are known to be more stable than the $[M+H]^+$ ions for some lipid classes. In the present study, lipids corresponding to the families of TAG, DAG, and CE were identified as ammonium adducts, whereas the rest of lipid groups were identified in the monoprotonated form. However, the use of ammonium formate requires the addition of buffering acids, such as the formic acid added in the present study, to avoid the formation of double-peak chromatograms (Sommer et al. 2006). Regarding elution program, the gradient conditions slightly changed when using the TOF or the Orbitrap with the aim to improve and adapt the chromatographic separation to each instrument. Both gradients presented in conditions A and B of Table 1 allowed good separation of main lipid classes. They both started at high percentage of the organic phase A, 80 and 85 %, respectively, and increased up to 99 % to allow the

desired elution of lipid species. With the Orbitrap, the two gradients were tested, and enhanced separation of lipid species was achieved when using the latter conditions, despite having a longer chromatogram than the one used with TOF. Figure 1 shows UHPLC chromatograms of TOF (Fig. 1a) and Orbitrap (Fig. 1b) when working at their respective optimum conditions (Table 1).

MS conditions

As observed in Table 1, the main difference among MS parameters used with TOF and Orbitrap was the acquisition range. The shorter range used in Orbitrap with respect to the one used in TOF was necessary to suppress high contribution of background ions in the system.

Lipid identification

Lipid species were successfully identified with both high-resolution TOF and Orbitrap. As shown in the UHPLC chromatograms of Fig. 1a and b, equivalent chromatographic distribution profiles were obtained when using both TOF and Orbitrap. Lyso PC and lyso plasmalogen PC were the first groups of lipids to elute and appeared in the early 5 min of the UHPLC-TOF chromatogram and between 4 and 7 min of the UHPLC-Orbitrap chromatogram. These groups of lipids were totally resolved from PC, plasmalogen PC, PE, SM, and DAG, which eluted together in the subsequent 10 min of the chromatogram. TAG and CE appeared together in the final minutes of the chromatogram. Individual lipid species unresolved in the total ion chromatogram were successfully isolated when their exact masses were selected. Thus, despite the incomplete chromatographic resolution of the complex lipid mixture, identification of individual lipids was possible using both the high-resolution TOF and Orbitrap. A total of 178 species of lipids were identified by TOF and Orbitrap and are shown in Table 2. In the group of glycerophospholipids, 107 species were identified containing 37 PC, 32 plasmalogen PC, 9 lyso PC, 4 lyso plasmalogen PC, and 25 PE. In the group of

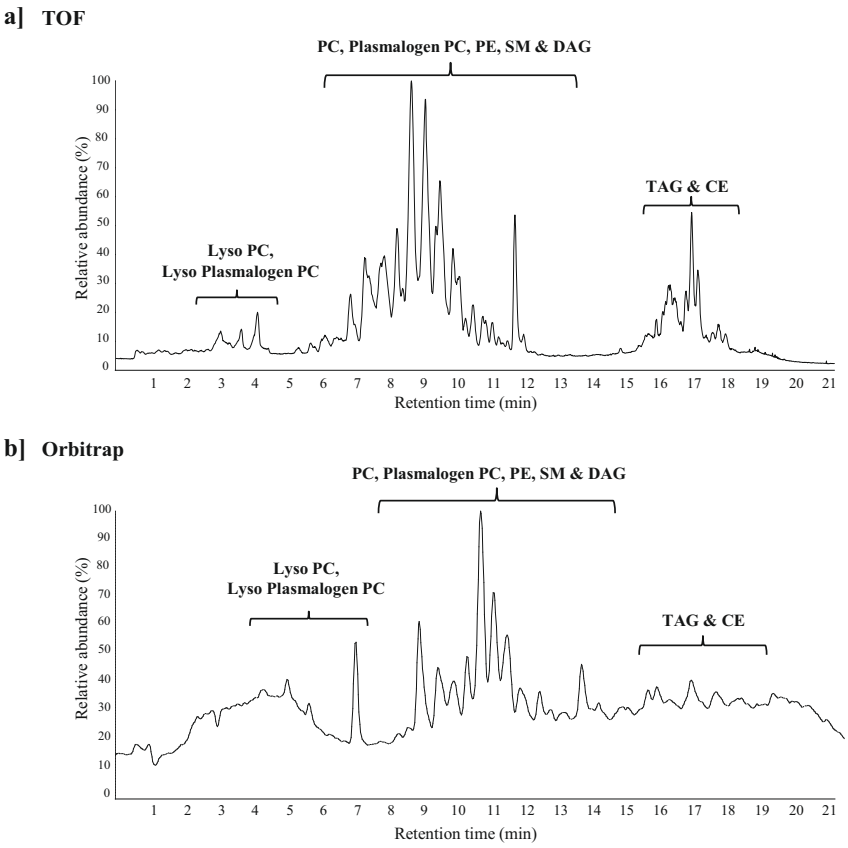

Fig. 1 UHPLC-MS total ion chromatograms of extracted lipids from JEG-3 cells when using **a** the TOF analyzer and **b** the Orbitrap analyzer, under conditions A and B of Table 1, respectively

Table 2 Lipid species identified using both TOF and Orbitrap analyzers

Glycerophospholipids	
PC	30:0[##], 32:0, 32:1, 32:2, 34:0, 34:1, 34:2, 34:3, 34:4, 34:5[##], 34:6[#], 36:0, 36:1, 36:2, 36:3, 36:4, 36:5, 36:6, 38:1, 38:2, 38:3, 38:4, 38:5, 38:6[##], 38:8[##], 40:0, 40:1, 40:2, 40:3, 40:4, 40:5, 40:6, 42:2, 42:3, 42:4, 42.5, 42:6
Plasmalogen PC	30:0, 30:1, 30:2[##], 32:0, 32:1, 32:2, 34:0, 34:1, 34:2, 34:3, 34:4[##], 36:0, 36:1, 36:2, 36:3, 36:4, 36:5, 38:1, 38:2, 38:3, 38:4, 38:5, 38:6, 38:7, 40:1, 40:2, 40:3, 40:4, 40:5, 40:6, 40:7, 40:8[##]
Lyso PC	16:0, 16:1, 18:0, 18:1, 18:2, 20:1, 20:2, 20:3, 20:4
Lyso plasmalogen PC	16:0, 16:1[##], 18:0, 18:1
PE	32:0, 32:1, 34:0, 34:1, 34:2, 34:3[#], 36:0[##], 36:1, 36:2, 36:3, 36:4, 36:6[##], 38:1, 38:2, 38:3, 38:4, 38:5, 38:6, 38:7[#], 40:1, 40:2[#], 40:3, 40:4[##], 40:5[##], 40:6[##]
Glycerolipids	
TAG	48:0, 48:1, 48:2, 48:3, 48:4, 48:6[##], 50:0, 50:1, 50:2, 50:3, 50:4, 50:5, 50:6, 52:0, 52:1, 52:2, 52:3, 52:4, 52:5, 52:6, 52:7, 54:1[#], 54:2, 54:3, 54:4, 54:5, 54:6, 54:7, 54:8, 54:9
DAG	32:0, 32:1, 32:2, 32:3, 34:0, 34:1, 34:2, 34:3, 34:4, 36:0, 36:1, 36:2, 36:3, 36:4, 36:5, 36:6, 38:0[##], 38:1[#], 38:2, 38:3, 38:4, 38:5
Sterol lipids	
CE	18:0, 18:1, 18:2, 18:3, 20:4, 20:5, 22:6
Sphingolipids	
SM	14:0, 16:0, 16:1, 18:0, 18:1, 20:0, 20:1, 22:0, 24:0, 24:1, 24:2, 24:3

Symbols (#) indicate lipid species only identified using TOF and (##) using Orbitrap. Lipid species GL, GP SP, and ST are annotated as < total fatty acyl chain length>:<total number of unsaturated bonds > and SM as < total fatty acyl chain length>:<total number of unsaturated bonds in the acyl chain>

glycerolipids, 52 species were identified containing 30 TAG and 22 DAG. As sterols, 7 CE were identified, and in the group of sphingolipids, 12 SM were determined. The compounds identified with their accurate mass measurement, elemental composition, calculated mass, error, double-bond equivalents and retention times are shown in the Table S1. Although not all lipids present in the cells were analyzed, the reported classes are quite representative since account for the 70 % of cellular lipidome. Phosphatydilserine and phosphatidylinositol were not determined since they can only be detected in negative electrospray ionization mode and the sensitivity was too low. considering the amount of extracted lipids from JEG-3 cells.

The distinct resolution of TOF and Orbitrap, 11,500 and 30,000 FWHM at *m*/*z* 556 and 400, respectively, resulted in a high lipid identification power. The use of 30,000 resolution with the Orbitrap would allow the resolution of isobaric species, although in our specific case, such species were chromatographically resolved. Figure 2 shows the identification ratio of the different target lipids when using both mass spectrometers. Equal results were obtained in families of lyso PC, TAG, DAG, CE, and SM. In the rest of the lipid groups, PC, plasmalogen PC, lyso plasmalogen PC and PE, identification was slightly superior with Orbitrap but with no significant differences. Of all the 178 lipids identified in the present study, 88 % were found by both analyzers, 4 % were only seen by TOF, and 8 % were only found with Orbitrap. Thus, the two high-performance platforms, TOF and Orbitrap analyzers, showed equivalent capability for lipidomic analysis in human placental choriocarcinoma JEG-3 cells.

Lipidome changes in PFC/TBT-exposed cells

The chromatographic profiles of PFC/TBT-exposed cells were compared to controls. TBT effects were studied at the low concentration of 0.1 μM, since it was the reported level at

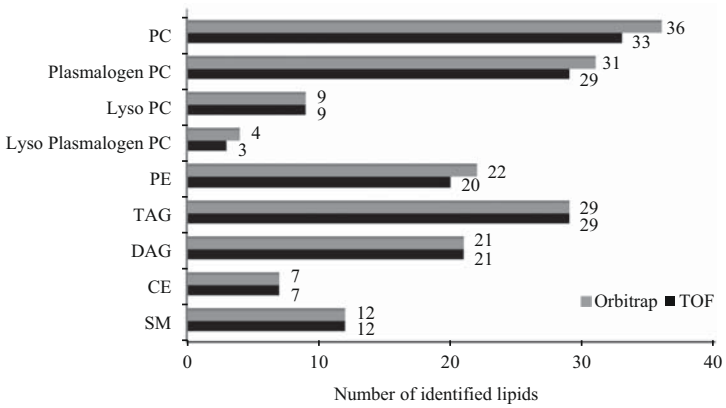

Fig. 2 Number of identified lipid species when using TOF and Orbitrap analyzers

which this compound promoted adipogenesis in vertebrates (Grün et al. 2006). In contrast, PFC effects were studied at two levels of concentration, 0.6 and 6 μM, the first close to the TBT exposure level and the latter about ten times higher. The selected doses of exposure were nontoxic for JEG-3 cells, as shown in a previous study (Gorrochategui et al. 2014).

Figure 3 represents differences in lipid amounts of exposed cells and controls caused by the distinct treatments, expressed as increasing rates, calculated as:

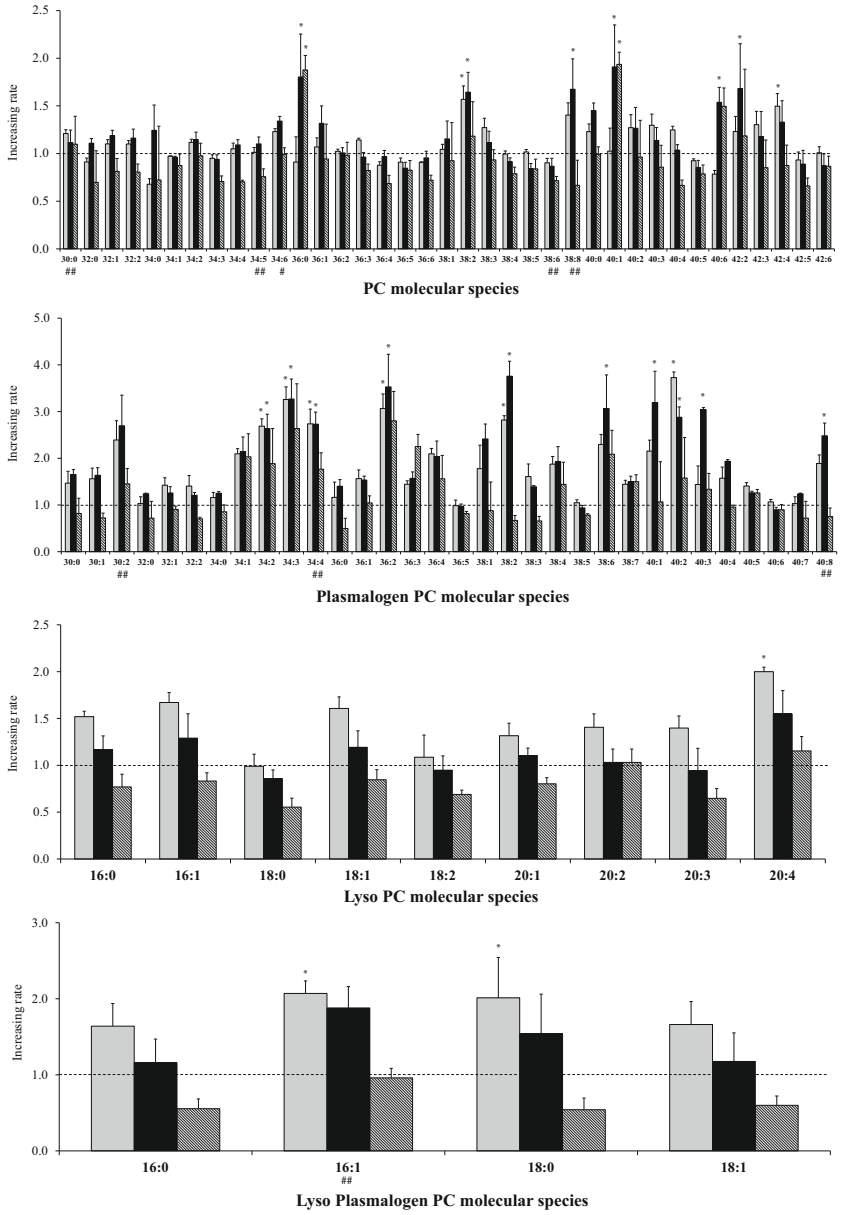

Fig. 3 Increasing rates of **a** PC, plasmalogen PC, lyso PC and lyso plasmalogen PC, **b** TAG, DAG and CE and **c** PE and SM in JEG-3 cells exposed to a mixture of PFCs, at 0.6 μM (□) and 6 μM (■) and TBT at 0.1 μM (▨). Values are relative to the cell control (set to 1) and are means±SEM (n=3), analyzed by TOF. Symbols (#) indicate lipid species only identified using TOF and (##) using Orbitrap. One-way ANOVA was performed to indicate statistical significant differences against the control (*P<0.05). Species of lipids are defined by their number of carbon atoms and the unsaturations of their fatty acid chains

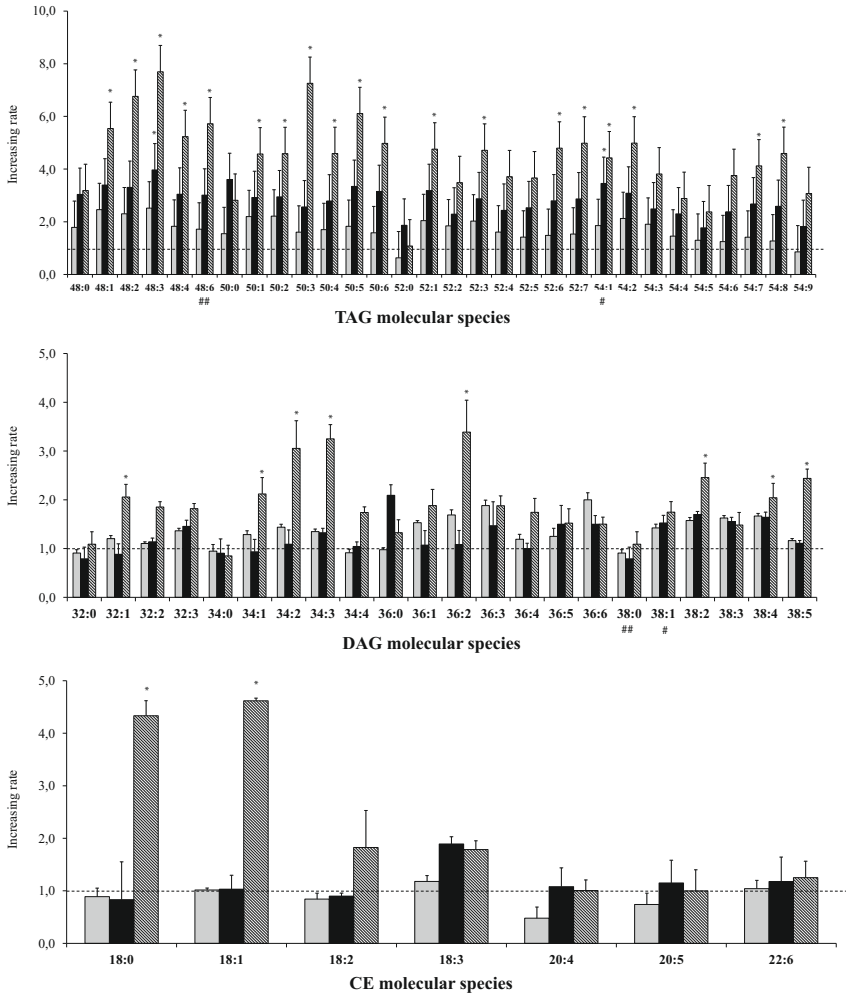

Fig. 3 (continued)

$$\text{Increasing rate} = \frac{\sum_{i=1}^{n} Ai, \text{exposed cell}}{\sum_{i=1}^{n} Ai, \text{control}}$$

where A_i represents the peak area of the lipid, and n the number of replicates of the four groups of samples (controls, cells exposed to PFCs at 0.6 μM, PFCs at 6 μM, and TBT), which was three in our experiment conditions. In each case, the variance associated to the increasing rate was calculated as the quotient of the standard error of the mean (SEM) of the corresponding cell treatment and SEM of controls.

Despite most lipid species were identified using both analyzers, the results shown correspond to the TOF analysis with the exception of few lipid species only identified with Orbitrap. Lipid species exclusively identified with TOF and Orbitrap are highlighted with symbols # and ##, respectively.

As shown in Fig. 3a, distinct effects were observed in four groups of the GP analyzed, PC, plasmalogen PC, lyso PC, and lyso plasmalogen PC, when exposed to PFCs and TBT. While exposure to PFCs produced significant increase in some lipid species, there was no significant alteration resulting from TBT exposure in the majority of cases. Even more, in groups of lyso PC and lyso plasmalogen PC, levels of lipids of cells exposed to the

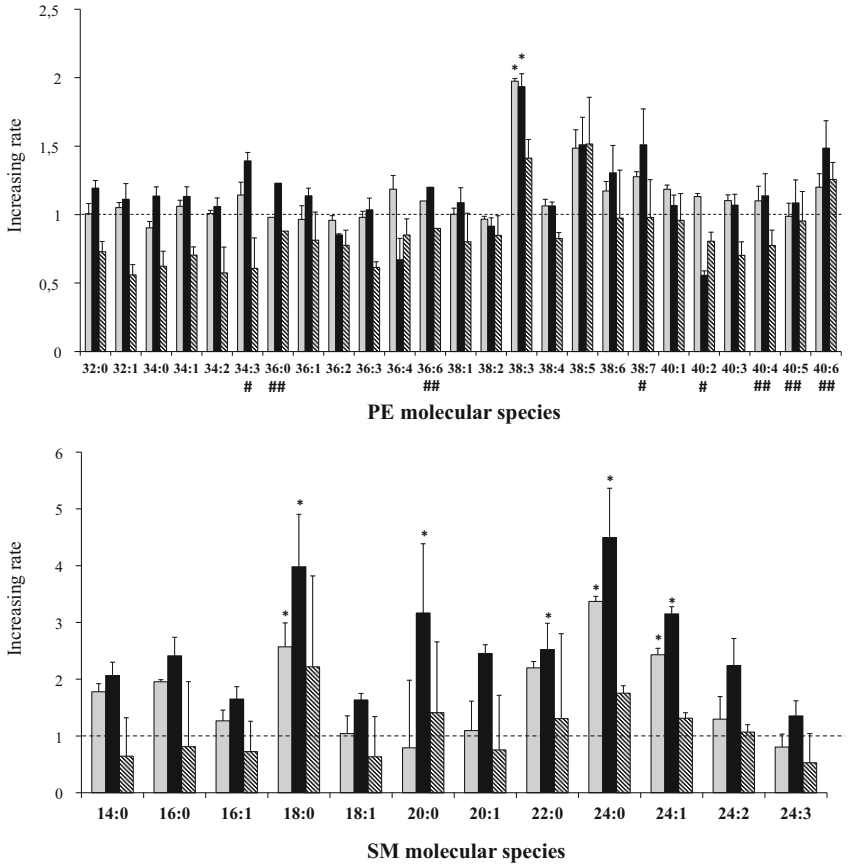

Fig. 3 (continued)

organotin compound were lower than in control samples. Surprisingly, effects of TBT were highly visible in families of TAG and DAG, whose levels suffered a dramatic increase after the exposure to the organotin compound. The effect of PFCs was considerably minor, even in the high concentration exposure of 6 μM, producing a low increase in the amount of some TAG and no significant effect on DAG. In the case of CE species, only two of them, 18:0 and 18:1, suffered a significant increase when exposed to TBT. Finally, effects on PE were practically undetectable and were only noticed in lipid species 38:3, whereas effects on SM resulted higher and were attributed to the presence of PFCs.

The observed increase in the amount of lipids resulting from the presence of TBT is in accordance to the findings of several studies which report the obesogenic effects of the organotin compound. According to our findings, Janer et al. (2007) reported increased accumulation of lipids and fatty acids in ramshorn snail *Marisa cornuarietis*. Moreover, Grün et al. (2006) reported promoted adipogenesis in murine 3 T3-L1 cell model and elevated lipid accumulation in adipose depots, liver and testis of neonate mice exposed to TBT. The observed effects of PFCs suggested a major influence on membrane lipids containing phosphorylcholine, such as PC, plasmalogen PC, lyso PC, and lyso plasmalogen PC, and sphingomyelins. In contrast, alterations of TBT where highly noticeable in TAG, DAG, and CE species.

In conclusion, the presented UHPLC-TOF/Orbitrap approaches allowed successful lipid profiling of JEG-3 cells. The proposed methodology was applied for the study of lipid alterations in PFC/TBT-exposed cells observing significant effects of both xenobiotics.

Acknowledgments This study was financed by the INNPACTO project (IPT-2011-0709-060000). Dr. R. Chaler, D. Fanjul, and Eva Dalmau are acknowledged for TOF-MS support and Dr. Alberto Adeva for Orbitrap-MS support.

References

Bennett RD, Heftmann E (1962) Thin-layer chromatography of sterols. J Chromatogr A 9:359–362

Bligh EG, Dyer WJ (1959) A rapid method of total lipid extraction and purification. Can J Biochem Phys 37:911–917

Castro-Perez JM, Kamphorst J, Degroot J, Lafeber F, Goshawk J, Yu K, Shockcor JP, Vreeken RJ, Hankemeier T (2010) Comprehensive LC-MSE lipidomic analysis using a shotgun approach and its application to biomarker detection and identification in osteoarthritis patients. J Proteome Res 9:2377–2389

Christie WW (1985) Rapid separation and quantification of lipid classes by high performance liquid chromatography and mass (light-scattering) detection. J Lipid Res 26:507–512

Fahy E, Subramaniam S, Murphy RC, Nishijima M, Raetz CRH, Shimizu T, Spener F, Van Meer G, Wakelam MJO, Dennis EA (2009) Update of the LIPID MAPS comprehensive classification system for lipids. J Lipid Res 50:S9–S14

Folch J, Lees M, Sloane Stanley GH (1957) A simple method for the isolation and purification of total lipids from animal tissues. J Biol Chem 226:497–509

Garanto A, Mandal NA, Egido-Gabás M, Marfany G, Fabriàs G, Anderson RE, Casas J, Gonzàlez-Duarte R (2013) Specific sphingolipid content decrease in Cerkl knockdown mouse retinas. Exp Eye Res 110:96–106

Gilliland FD, Mandel JS (1996) Serum perfluorooctanoic acid and hepatic enzymes, lipoproteins, and cholesterol: a study of occupationally exposed men. Am J Ind Med 29:560–568

Gorrochategui E, Pérez-Albaladejo E, Casas J, Lacorte S, Porte C (2014) Perfluorinated chemicals: differential toxicity, inhibition of aromatase activity and alteration of cellular lipids in human placental cells. Toxicol Appl Pharmacol 277(2):124–130. doi:10.1016/j.taap.2014.03.012

Grün F, Blumberg B (2006) Environmental obesogens: organotins and endocrine disruption via nuclear receptor signaling. Endocrinol 147: S50–S55

Grün F, Watanabe H, Zamanian Z, Maeda L, Arima K, Cubacha R, Gardiner DM, Kanno J, Iguchi T, Blumberg B (2006) Endocrine-disrupting organotin compounds are potent inducers of adipogenesis in vertebrates. Mol Endocrinol 20:2141–2155

Hughes MA, Brash AR (1991) Investigation of the mechanism of biosynthesis of 8-hydroxyeicosatetraenoic acid in mouse skin. BBA-Lipid Lipid. Met 1081:347–354

Janer G, Navarro JC, Porte C (2007) Exposure to TBT increases accumulation of lipids and alters fatty acid homeostasis in the ramshorn snail *Marisa cornuarietis*. Comp Biochem Phys C 146:368–374

Nelson JW, Hatch EE, Webster TF (2010) Exposure to polyfluoroalkyl chemicals and cholesterol, body weight, and insulin resistance in the general U.S. population. Environ Health Persp 118:197–202

Oresic M, Hänninen VA, Vidal-Puig A (2008) Lipidomics: a new window to biomedical frontiers. Trends Biotechnol 26:647–652

Pulfer M, Murphy RC (2003) Electrospray mass spectrometry of phospholipids. Mass Spectrom Rev 22:332–364

Ruggieri S (1962) Separation of the methyl esters of fatty acids by thin layer chromatography. Nature 193:1282–1283

Shi Y, Burn P (2004) Lipid metabolic enzymes: emerging drug targets for the treatment of obesity. Nat Rev Drug Discov 3: 695–710

Shui G, Bendt AK, Pethe K, Dick T, Wenk MR (2007) Sensitive profiling of chemically diverse bioactive lipids. J Lipid Res 48:1976–1984

Sommer U, Herscovitz H, Welty FK, Costello CE (2006) LC-MS-based method for the qualitative and quantitative analysis of complex lipid mixtures. J Lipid Res 47:804–814

Van Meer G (2005) Cellular lipidomics. EMBO J 24:3159–3165

Wang S, Li J, Shi X, Qiao L, Lu X, Xu G (2013) A novel stop-flow two-dimensional liquid chromatography-mass spectrometry method for lipid analysis. J Chromatogr A 1321:65–72

Watson AD (2006) Thematic review series: systems biology approaches to metabolic and cardiovascular disorders. Lipidomics: a global approach to lipid analysis in biological systems. J Lipid Res 47: 2101–2111

SUPPLEMENTARY MATERIAL OF SCIENTIFIC ARTICLE V

Characterization of complex lípid mixtures in contaminant exposed JEG-3 cells using líquid chromatography and high-resolution mass spectrometry

E. Gorrochategui, J. Casas, E. Pérez-Albaladejo, O. Jáuregui, C. Porte, S. Lacorte

Environmental Science and Pollution Research (2014) **21 (20)**, 11907-11916

SUPPLEMENTARY TABLE 1- Elemental composition of glycerophospholipid, glycerolipid, sterol lipid and sphingolipid species found in human placental choriocarcinoma JEG-3 cells, calculated by mass accuracy within error of 5 ppm, with atom constraints and with -0.5 ≤ DBE ≤ 15.0. DBE: double-bond equivalent. Elemental composition of PC, Plasmalogen PC, Lyso PC, Lyso plasmalogen PC, PE and SM refer to the $[M+H]^+$ ions whereas TAG, DAG and CE refer to ammonium adducts $[M+NH_4]^+$. Lipid species were detected under ESI (+) using an UHPLC system coupled to a TOF analyzer with an Acquity UPLC BEH C_8 column (1.7 µm particle size, 100 mm x 2.1 mm), with the exception of lipid species highlighted with symbol (*), which were identified using an UHPLC-Orbitrap system with the same column.

GLYCEROPHOSPHOLIPIDS							
Lipid subclass	**Lipid specie**	**Measured mass (Da)**	**Elemental composition**	**Calculated mass (Da)**	**Error (ppm)**	**DBE**	**RT (min)**
PC							
	30:0	706.5383	$C_{38}H_{77}NO_8P$	706.5381	0.3	1.5	5.7*
	32:0	734.5694	$C_{40}H_{81}NO_8P$	734.5694	0.0	1.5	7.7
	32:1	732.5553	$C_{40}H_{79}NO_8P$	732.5538	2.0	2.5	6.8
	32:2	730.5377	$C_{40}H_{77}NO_8P$	730.5381	-0.5	3.5	6.2
	34:0	762.6012	$C_{42}H_{85}NO_8P$	762.6007	0.7	1.5	9
	34:1	760.5856	$C_{42}H_{83}NO_8P$	760.5851	0.7	2.5	8
	34:2	758.5708	$C_{42}H_{81}NO_8P$	758.5694	1.8	3.5	7.1
	34:3	756.5551	$C_{42}H_{79}NO_8P$	756.5538	1.7	4.5	6.2-7
	34:4	754.5381	$C_{42}H_{77}NO_8P$	754.5381	0.0	5.5	6.1
	34:5	752.5231	$C_{42}H_{75}NO_8P$	752.5225	0.8	6.5	5.5*
	34:6	754.5071	$C_{42}H_{73}NO_8P$	754.5068	0.4	7.5	5.2
	36:0	790.6328	$C_{44}H_{89}NO_8P$	790.6320	1.0	1.5	10.3
	36:1	788.6169	$C_{44}H_{87}NO_8P$	788.6164	0.6	2.5	9.4
	36:2	786.6012	$C_{44}H_{85}NO_8P$	786.6007	0.6	3.5	8.5
	36:3	784.5855	$C_{44}H_{83}NO_8P$	784.5851	0.5	4.5	7.6
	36:4	782.5698	$C_{44}H_{81}NO_8P$	782.5694	0.5	5.5	7.2
	36:5	780.5541	$C_{44}H_{79}NO_8P$	780.5538	0.4	6.5	6.5
	36:6	778.5384	$C_{44}H_{77}NO_8P$	778.5381	0.4	7.5	5.8
	38:1	816.6482	$C_{46}H_{91}NO_8P$	816.6478	0.5	2.5	10.4
	38:2	814.6325	$C_{46}H_{89}NO_8P$	814.6320	0.6	3.5	9.6
	38:3	812.6168	$C_{46}H_{87}NO_8P$	812.6164	0.5	4.5	8.8
	38:4	810.6011	$C_{46}H_{85}NO_8P$	810.6007	0.5	5.5	8.4
	38:5	808.5854	$C_{46}H_{83}NO_8P$	808.5851	0.4	6.5	7.6
	38:6	806.5697	$C_{46}H_{81}NO_8P$	806.5694	0.4	7.5	7.0*
	38:8	802.5388	$C_{46}H_{77}NO_8P$	802.5381	0.9	9.5	6.1*
	40:0	846.6958	$C_{48}H_{97}NO_8P$	846.6946	1.4	1.5	12.2
	40:1	844.6789	$C_{48}H_{95}NO_8P$	844.6790	-0.1	2.5	11.6
	40:2	842.6638	$C_{48}H_{93}NO_8P$	842.6633	0.6	3.5	10.8
	40:3	840.6481	$C_{48}H_{91}NO_8P$	840.6477	0.5	4.5	10
	40:4	838.6330	$C_{48}H_{89}NO_8P$	838.6320	1.2	5.5	9.4
	40:5	836.6172	$C_{48}H_{87}NO_8P$	836.6164	1.0	6.5	8.8
	40:6	834.6012	$C_{48}H_{85}NO_8P$	834.6007	0.6	7.5	7.8

	42:2	870.6950	C50H97NO8P	870.6946	0.5	3.5	11.8
	42:3	868.6796	C50H95NO8P	868.6790	0.7	4.5	11.1
	42:4	866.6638	C50H93NO8P	866.6633	0.6	5.5	10.4
	42:5	864.6482	C50H91NO8P	864.6477	0.6	6.5	9.8
	42:6	862.6327	C50H89NO8P	862.6320	0.8	7.5	9.0
Plasmalogen PC							
	30:0	692.5588	C38H79NO7P	692.5589	-0.1	0.5	7.3
	30:1	690.5449	C38H77NO7P	690.5432	2.5	1.5	6.5
	30:2	688.5280	C38H75NO7P	688.5276	0.6	2.5	5.9*
	32:0	720.5901	C40H83NO7P	720.5902	-0.1	0.5	8.6
	32:1	718.5750	C40H81NO7P	718.5745	0.7	1.5	7.8
	32:2	716.5592	C40H79NO7P	716.5589	0.4	2.5	7.4
	34:0	748.6215	C42H87NO7P	748.6215	0.0	0.5	9.9
	34:1	746.6050	C42H85NO7P	746.6058	-1.1	1.5	8.9
	34:2	744.5919	C42H83NO7P	744.5902	2.3	2.5	8.2
	34:3	742.5738	C42H81NO7P	742.5745	-0.9	3.5	7.7
	34:4	740.5589	C42H79NO7P	740.5589	0.0	4.5	7.1*
	36:0	776.6532	C44H91NO7P	776.6528	0.5	0.5	11.1
	36:1	774.6365	C44H89NO7P	774.6371	-0.8	1.5	10.3
	36:2	772.6228	C44H87NO7P	772.6215	1.7	2.5	9.3
	36:3	770.6061	C44H85NO7P	770.6058	0.4	3.5	9
	36:4	768.5919	C44H83NO7P	768.5902	2.2	4.5	8.2
	36:5	766.5760	C44H81NO7P	766.5745	2.0	5.5	7.3
	38:1	802.6688	C46H93NO7P	802.6684	0.5	1.5	11.2
	38:2	800.6534	C46H91NO7P	800.6528	0.7	2.5	10.5
	38:3	798.6379	C46H89NO7P	798.6371	1.0	3.5	9.9-10.3
	38:4	796.6250	C46H87NO7P	796.6215	4.4	4.5	9.3-9.5
	38:5	794.6060	C46H85NO7P	794.6058	0.3	5.5	8.5
	38:6	792.5885	C46H83NO7P	792.5902	-2.1	6.5	7.9-8.4
	38:7	790.5747	C46H81NO7P	790.5745	0.3	7.5	5.5-7.8
	40:1	830.7002	C48H97NO7P	830.6997	0.6	1.5	12.3
	40:2	828.6847	C48H95NO7P	828.6841	0.7	2.5	11.5
	40:3	826.6680	C48H93NO7P	826.6684	-0.5	3.5	10.8-11
	40:4	824.6545	C48H91NO7P	824.6528	2.1	4.5	10.2
	40:5	822.6376	C48H89NO7P	822.6371	0.6	5.5	9.5
	40:6	820.6219	C48H87NO7P	820.6215	0.5	6.5	8.6-9.2
	40:7	818.6071	C48H85NO7P	818.6058	1.6	7.5	8.2
	40:8	816.5906	C48H83NO7P	816.5902	0.5	8.5	7.5*
Lyso PC							
	16:0	496.3401	C24H51NO7P	496.3398	0.6	0.5	2.4
	16:1	493.3167	C24H48NO7P	493.3163	0.8	1.5	2.1
	18:0	524.3715	C26H55NO7P	524.3711	0.8	0.5	3.1
	18:1	522.3555	C26H53NO7P	522.3554	0.2	1.5	2.6
	18:2	520.3404	C26H51NO7P	520.3398	1.2	2.5	2.3
	20:1	550.3872	C28H57NO7P	550.3867	0.9	1.5	3.2
	20:2	548.3718	C28H55NO7P	548.3711	1.3	2.5	2.9
	20:3	546.3558	C28H53NO7P	546.3554	0.7	3.5	2.5
	20:4	544.3401	C28H51NO7P	544.3398	0.6	4.5	2.2
Lyso Plasmalogen PC							
	16:0	482.3597	C24H53NO6P	482.3605	-1.7	-0.5	2.8

	16:1	480.3455	$C_{24}H_{51}NO_6P$	480.3449	1.2	0.5	2.0*
	18:0	510.3912	$C_{26}H_{57}NO_6P$	510.3918	-1.2	-0.5	3.5
	18:1	508.3750	$C_{26}H_{55}NO_6P$	508.3762	-2.4	0.5	3
PE							
	32:0	692.5229	$C_{37}H_{75}NO_8P$	692.5225	0.6	1.5	5.9
	32:1	690.5080	$C_{37}H_{73}NO_8P$	690.5068	1.7	2.5	5.3
	34:0	720.5550	$C_{39}H_{79}NO_8P$	720.5538	1.7	1.5	7.0
	34:1	718.5381	$C_{39}H_{77}NO_8P$	718.5381	0.0	2.5	6.2
	34:2	716.5229	$C_{39}H_{75}NO_8P$	716.5225	0.6	3.5	6.0
	34:3	714.5073	$C_{39}H_{73}NO_8P$	714.5068	0.7	4.5	5.3
	36:0	748.5857	$C_{41}H_{83}NO_8P$	748.5851	0.8	1.5	8.0*
	36:1	746.5701	$C_{41}H_{81}NO_8P$	746.5694	0.9	2.5	7.4
	36:2	744.5553	$C_{41}H_{79}NO_8P$	744.5538	2.0	3.5	6.6
	36:3	742.5386	$C_{41}H_{77}NO_8P$	742.5381	0.7	4.5	6.3
	36:4	740.5231	$C_{41}H_{75}NO_8P$	740.5225	0.8	5.5	6.2
	36:6	736.4919	$C_{41}H_{71}NO_8P$	736.4912	1.0	7.5	5.8*
	38:1	774.6023	$C_{43}H_{85}NO_8P$	774.6007	2.1	2.5	8.7
	38:2	772.5866	$C_{43}H_{83}NO_8P$	772.5851	1.9	3.5	7.8
	38:3	770.5702	$C_{43}H_{81}NO_8P$	770.5694	1.0	4.5	7.4
	38:4	768.5547	$C_{43}H_{79}NO_8P$	768.5538	1.2	5.5	6.5
	38:5	766.5389	$C_{43}H_{77}NO_8P$	766.5381	1.0	6.5	7.6
	38:6	764.5235	$C_{43}H_{75}NO_8P$	764.5225	1.3	7.5	6.8
	38:7	762.5079	$C_{43}H_{73}NO_8P$	762.5068	1.4	8.5	6.2
	40:1	800.6172	$C_{45}H_{87}NO_8P$	800.6164	1.0	3.5	9.0
	40:2	798.6023	$C_{45}H_{85}NO_8P$	798.6007	2.0	4.5	8.2
	40:3	796.5876	$C_{45}H_{83}NO_8P$	796.5851	3.1	5.5	7.8
	40:4	794.5703	$C_{45}H_{81}NO_8P$	794.5694	1.1	6.5	6.5*
	40:5	792.5542	$C_{45}H_{79}NO_8P$	792.5538	0.5	7.5	5.9*
	40:6	790.5386	$C_{45}H_{77}NO_8P$	790.5381	0.6	8.5	5.4*
GLYCEROLIPIDS							
Lipid subclass	**Lipid specie**	**Measured mass (Da)**	**Elemental composition**	**Calculated mass (Da)**	**Error (ppm)**	**DB E**	**RT (min)**
TAG							
	48:0	824.7722	$C_{51}H_{102}NO_6$	824.7702	2.4	1.5	16.0
	48:1	822.7565	$C_{51}H_{100}NO_6$	822.7545	2.4	2.5	15.5
	48:2	820.7393	$C_{51}H_{98}NO_6$	820.7389	0.5	3.5	15.0
	48:3	818.7237	$C_{51}H_{96}NO_6$	818.7232	0.6	4.5	14.7
	48:4	816.7079	$C_{51}H_{94}NO_6$	816.7076	0.4	5.5	14.2
	48:6	812.6767	$C_{51}H_{90}NO_6$	812.6763	0.5	7.5	13.1*
	50:0	852.8024	$C_{53}H_{106}NO_6$	852.8015	1.1	1.5	16.7
	50:1	850.7867	$C_{53}H_{104}NO_6$	850.7858	1.1	2.5	16.1
	50:2	848.7706	$C_{53}H_{102}NO_6$	848.7702	0.5	3.5	15.6
	50:3	846.7552	$C_{53}H_{100}NO_6$	846.7545	0.8	4.5	15.2-15.4
	50:4	844.7392	$C_{53}H_{98}NO_6$	844.7389	0.4	5.5	14.9
	50:5	842.7236	$C_{53}H_{96}NO_6$	842.7232	0.5	6.5	14.4
	50:6	840.7078	$C_{53}H_{94}NO_6$	840.7076	0.2	7.5	14.0
	52:0	880.8336	$C_{55}H_{110}NO_6$	880.8328	0.9	1.5	17.6
	52:1	878.8176	$C_{55}H_{108}NO_6$	878.8171	0.6	2.5	16.7
	52:2	876.8029	$C_{55}H_{106}NO_6$	876.8015	1.6	3.5	16.2
	52:3	874.7863	$C_{55}H_{104}NO_6$	874.7858	0.6	4.5	15.8

	52:4	872.7705	C55H102NO6	872.7702	0.3	5.5	15.6
	52:5	870.7549	C55H100NO6	870.7545	0.5	6.5	15.1
	52:6	868.7391	C55H98NO6	868.7389	0.2	7.5	14.7
	52:7	866.7237	C55H96NO6	866.7232	0.6	8.5	14.2
	54:1	906.8488	C57H112NO6	906.8484	0.4	2.5	17.5
	54:2	904.8334	C57H110NO6	904.8328	0.7	3.5	16.9
	54:3	902.8170	C57H108NO6	902.8171	-0.1	4.5	16.4
	54:4	900.8021	C57H106NO6	900.8015	0.7	5.5	16.0-16.1
	54:5	898.7871	C57H104NO6	898.7858	1.4	6.5	15.7
	54:6	896.7712	C57H102NO6	896.7702	1.1	7.5	15.4
	54:7	894.7553	C57H100NO6	894.7545	0.9	8.5	14.9
	54:8	892.7395	C57H98NO6	892.7389	0.7	9.5	14.5-14.7
	54:9	890.7237	C57H96NO6	890.7232	0.6	10.5	14.2
DAG							
	32:0	586.5409	C35H72NO5	586.5405	0.7	0.5	9.2
	32:1	584.5235	C35H70NO5	584.5249	-2.4	1.5	8.2
	32:2	582.5097	C35H68NO5	582.5092	0.9	2.5	7.3
	32:3	580.4937	C35H66NO5	580.4936	0.2	3.5	6.7
	34:0	614.5698	C37H76NO5	614.5718	-3.3	0.5	10.5
	34:1	612.5588	C37H74NO5	612.5562	4.2	1.5	9.5
	34:2	610.5388	C37H72NO5	610.5405	-2.8	2.5	8.7
	34:3	608.5241	C37H70NO5	608.5249	-1.3	3.5	7.9
	34:4	606.5076	C37H68NO5	606.5092	-2.6	4.5	7.2
	36:0	642.6028	C39H80NO5	642.6031	-0.5	0.5	11.6
	36:1	640.5859	C39H78NO5	640.5875	-2.5	1.5	10.8
	36:2	638.5723	C39H76NO5	638.5718	0.8	2.5	9.9
	36:3	636.5568	C39H74NO5	636.5562	0.9	3.5	9.1
	36:4	634.5424	C39H72NO5	634.5405	3.0	4.5	8.7
	36:5	632.5261	C39H70NO5	632.5249	1.9	5.5	7.8
	36:6	630.5097	C39H68NO5	630.5092	0.8	6.5	7.0
	38:0	670.6335	C41H84NO5	670.6344	-1.3	0.5	12.3*
	38:1	668.6190	C41H82NO5	668.6188	0.3	1.5	11.8
	38:2	666.6035	C41H80NO5	666.6031	0.6	2.5	11
	38:3	664.5875	C41H78NO5	664.5875	0.0	3.5	10.3
	38:4	662.5716	C41H76NO5	662.5718	-0.3	4.5	9.8
	38:5	660.5548	C41H74NO5	660.5562	-2.1	5.5	9
STEROL LIPIDS							
Lipid subclass	**Lipid specie**	**Measured mass (Da)**	**Elemental composition**	**Calculated mass (Da)**	**Error (ppm)**	**DB E**	**RT (min)**
CE							
	18:0	670.6500	C45H84NO2	670.6497	0.4	4.5	17.2
	18:1	668.6337	C45H82NO2	668.6340	-0.4	5.5	16.3
	18:2	666.6193	C45H80NO2	666.6184	1.4	6.5	15.7
	18:3	664.6057	C45H78NO2	664.6027	4.5	7.5	15.2
	20:4	690.6190	C47H80NO2	690.6184	0.9	8.5	15.4
	20:5	688.6032	C47H78NO2	688.6027	0.7	9.5	14.89
	22:6	714.6185	C49H80NO2	714.6184	0.1	10.5	15.4

SPHINGOLIPIDS							
Lipid subclass	**Lipid specie**	**Measured mass (Da)**	**Elemental composition**	**Calculated mass (Da)**	**Error (ppm)**	**DBE**	**RT (min)**
SM							
	14:0	675.5435	$C_{37}H_{76}N_2O_6P$	675.5436	-0.1	1.5	5.5
	16:0	703.5749	$C_{39}H_{80}N_2O_6P$	703.5749	0.0	1.5	6.5
	16:1	701.5588	$C_{39}H_{78}N_2O_6P$	701.5592	-0.6	2.5	5.8
	18:0	731.6070	$C_{41}H_{84}N_2O_6P$	731.6062	1.1	1.5	7.9
	18:1	729.5903	$C_{41}H_{82}N_2O_6P$	729.5905	-0.3	2.5	6.9
	20:0	759.6375	$C_{43}H_{88}N_2O_6P$	759.6375	0.0	1.5	9.4
	20:1	757.6225	$C_{43}H_{86}N_2O_6P$	757.6218	0.9	2.5	8.3
	22:0	787.6695	$C_{45}H_{92}N_2O_6P$	787.6688	0.9	1.5	9.9
	24:0	815.7008	$C_{47}H_{96}N_2O_6P$	815.7001	0.9	1.5	11
	24:1	813.6852	$C_{47}H_{94}N_2O_6P$	813.6844	1.0	2.5	10.6
	24:2	811.6697	$C_{47}H_{92}N_2O_6P$	811.6689	1.0	3.5	9.8
	24:3	809.6542	$C_{47}H_{90}N_2O_6P$	809.6531	1.4	4.5	9.0

(*) Lipid species identified with UHPLC-Orbitrap system.

3.2.3. SCIENTIFIC ARTICLE VI

Chemometric strategy for untargeted lipidomics: Biomarker detection and identification in stressed human placental cells

E. Gorrochategui, J. Casas, C. Porte, S. Lacorte, R. Tauler

Analytica Chimica Acta (2015) **854**, 20-33

Analytica Chimica Acta 854 (2015) 20–33

Contents lists available at ScienceDirect

Analytica Chimica Acta

journal homepage: www.elsevier.com/locate/aca

Chemometric strategy for untargeted lipidomics: Biomarker detection and identification in stressed human placental cells

Eva Gorrochategui [a], Josefina Casas [b], Cinta Porte [a], Sílvia Lacorte [a], Romà Tauler [a,*]

[a] Department of Environmental Chemistry, Institute of Environmental Assessment and Water Research (IDAEA), Consejo Superior de Investigaciones Científicas (CSIC), Barcelona 08034, Catalonia, Spain
[b] Department of Biomedicinal Chemistry, Institute of Advanced Chemistry of Catalonia (IQAC), Jordi Girona 18-26, Barcelona 08034, Catalonia, Spain

HIGHLIGHTS

- The lipidome of human placental cells exposed to xenobiotics is studied.
- Multiple liquid chromatographic coelutions are resolved by MCR-ALS.
- Two untargeted strategies are proposed to discover lipid disruption biomarkers.
- Biomarker identification allows interpretation of lipid changes in stressed cells.
- The proposed method is a powerful alternative to targeted lipidomic strategies.

GRAPHICAL ABSTRACT

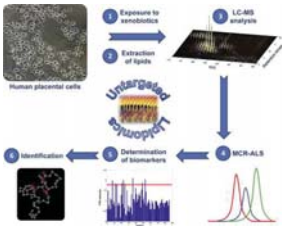

ARTICLE INFO

Article history:
Available online 11 November 2014

Keywords:
Untargeted lipidomics
Liquid chromatography–mass spectrometry
Multivariate curve resolution-alternating least squares
Partial least squares-discriminant analysis
Biomarkers
Obesogens

ABSTRACT

A lipidomic study was developed in a human placental choriocarcinoma cell line (JEG-3) exposed to tributyltin (TBT) and to a mixture of perfluorinated chemicals (PFCs). The method was based on the application of multivariate curve resolution-alternating least squares (MCR-ALS) to data sets obtained by ultra-high performance liquid chromatography coupled to time-of-flight mass spectrometry (UHPLC–TOF-MS) using an untargeted approach. Lipids from exposed JEG-3 cells were solid–liquid extracted and analyzed by UHPLC–TOF-MS in full scan mode, together with control samples. Raw UHPLC–TOF-MS data of the different cell samples were subdivided into 20 distinct chromatographic windows and each window was further organized in a column-wise augmented data matrix, where data from every sample was in an individual data matrix. Then, the 20 new augmented data matrices were modeled by MCR-ALS. A total number of 86 components were resolved and a statistical comparative study of their elution profiles showed distinct responses for the lipids of exposed versus control cells, evidencing a lipidome disruption attributed to the presence of the xenobiotics. Results from one-way ANOVA followed by a multiple comparisons test and from discriminant partial least squares (PLS-DA) analysis were compared as usual strategies for the determination of potential biomarkers. Identification of 24 out of the 33 proposed biomarkers contributed to the better understanding of the effects of PFCs and TBT in the lipidome of human placental cells. Overall, this study proposes an innovative untargeted LC–MS MCR-ALS approach valid for -omic sciences such as lipidomics.

* Corresponding author. Tel.: +34 934006140; fax: +34 93 204 59 04.
E-mail address: roma.tauler@cid.csic.es (R. Tauler).

http://dx.doi.org/10.1016/j.aca.2014.11.010
0003-2670/

1. Introduction

Lipids play essential roles in energy production and storage, structure and signaling in the human body [1,2]. Information about lipids and their individual classes can aid in understanding the pathogenesis of many disease states. Among others, obesity is characterized by a series of lipid disturbances [3], producing far-ranging effects on human health. Despite generally accepted causes for obesity are the consumption of calorie-dense food and diminished physical activity, the environmental obesogen hypothesis is raising acceptance in recent years. This hypothesis proposes that chemical exposure to molecules called "obesogens" during critical developmental stages influences subsequent adipogenesis, lipid balance and obesity [4]. Tributyltin (TBT) is a well-known endocrine disruptor previously used as a biocide in anti-fouling paints. TBT is a high-affinity agonist of the retinoic X receptor (RXR) and peroxisome proliferator activated receptor gamma (PPARγ), which are key components in adipogenesis and the function of adipocytes. TBT exposure has reported to promote inappropriate activation of RXR–PPARγ, causing a direct alteration of adipose tissue homeostasis [4]. Perfluorinated chemicals (PFCs) are potential obesogens used for many years in numerous industrial products, such as Teflon and have emerged as global environmental pollutants [5]. Among the variety of PFCs, perfluorooctanesulfonate (PFOS) and perfluorooctanoic acid (PFOA) are the most deeply investigated compounds in the last decades, whereas, other PFC homologs have been rarely studied. Recently, shorter chain length PFCs have been proposed as safe substitutes for the longer chain length ones, since they are expected to be less bioaccumulative and less toxic [6]. PFCs have been reported to alter lipid levels in some animal species and humans [7,8], but their mechanism of action is still unknown.

The study of lipids emerges as a complicated area of research due to their structural diversity and the considerable technical challenges associated with their identification within complex samples [9]. "The large-scale analysis of lipid profiles in cells and tissues" [10] was made possible by the dawn of lipidomics [11,12]. Lipidomics is a field that aims at the study of lipids and their interaction with other biochemicals [13]. While lipid-, and metabolome research in general, over past decades was overshadowed by the progress of genomics, recently revived and burgeoning interest in lipids illustrates their critical biological importance [14].

Mass spectrometry-based analytical methods come out as powerful strategies for lipidomics, since, they offer high sensitivity and resolution for the characterization of global lipid profiles in cells or organisms. Moreover, recent advances in mass spectrometry techniques have allowed the screening of many lipid molecular species in parallel [14]. These advances, however, pose a greater challenge for researchers to handle massive amounts of information-rich MS data from modern analytical instruments in order to understand the complexity of lipid systems. The application of modern chemometric methods to these complex megavariate data systems is opening new ways in bio and environmental sciences, facilitating a shift from the concept of studying one chemical compound or process at a single experiment. Thus, there is an urgent need to improve and automate all the steps involved in analyzing the data generated in -omic studies such as lipidomics by means of chemometric and multivariate data analysis methods.

Chemometrics is presently a well established field in chemical data analysis and has recently been proven to be valuable in the analysis of -omic data [15–17]. There is a considerable number of techniques especially suited for the study of complex megavariate -omic data sets, meant for exploratory or modelling purposes, such as principal component analysis (PCA), partial least squares (PLS) and its orthogonal variant (OPLS). Moreover, other less explored chemometric methodologies in -omic studies, such as multivariate curve resolution (MCR) methods evolve as powerful tools to properly resolve the profiling problem in -omic data sets [17,18]. In addition, chemometric methods can be used for biomarker detection in the context of finding sample descriptors which show systematic differences between normal and environmentally injured organisms in an untargeted approach. However, in areas of biology and toxicology, chemometric methodologies are still largely overlooked in favor of traditional statistical methods, which are generally focused on targeted evaluation of specific classes of compounds.

The aim of this study was to elucidate the lipidomic disruption produced in JEG-3 cells exposed to TBT and a mixture of PFCs, using MCR-ALS resolved profiles. Determination of biomarkers was based on the use of a traditional statistical approach, one-way ANOVA followed by a multiple comparisons test, versus the analysis by PLS-DA. The untargeted chemometric strategy presented in this study was designed as a novel alternative to the classical targeted approach generally used in lipidomics.

2. Theory

A brief description of the chemometric and statistical methods used in this study is shown below.

2.1. Multivariate curve resolution-alternating least squares (MCR-ALS)

Multivariate curve resolution methods [19] are based on the same bilinear decomposition of original data sets used by PCA, but under completely different constraints and with a different goal. The mathematical basis of the bilinear model used by MCR is shown in Eq. (1):

$$\mathbf{D} = \mathbf{C}\mathbf{S}^{\mathbf{T}} + \mathbf{E} \quad (1)$$

In this equation, matrix $\mathbf{D}$ ($I \times J$) represents the data output of a second-order instrument. In the case of LC–MS data, $\mathbf{D}$ matrix contains the MS spectra at all retention times ($i = 1, \ldots I$) in its rows, and the chromatograms at all spectra m/z channels ($j = 1, \ldots J$) in its columns. This matrix is decomposed in the product of two small factor matrices, $\mathbf{C}$ and $\mathbf{S}^{\mathbf{T}}$. The $\mathbf{C}$ ($I \times N$) matrix contains column vectors which correspond to the elution profiles of the N ($n = 1, \ldots N$) pure components of matrix $\mathbf{D}$. In $\mathbf{S}^{\mathbf{T}}$ ($N \times J$) matrix, row vectors correspond to the spectra of the N pure components. The part of $\mathbf{D}$ that is not explained by the model forms the residual matrix, $\mathbf{E}$ ($I \times J$).

MCR-ALS methods assume that the variation measured in all samples in the original data set can be described by a combination of a small number of chemically meaningful profiles. In the case of LC–MS data sets, information of the data table can be reproduced by the combination of a small number of pure mass spectra (row profiles in the $\mathbf{S}^{\mathbf{T}}$ matrix) weighted by the concentration of each of them along the elution direction (the related chromatographic elution peaks, column profiles in $\mathbf{C}$).

2.1.1. Column-wise augmented data matrices

In second order data, MCR-ALS can be implemented through different sample types simultaneously, conforming column-wise augmented data matrices ($\mathbf{D}_{\mathbf{aug}}$) containing distinct matrices correlated to different processes attached one at the top of each other. Thus, spectral direction is equal for all of them and the data matrix length is augmented in the process direction. Resolved pure mass spectra are equivalent to all experiments ($\mathbf{S}^{\mathbf{T}}$) whereas concentration profiles can differ from experiment to experiment, conforming $\mathbf{C}_{\mathbf{aug}}$, as shown in Eq. (2):

$$\mathbf{D}_{aug} = \begin{bmatrix} \mathbf{D}_1 \\ \mathbf{D}_2 \\ \mathbf{D}_3 \\ \vdots \end{bmatrix} = \begin{bmatrix} \mathbf{C}_1 \\ \mathbf{C}_2 \\ \mathbf{C}_3 \\ \vdots \end{bmatrix} \mathbf{S}^T + \begin{bmatrix} \mathbf{E}_1 \\ \mathbf{E}_2 \\ \mathbf{E}_3 \\ \vdots \end{bmatrix} = \mathbf{C}_{aug}\mathbf{S}^T + \mathbf{E}_{aug}$$

Process direction

(2)

In the MCR-ALS method, bilinear models expressed by Eq. (1) (single data matrix case) or Eq. (2) (augmented data matrix) are solved by means of an alternating least squares optimization under constraints (see [19]). In the cases under study in this work, the constraints applied during the ALS optimization were non-negativity for concentration (elution), **C**, and spectra, $\mathbf{S}^T$, profiles, and normalization for the later. See below in Sections 3.5 and 4.2 a more detailed description of the adaptation of the MCR-ALS to the analysis of the lipidomic data of this work. One of the main advantages of MCR-ALS analysis of several data matrices is that the alignment of chromatograms is not necessary since single spectrum dimensions coincide among matrices because are invariant for all runs [20].In summary, MCR-ALS procedure was applied in this work to acquire the resolved elution and mass spectral profiles corresponding to the lipidic components extracted from the distinct sample types related to the distinct stress experiments.

The quality of MCR-ALS models was measured evaluating the lack of fit, which is the difference among the input data $\mathbf{D}_{aug}$ and the data reproduced from the product obtained by MCR-ALS ($\mathbf{C}_{aug}\mathbf{S}^T$) and the percent of explained variance (R^2), defined in Eq. (3):

$$R^2(\%) = \frac{\sum d_{ij}^{*2}}{\sum d_{ij}^2} \times 100 \quad (3)$$

where $i = 1, \ldots, I$ and $j = 1, \ldots, J$, d_{ij} is an element of the experimental matrix **D**, d_{ij}^* is the element of the MCR-ALS reproduced matrix $\mathbf{D}^*$ and $I \times J$ is the total number of elements in the data set.

2.2. Partial least squares-discriminant analysis (PLS-DA)

Partial least squares (PLS) was first designed as a tool for statistical regression but later modified for classification purposes. Barker and Rayens [21] showed that PLS-DA corresponds to the inverse-least-squares approach to linear discriminant analysis and produces essentially the same results but with noise reduction and variable selection advantages of PLS [22]. In fact, PLS-DA is oriented to discriminate among different groups of samples by partitioning the hyperspace in a number of regions equal than the number of groups. Thus, if a sample is represented in the region of the space corresponding to a particular category, it is classified as belonging to that category.

PLS-DA is essentially based on PLS1 and PLS2 algorithms which search for latent variables with a maximum covariance with the *Y*-variables. The main difference respect to these algorithms is related to the dependent variables, since these represent qualitative (and not quantitative) values, when dealing with classification. For more details about PLS-DA analysis see [21].

2.3. Statistical tests

2.3.1. One-way ANOVA

One-way ANOVA is a statistical test oriented to determine whether data from distinct groups have a common mean. This test is a simple special case of a linear model where the input data is a matrix of observations $\mathbf{y_{ij}}$ in which columns represent distinct groups and rows the different samples. This matrix is decomposed into matrix $\mathbf{a_j}$, whose columns represent group means and are equal for all rows, "dot *j*" notation, and a matrix of random disturbances $\boldsymbol{\varepsilon_{ij}}$ (Eq. (4)). The model assumes that the columns of *y* are a constant plus a random disturbance and elucidates the similarity among these constants.

$$\mathbf{y_{ij}} = \mathbf{a_j} + \boldsymbol{\varepsilon_{ij}} \quad (4)$$

One-way ANOVA returns a table with information of sums of squares, degrees of freedom, mean squares and an *F* statistic and its *P* value. The *F* statistic is used as a hypothesis test to find out if column means of matrix $\mathbf{y_{ij}}$ are the same and the *P* value from this test is returned. The *P* value returned by one-way ANOVA depends on assumptions about the random disturbances $\boldsymbol{\varepsilon_{ij}}$ in the model equation. For the *P* value to be correct, these disturbances need to be independent, normally distributed, and have a constant variance. A *P* value lower than 0.05 indicates that means of the groups are significantly different at this significance level (i.e., only in 5% of cases or lower such a difference could be caused randomly).

The application of ANOVA analysis requires data to accomplish some assumptions such as "normality of residuals" and "homogeneity of variance between groups". In this study, a table of residuals was constructed and studied to ensure they varied randomly so that the "normality" assumption was fulfilled. In addition, variances among groups were compared to ensure they were homogeneous. Thus, in the present study no data transformation was required to meet the underlying assumptions of ANOVA.

2.3.2. Multiple comparisons test

Comparative studies often require the contrast among various groups of samples, such as pairwise comparisons among group means. One possible strategy to perform such multiple comparisons is to assess each comparison separately by a suitable procedure (a hypothesis test or confidence estimate) at a level appropriate for that single interference. This is known as per-comparison or separate inferences approach [23]. An example of this approach is the detection of differences among the means of $k \geq 3$ treatments, performing separating $\binom{k}{2}$ pairwise two-sided *t*-tests, each at level α appropriate for a single test. Such multiple *t*-tests (without a preliminary *F*-test of the overall homogeneity hypothesis H_0), despite used so frequently [24], do not cope with the multiplicity or selection effect [25]. This effect is related to the fact that in a multiple *t*-test any significant pairwise difference also implies overall significance, i.e., rejection of H_0. For instance, in the example presented above of the $\binom{k}{2}$ pairwise *t*-tests applied separately each at level α, the probability of concluding overall significance, when in fact H_0 is true, can be well in excess of α and close to 1 for sufficiently large *k*. The probability of concluding any false pairwise significance will equal α when exactly one pairwise null hypothesis is true, and will exceed α when two or more pairwise null hypothesis are true. Thus, with multiple *t*-tests, spurious overall and detailed (pairwise) significant results are obtained more frequently than is indicated by the per-comparison level α. These are the negative consequences defined by the called multiplicity or selection effect.

In this way, multiple comparisons procedures (MCPs) are statistical procedures designed to consider and properly control the multiplicity effect through some combined or joint measure of erroneous inferences [23]. In this study, a multiple comparisons test from the Statistics Toolbox of MATLAB (The MathWorks, Inc., Natick, MA, USA) has been used to specifically determine which pairs of means compared among the treatments are different.

This test uses as input, the stats output from ANOVA. The first output from multcompare has one row for each pair of groups compared, with an estimate of the difference in group means and a confidence interval for that group which is 0.05 as default. The second output contains the mean and its standard error for each group. All this information can be computed in a graph which allows a simple visualization of the differences encountered among groups.

Distinct types of critical values can be used for the multiple comparison procedures, and must be specified before computing them. Among all the possibilities the most common are the Tukey–Kramer, Bonferroni, Dunn–Sidak, lsd or Scheffe. The type of critical value used as default in the MATLAB implementation is the Tukey–Kramer and is the one used in the present study. Tukey–Kramer test [26,27] is based on a formula very similar to that of the *t*-test but using a studentized range distribution (q). The formula for Tukey's test is the one of Eq. (5).

$$q_s = \frac{Y_a - Y_b}{SE} \quad (5)$$

where Y_a is the larger of the two means being compared, Y_b is the smaller of the two means being compared, and SE the standard error of the data in question. This q_s value can then be compared to a q value from the studentized range distribution. If the q_s value is larger than the $q_{critical}$ value obtained from the distribution, the two means are said to be significantly different.

Since the null hypothesis for Tukey's test states that all means being compared are from the same population (i.e., $\mu_1 = \mu_2 = \mu_3 = \ldots = \mu_n$), the means should be normally distributed. This gives rise to the normality assumption of Tukey's test. The other assumption of this test is that observations being tested must be independent.

3. Experimental

3.1. Chemicals and reagents

Minimum essential medium, foetal bovine serum, L-glutamine, sodium pyruvate, nonessential amino acids, penicillin G, streptomycin, PBS and trypsin-EDTA were from Gibco BRL Life Technologies (Paisley, Scotland, UK). Tributyltin (TBT), perfluorobutanoic acid (PFBA), perfluorohexanoic acid (PFHxA), perfluorooctanoic acid (PFOA), perfluorononanoic acid (PFNA), perfluorododecanoic acid (PFDoA) and perfluorohexanesulfonate (PFHxS) were purchased from Sigma–Aldrich (Steinheim, Germany) and perfluorobutanesulfonate (PFBS) and perfluorooctanesulfonate (PFOS) were obtained from Fluka (Austria). Stock standard solutions containing the mixture of the eight PFCs were prepared in ethanol and the stock solution of TBT was prepared in dimethyl sulfoxide (DMSO). These solutions were stored at −20 °C. HPLC grade water, methanol (>99.8%) and acetonitrile (>99.8%) were purchased from Merck (Darmstadt, Germany). Chloroform was supplied by Carlo Erba (Peypin, France) and butylated hydroxytoluene (BHT) by Sigma–Aldrich (St. Louis, MO, USA).

3.2. Instrumentation

LC separation of lipids was carried out with an Acquity UHPLC system (Waters, USA) coupled to a Waters/LCT Premier XE time-of-flight (TOF) analyzer. The analytical separation was performed with an Acquity UPLC BEH C_8 column (1.7 μm particle size, 100 mm × 2.1 mm, Waters, Ireland). A positive ESI interface was used to detect the compounds in the LC column effluent. The chromatographic conditions and MS parameters used were the ones reported in previous studies [28,29].

3.3. Sample preparation and experimental design

3.3.1. Cell culture

JEG-3 cells derived from a placental carcinoma in humans were obtained from American Type Culture Collection (ATCC HTB-36, passage 127). They were grown in Eagle's minimum essential medium supplemented with 5% foetal bovine serum, 2 mM L-glutamine, 1 mM sodium pyruvate, 0.1 mM nonessential amino acids, 1.5 g L^{-1} sodium bicarbonate, 50 U mL^{-1} penicillin G and 50 μg mL^{-1} streptomycin in a humidified incubator with 5% CO_2 at 37 °C. Cells were routinely cultured in 75 cm^2 polystyrene flasks. When 90% confluence was reached, cells were dissociated with 0.25% (w/v) trypsin and 0.9 mM EDTA for subculturing and experiments. Experiments were carried out on confluent cell monolayers [28].

3.3.2. Cell exposure to PFCs and TBT

Three different cell stress treatments were designed in order to study the effects of TBT and two distinct concentrations of a mixture of PFCs, separately, in the lipidome of JEG-3 cells. Treatment A consisted in the addition of a stock solution containing the mixture of the eight PFCs (PFBA, PFHxA, PFOA, PFNA, PFDoA, PFBS, PFHxS and PFOS) so that the final concentration of each PFC in cells was 0.6 μM. Treatment B consisted in the addition of a stock solution containing the same mixture of the eight PFCs at a final concentration of 6 μM each. Treatment C was based on the addition of a stock solution of TBT at a final concentration of 0.1 μM. The selected concentrations were nontoxic for JEG-3 cells, as shown in a previous study [28] and were similar to the ones reported in a study carried out in occupationally exposed workers [30]. Control samples consisted of cells exposed to 0.4% ethanol. In all cases, addition of xenobiotics was done in triplicate so that a total of 12 samples were obtained, grouped in 4 classes (treatments A, B, C and controls).

As shown in one of the images of Fig. 1, cells were seeded in 6-well plates at a rate of 0.67×10^6 cells per well and allowed to attach overnight in an incubator at 37 °C, 5% CO_2. In the exposure to the xenobiotics, 6 μL of a 0.02 mM stock solution of TBT or 6 μL of 0.1 and 1 mM stock solutions containing the eight PFCs of study. After 24 h of exposure, the medium was aspirated and cells were washed with PBS, trypsinized and centrifuged at 5400 × *g* for 10 min. The supernatant was aspirated and cells were stored at −80 °C until analysis [28].

3.3.3. Extraction step and UHPLC–TOF-MS analysis

Lipids were extracted from JEG-3 cells with similar extraction conditions of a previous study [31]. To the cell pellets, 540 μL of a methanol:chloroform (1:2, v/v) solution containing 0.01% of butylated hydroxytoluene (BHT) were added. Samples were shaken with a vortex mixer (1 min) and after 30 min, extracted in an ultrasonic bath for 5 min at room temperature (2 times). Between each period of 5 min, samples were thoroughly mixed. Afterwards, samples were centrifuged at 13,000 rpm for 5 min. The supernatant was transferred to a new micro vial, evaporated to

dryness, reconstituted with 160 μL of acetonitrile and stored in an argon atmosphere.

The chromatographic separation was that of a previous study, using the instrumentation previously described [29].

3.4. Peak assignment and identification of lipids

Positive identification of lipids was based on the accurate mass measurement with an error < 5 ppm using high resolution TOF and its relative LC retention times, compared to that of some standards (±2) used in a previous study, analyzed under the same chromatographic conditions [32]. In addition, a homemade database generated in a previous study [29], working under the

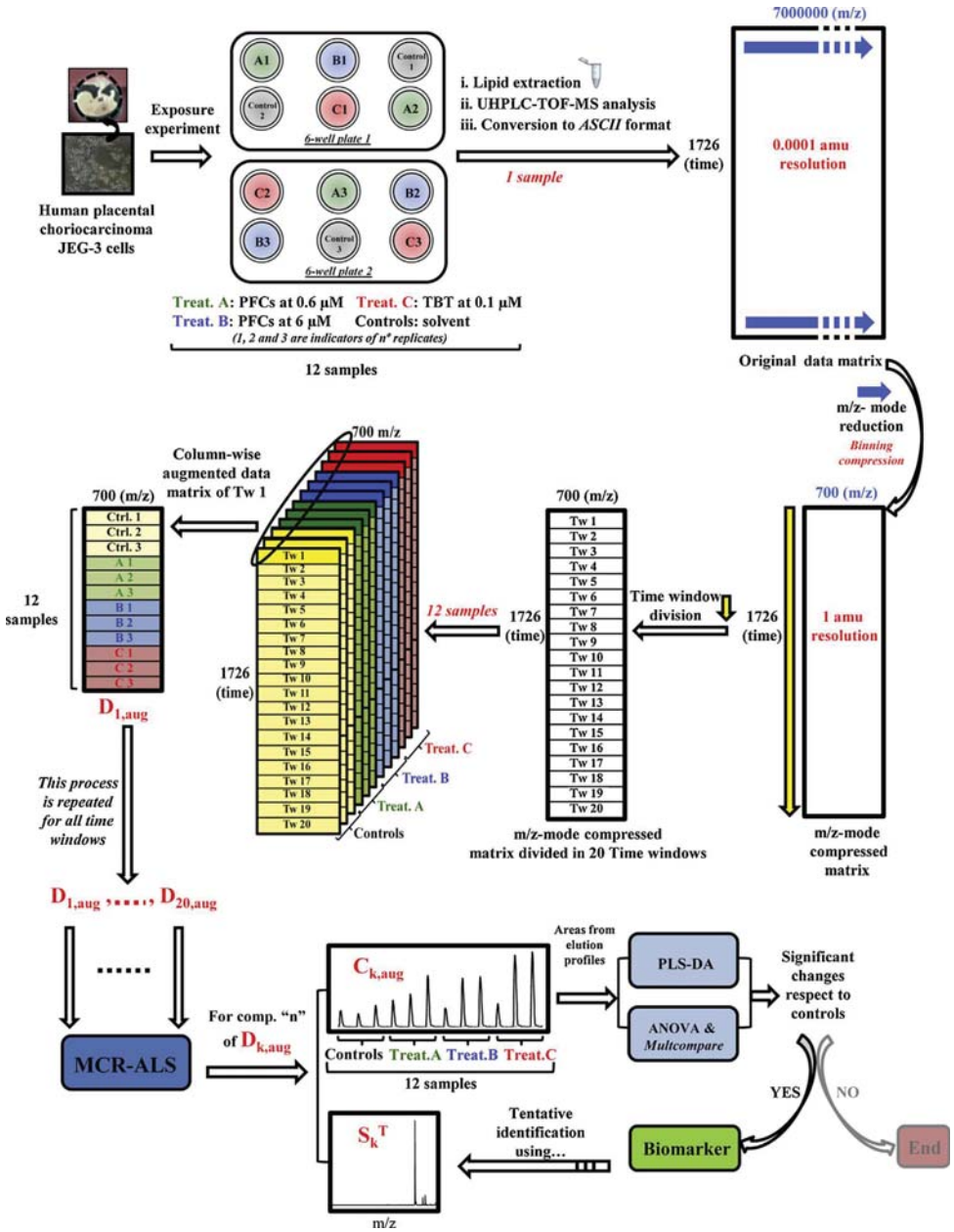

Fig. 1. Scheme of the steps of the untargeted LC–MS MCR-ALS strategy proposed in this study for the analysis of lipid profiles in order to determine potential biomarkers for lipid disruption.(For interpretation of the references to color in this figure legend, the reader is referred to the web version of this article.)

same LC–MS conditions, was also used to enable the identification of lipid species.

3.5. Data sets arrangement and their multivariate analysis by MCR-ALS

The workflow used in this study was similar to a previous work [17] with some modifications, specially focused on biomarker selection approach.

Once samples were analyzed by UHPLC–TOF-MS in positive ESI and full scan mode, every sample was represented by a $1726 \times 7{,}000{,}000$ data matrix, being the first number, the acquired retention times (20 min of chromatographic run with 1726 time points) and the second number, the detected m/z values (300–1000 amu with 0.0001 of resolution). These data files were stored in raw formats by the MassLynx software and they were transformed to ASCII by the Databridge function of MassLynx™ V 4.1 software to be further processed with MATLAB. According to this selected data arrangement, the simultaneous analysis of the whole data set (augmented data matrix of Eq. (2)) from the 12 samples would require 1.16 ($12 \times 1726 \times 7{,}000{,}000 \times 8$) terabytes of storage, which is not currently feasible for standard laboratory computers.

Therefore a proper data compression strategy was required, and data matrices in ASCII format from every sample were undergone to a reduction in its dimensionality in order to facilitate MCR-ALS modeling. This reduction was carried out by using a homemade routine which allowed m/z-mode dimension binning compression (grouping mass values into a number of "bins" containing values within a particular m/z range covering 1 amu) by ten thousand times its size. Thus, the obtained matrices were reduced to a size of 1726×700, so that final mass information obtained from spectra profiles ($\mathbf{S^T}$ in Eqs. (1) and (2)) of MCR-ALS resolved components was limited to 1 amu resolution. In addition to these matrices, a vector of retention times (1726) and a vector of m/z values were generated (700). Due to the complexity of the data sets (large number of possible components to be resolved by MCR-ALS in the simultaneous analysis of all cell samples) and to hardware limitations, each data matrix was also further reduced in its time-mode dimension by dividing the chromatogram in 20 different time windows. For each time window, a new column-wise augmented data matrix was generated, arranging all the 12 samples one at the top of each other (sample × elution time of the corresponding time window, m/z values). Finally and previous to the MCR-ALS analysis, the intensity scale of all chromatograms was divided by 10^4 so that data values were scaled to more computationally manageable sizes and facilitated their evaluation and graphical representation and comparison.

MCR-ALS was applied to the 20 windowed augmented column-wise matrices containing information of the 12 samples simultaneously. The elution profiles were compared against sample classes in other to elucidate the possible effects of the different cell stress treatments. Calculated areas of the MCR-ALS resolved elution profiles of the different components were further used to determine potential biomarkers for lipid disruption by the use of two strategies: one-way ANOVA followed by a multiple comparisons test and a PLS-DA discrimination analysis by the use of VIP-scores. Then, only for compounds determined as potential biomarkers, information of their $\mathbf{S^T}$ at low resolution from MCR-ALS analysis was used for their tentative identification. Fig. 1 shows a scheme of the steps involved in this study.

3.6. Software

MATLAB 8.1.0 R2013a (The MathWorks, Inc., Natick, MA, USA) was used as the development platform for data analysis and visualization. A graphical interface was used to apply MCR-ALS, which additionally provided detailed information about the implementation of this algorithm [33]. Statistics Toolbox™ for MATLAB, PLS Toolbox 7.3.1 (Eigenvector Research Inc., Wenatchee, WA, USA) and homemade routines were used in this work. Waters/Micromass MassLynx™ V 4.1 software was used for data set conversion from raw into ASCII format and as the formula identification platform through its elemental composition tool.

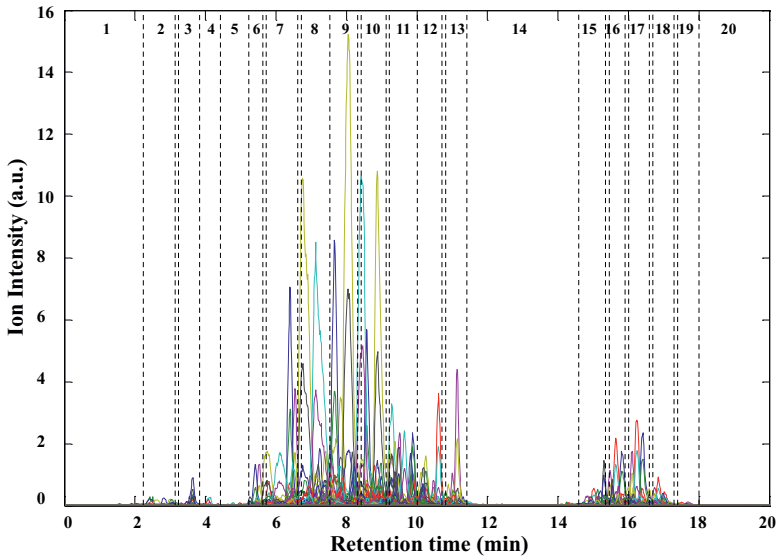

Fig. 2. UHPLC–TOF-MS chromatogram of a control sample divided in 20 time windows for the MCR-ALS analysis, after the m/z compression to 1 amu resolution. Colored lines are indicators of distinct m/z values.(For interpretation of the references to color in this figure legend, the reader is referred to the web version of this article.)

Table 1
Dimensions of the $k = 1–20$ chromatographic windows for one sample (D_k) and for the 12 samples distributed one at the top of each other conforming augmented data matrices ($D_{k,aug}$) (see Eq. (2)). MCR-ALS data fitting results are shown for the analysis of the augmented data matrices ($D_{k,aug}$).

Time window (k)	Dimensions of D_k	Dimensions of $D_{k,aug}$	RT (min)	Nr. estimated components	Nr. resolved components	Lack of fit (%)	R^2 [a](%)	Resolved peak nr.
1	190 × 700	2280 × 700	0.0–2.2	–	–	–	–	–
2	85 × 700	1020 × 700	2.2–3.2	11	9	15.4	97.6	1–9
3	65 × 700	780 × 700	3.1–3.8	12	8	6.3	99.6	10–17
4	50 × 700	600 × 700	3.8–4.4	8	5	10.9	98.8	18–22
5	68 × 700	816 × 700	4.4–5.2	4	2	31.6	90.0	23–24
6	42 × 700	504 × 700	5.2–5.7	5	3	5.1	99.7	25–27
7	95 × 700	1140 × 700	5.6–6.7	6	4	9.2	99.1	28–31
8	82 × 700	984 × 700	6.6–7.5	4	2	18.2	96.7	32–33
9	77 × 700	924 × 700	7.5–8.4	4	3	15.1	97.7	34–36
10	80 × 700	960 × 700	8.3–9.2	4	3	13.2	98.2	37–39
11	80 × 700	960 × 700	9.1–10.0	10	8	11.2	98.7	40–47
12	67 × 700	804 × 700	10.0–10.8	7	5	10.7	98.9	48–52
13	60 × 700	720 × 700	10.7–11.4	4	3	13.4	98.2	53–55
14	275 × 700	3300 × 700	11.4–14.6	–	–	–	–	–
15	75 × 700	900 × 700	14.6–15.5	9	6	8.5	99.3	56–61
16	55 × 700	660 × 700	15.4–16.0	8	5	5.1	99.7	62–66
17	67 × 700	804 × 700	15.9–16.7	8	6	5.6	99.7	67–72
18	65 × 700	780 × 700	16.6–17.4	9	7	7.1	99.5	73–79
19	55 × 700	660 × 700	17.3–18.0	10	7	9.1	99.2	80–86
20	176 × 700	2112 × 700	18.0–20.0	–	–	–	–	–

–Regions of the chromatogram with background noise.
[a] R^2 explained data variance according Eq. (3).

4. Results and discussion

4.1. Reduction of the time-mode dimension

After applying the reduction of the m/z-mode dimensions of original data matrices, time-mode dimensions were also reduced by subdividing chromatograms in 20 different time windows, as previously represented in Fig. 1.

The distinct time windows were established according to the position and shape of chromatographic profiles in the chromatogram, considering regions of peak clusters and avoiding the halving peaks, i.e., trying always to keep the full peak in the window. When time windows are selected avoiding halving peaks, the regions start one right after the end of its previous. For that cases in which it is impossible to avoid the splitting of a peak in two windows, the solution is overlapping these consecutive regions. As shown in Fig. 2, most of them covered a time interval between 0 and 1 min with the exception of three extensive zones 1, 14 and 20, which contained very little relevant chromatographic peaks. The dimensions of the resulting 20 submatrices are shown in Table 1.

4.2. MCR-ALS results

MCR-ALS allowed the resolution of multiple coeluted chromatographic peaks generated during the LC–MS analysis of complex lipid samples together with the evaluation of possible xenobiotic effects in the lipidome of cells.

As previously stated in Section 3.5, MCR-ALS analysis was performed simultaneously over the 12 samples (control and stressed samples with treatments A, B and C), but considering separately the 20 different chromatographic time windows (Fig. 1). Thus, a total number of 20 different column-wise augmented data matrices ($\mathbf{D_{k,aug}}$ where $k = 1–20$; Eq. (2)) was generated, one for each time window, containing in all cases the same number of columns (700 m/z values) and 12 submatrices, with the time-dimension of the individual time windows, which were different in each case. The dimensions of the new 20 column-wise augmented data matrices are also shown in Table 1.

Previous to the MCR-ALS analysis, the number of components explaining a reasonable amount of the total variance of each augmented data matrix at a particular time window was initially estimated throughout SVD algorithm [34], choosing those with a large size (larger than noisy ones). The number of selected components for each augmented data matrix at the different time windows was related to the number of identifiable chromatographic peaks but also considering extra components to explain the background noise. In order to select the optimum number of components, MCR-ALS was first undergone with an initial estimation considering few components and was consecutively repeated increasing this number. After each of these MCR-ALS analyses, the incorporation of a new component was considered appropriate only if a diminution in the lack of fit and an increase in the explained variance were observed. Thus, the addition of an extra component which caused a superior or equal value of lack of fit and a lower variance explained was considered incorrect and the corresponding component was automatically rejected. The number of selected components for each time window in the present study is shown in Table 1.

MCR-ALS was then directly applied to the 20 column-wise augmented data matrices (without applying any background correction) and matrices $\mathbf{C_{k,aug}}$ and $\mathbf{S_k^T}$ (where $k = 1–20$; Eq. (2)) were estimated. Initialization of MCR-ALS was performed using estimates of spectra profiles, using those measured experimentally at elution times giving the purest ones (like in the SIMPLISMA algorithm, [35]), and setting the noise level at 10% to avoid the selection of pure noise ones. Distinct constraints were considered during ALS optimization to diminish rotational and intensity ambiguities [24,36,37]. In the present study, non-negativity constraints for both elution and mass spectra profiles and pure mass spectra normalization (spectra equal length) were applied to reduce rotational and intensity ambiguities, respectively. ALS optimization resulted to be fast and reliable due to the high selectivity of MS measurements. Once ALS optimization reached its optimum, the resulting elution profiles were integrated and areas of the resolved peaks were obtained. Thus, areas of all resolved components present in control and exposed samples were estimated for each time window.

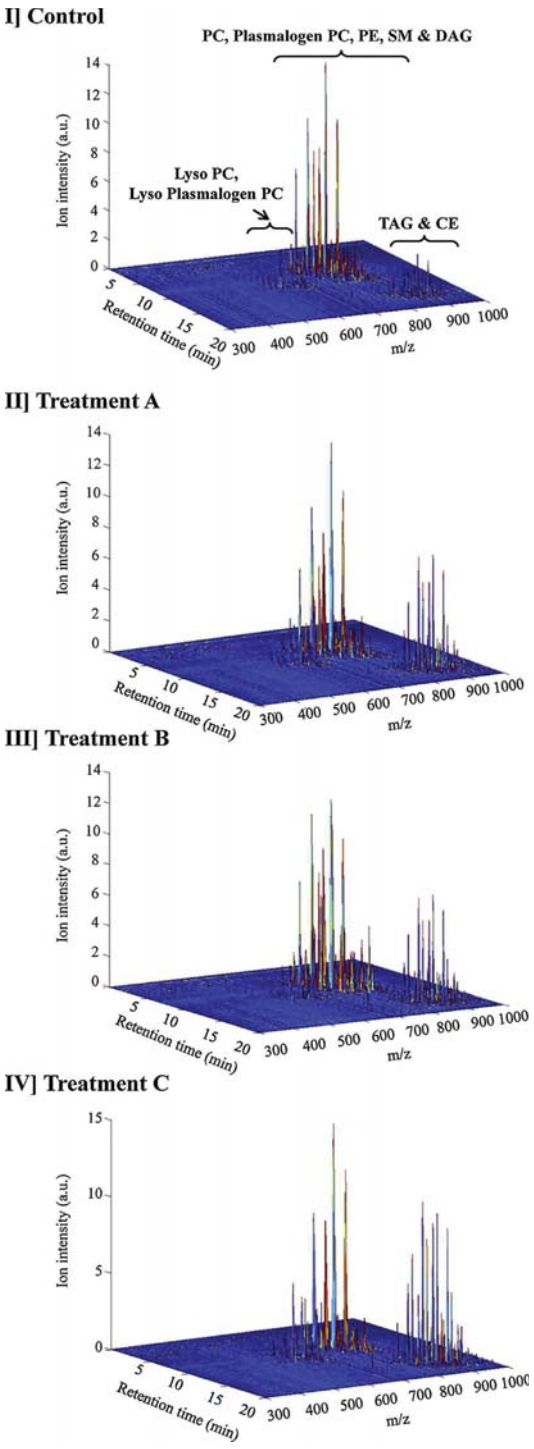

Fig. 3. Mesh plot of raw UHPLC–TOF-MS chromatograms corresponding to (I) control sample, (II) lipid sample from treatment A, (III) lipid sample from treatment B and (IV) lipid sample from treatment C.

The number of the estimated components, the number of resolved peaks in each region, the percentage of the variance explained in each case (see Eq. (3)) and the assigned numbers of the resolved peaks are summarized in Table 1. As it can be noticed, the number of estimated components was in all cases superior to the number of well resolved components with reliable chromatographic peak shape features, due to other possible signal contributions (such as background instrumental noise or solvent contributions). However, this small additional number of estimated components was required to better build and fit an adequate model where peaks corresponding to chemical compounds could be more properly resolved. Moreover, most of MCR-ALS analysis resulted in a percentage of lack of fit lower than 20% and in a percentage of explained variances higher than 96% with the exception of time window 5, with a lack of fit of 31.6% and an explained variance of 90%, possibly due to the low signal-to-noise ratio of that window, as observed in Fig. 2. Addition of extra components did not improve the results in any case.

The total number of MCR-ALS resolved components considering the 20 chromatographic time windows was 86.

4.3. First evaluation of raw LC–MS data and MCR-ALS results

Effects of treatments were first visible when raw UHPLC–TOF-MS chromatograms of distinct sample classes were compared. Fig. 3 is a mesh representation of four UHPLC–TOF-MS chromatograms corresponding to a control and 3 lipid samples exposed to the cell stress treatments A, B and C. Chromatographic separation of lipids was the same to the one achieved in a previous study [29], carried out in the same LC and MS conditions, and is shown in Fig. 3(I). The more significant change among control and stressed samples was observed in lipids eluting at the final minutes of the chromatogram, expected to correspond to families of diacylglycerols (DAG), triacylglycerols (TAG) and cholesterol esters (CE).

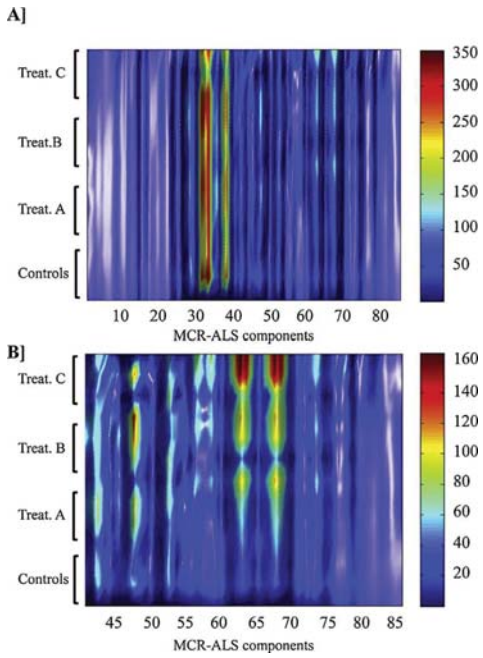

Fig. 4. Correlation map of sample type and components considering the calculated areas of MCR-ALS analysis. (A) For all the 86 resolved components and (B) For components 41–86.

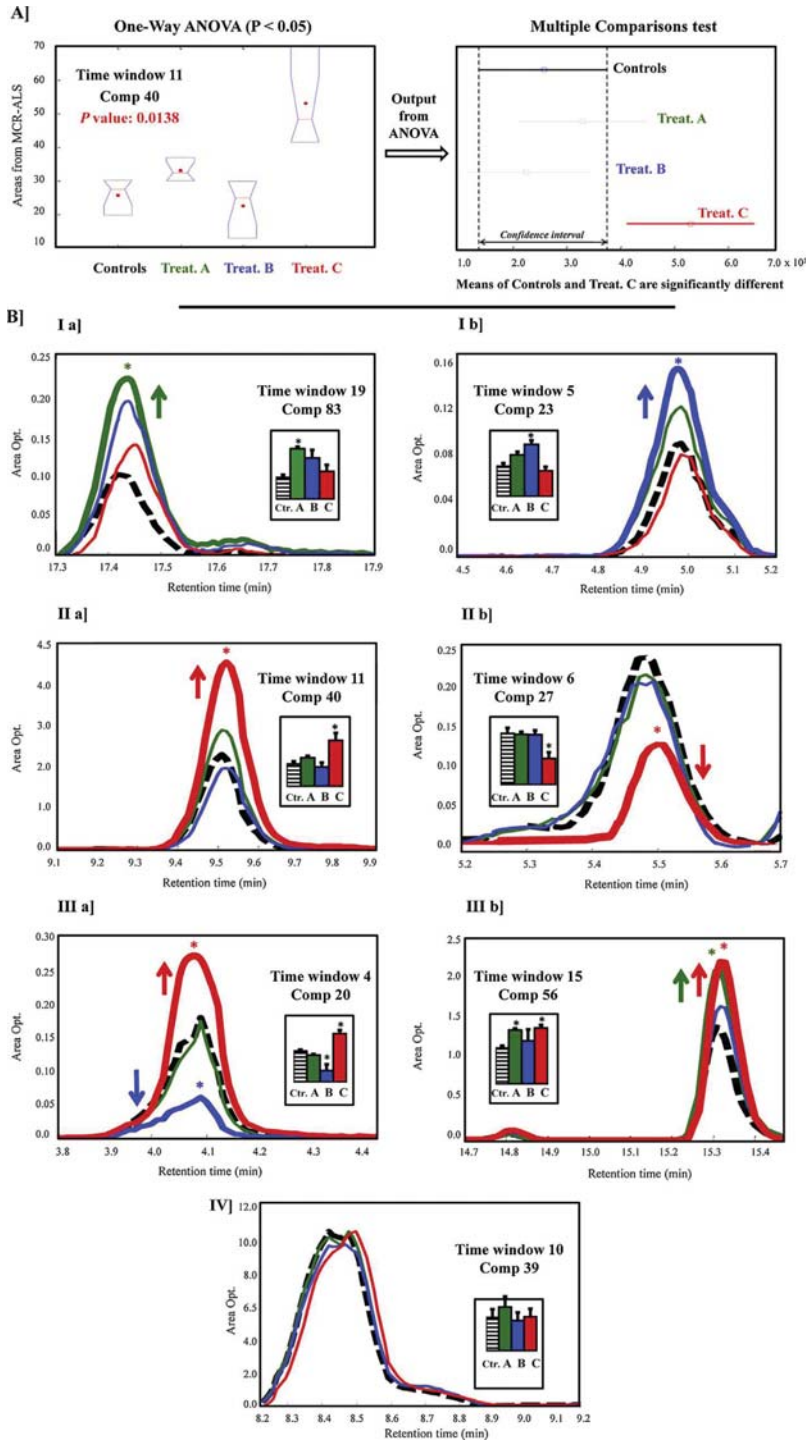

Fig. 5. (A) Example of results from one-way ANOVA followed by multiple comparisons test for component 40 of time window 11. (B) Elution/concentration profiles of 7 MCR-ALS resolved components (one per time window) as a representation of the distinct patterns of disruption observed: (I) effects of PFCs, (II) effects of TBT, (III) effects of both xenobiotics, (IV) no significant effects. Elution profiles are from mean areas of the three replicates from controls (_ _ _), cells exposed to PFCs at 0.6 μM ( ), cells exposed to PFCs at 6 μM ( ) and cells exposed to TBT (>). Thicker lines represent significant changing elution profiles. Bar graphics inside the boxes represent the means ± SEM ($n = 3$) of the controls and the three cell stress treatments. *Statistical significant differences respect to controls ($P < 0.05$).

Compared to the control (Fig. 3(I)), amount of these lipid species was superior in lipid samples from treatments A and B (Fig. 3(II and III)) and even higher in lipid sample from treatment C (Fig. 3(IV)).

Moreover, representation of the calculated areas of the 86 MCR-ALS resolved components for the distinct cell stress treatments allowed a detailed observation of the effects produced by the xenobiotics. Area values were stored in one data table containing the information of the 20 chromatographic time windows, conformed by a number of rows equal to the number of studied samples and a number of columns corresponding to all the MCR-ALS resolved components.

Correlations between cell stress treatments (A, B and C) and areas of the 86 MCR-ALS resolved components is shown in Fig. 4A and B. In both representations, intense red colors represent high correlations, so this means high amount of lipids produced by the treatments, whereas intense blue colors symbolize low correlations, so this means basal amount of lipids, as in controls. As shown in Fig. 4A, when the totality of variables were represented, no significant differentiation among control lipid samples and exposed lipid samples was noticeable. Thus, most of the correlation map was blue-colored, indicating a similar basal lipid abundance among samples, except for an intense red region between compounds 30 and 40. The high amount of those lipid species impeded the observation of the effects produced by the xenobiotics in the rest of compounds. Thus, when variables starting from 41 to 86 were only considered (Fig. 4B), the contrast in lipid abundance among different sample types became more evident, specially in compound 49 and in a major extent in compounds 63, 64, 68 and 69. Interestingly, the observed differences in the latter four compounds were higher in cells exposed to TBT (treatment C, up to 8-fold) whereas the exposure to the mixture of PFCs produced minor increase in lipid content (treatments A, B, approximately up to 5-fold). In contrast, no significant effects were noticed in the representation of variables 1 to 29. Thus, the preliminary study of raw LC–MS data and MCR-ALS results concluded that exposure to xenobiotics caused a change in the lipidome of JEG-3 cells, producing an increase in some lipid areas, mainly attributed to the presence of TBT (treatment C).

4.4. Comparison of elution profiles among treatments

Exhaustive study of the MCR-ALS results was necessary in order to draw significant conclusions of the disruption caused by the xenobiotics. Thus, effects of distinct cell stress treatments were thoroughly studied by a statistical comparison of the calculated areas of the 86 MCR-ALS resolved chromatographic peaks. One-way ANOVA was applied to these data followed by a multiple comparisons test (see Section 2.3). A rearrangement of the data output of MCR-ALS calculated areas was necessary previous to the ANOVA test. Thus, calculated areas of resolved MCR-ALS components, which were disposed in a matrix of size number of components × 12 samples, were further rearranged for every component in a 3 × 4 table disposition (sample replicates × sample classes). Fig. 5A represents an example of the one-way ANOVA and multcompare evaluation of component 40 of chromatographic window 11, in which it is shown that treatment C produces an increment respect to controls whereas no significant effects are derived from treatments A and B.

The one-way ANOVA and multcompare analysis of the 86 MCR-ALS resolved components evidenced that 23 of them showed significant differences ($P < 0.05$) respect to controls, indicating a disruption caused by the xenobiotics.

Detailed evaluation of those 23 components evidenced three distinct patterns of disruption. Fig. 5B (I–III) show elution profiles of 6 components, grouped in three classes, as an example of the three patterns of disruption observed within the 23 components. In contrast, in Fig. 5B IV is represented one component as an example of the 63 remaining components not showing significant differences in the one-way ANOVA and multcompare analysis. In each case, elution profiles represented with distinct colors correspond to mean area values of the three replicates of the four sample classes (treatment A, B and C and controls).

`First pattern of disruption explained significant effects produced by the mixture of the eight PFCs at both levels of concentration but no significant consequences derived from TBT exposure (Fig. 5B I). As observed in Fig. 5B (I a) and (I b), both doses of exposure of the mixture of PFCs, 0.6 and 6 μM, respectively, produced significant increments in lipid areas of exposed cells compared to controls. However, significant effects of the mixture of PFCs at the lower dose occurred in 3 components (8, 36 and 83) but only in compound 23 at the higher dose. Second pattern of disruption explained changes exclusively caused by the presence of TBT (Fig. 5B II). Exposure to the organotin compound caused an increase or a decrease in some lipid areas of exposed cells respect to controls. In 16 MCR-ALS resolved components (10, 11, 12, 40, 44, 57, 59, 63, 64, 65, 66, 68, 69, 71, 72 and 79), effects of TBT resulted in an increase in lipid areas and in only one case, compound 27, the effects ended in a decrease, Fig. 5B (II a and b), respectively. The third pattern of disruption explained few cases in which the effects produced in the lipidome of JEG-3 cells were attributed to the presence of both xenobiotics, the mixture of PFCs and TBT (Fig. 5B III). In compound 20, TBT produced and increase in the lipid area whereas the mixture of PFCs at 6 μM caused a decrease (Fig. 5B (III a)). In contrast, in compound 56, both TBT and the mixture

Table 2
Potential biomarkers for lipid disruption produced by three different treatments: (A) mixture of PFCs at 0.6 μM, (B) mixture of PFCs at 6 μM and (C) TBT at 0.1 μM. Results are shown for the two distinct approaches used, one-way ANOVA followed by a multiple comparisons test and a PLS-DA analysis for the extraction of variables important in projection (VIPs), fixing distinct VIP scores threshold values.

Biomarkers for lipidome disruption					
	ANOVA and multcompare test		PLS-DA		Combination of both strategies
Treatment	($P < 0.05$)	VIP scores > 1.5	VIP scores > 1.8	VIP scores > 2.0	(Considering VIP scores > 1.9)
A	8, 36, 56,83	8, 10, 13, 15, 16, 36, 56, 75, 76, 77, 82, 83, 84, 86	8, 10, 56, 76, 82, 83, 86	83, 86	8, 10, 36, 56, 76, 82, 83, 86
B	20[a], 23	8, 12, 14, 21, 23, 25, 28, 36, 40[a], 48, 49, 53	8, 12, 14, 21, 23, 25, 36, 49, 53	23, 36, 53	8, 12, 14, 20, 21, 23, 25, 36, 49, 53
C	10, 11, 12, 20, 27[a], 40, 44, 56, 57, 59, 63, 64, 65, 66, 68, 69, 71, 72, 79	7, 8, 10, 11, 12, 17, 20, 21, 27[a], 53, 56, 59, 64, 68, 69, 71, 72, 79	7, 10, 11, 17, 53, 56, 72, 79	10, 79	7, 10, 11, 12, 17, 20, 27, 40, 44, 53, 56, 57, 59, 63, 64, 65, 66, 68, 69, 71, 72, 79
Total(*)	23	39	21	7	33

(*)Total number of biomarkers count coincident components among treatments only one time.
Underlined components are common among the two preferred strategies.
[a] Diminution of peak areas respect to controls.

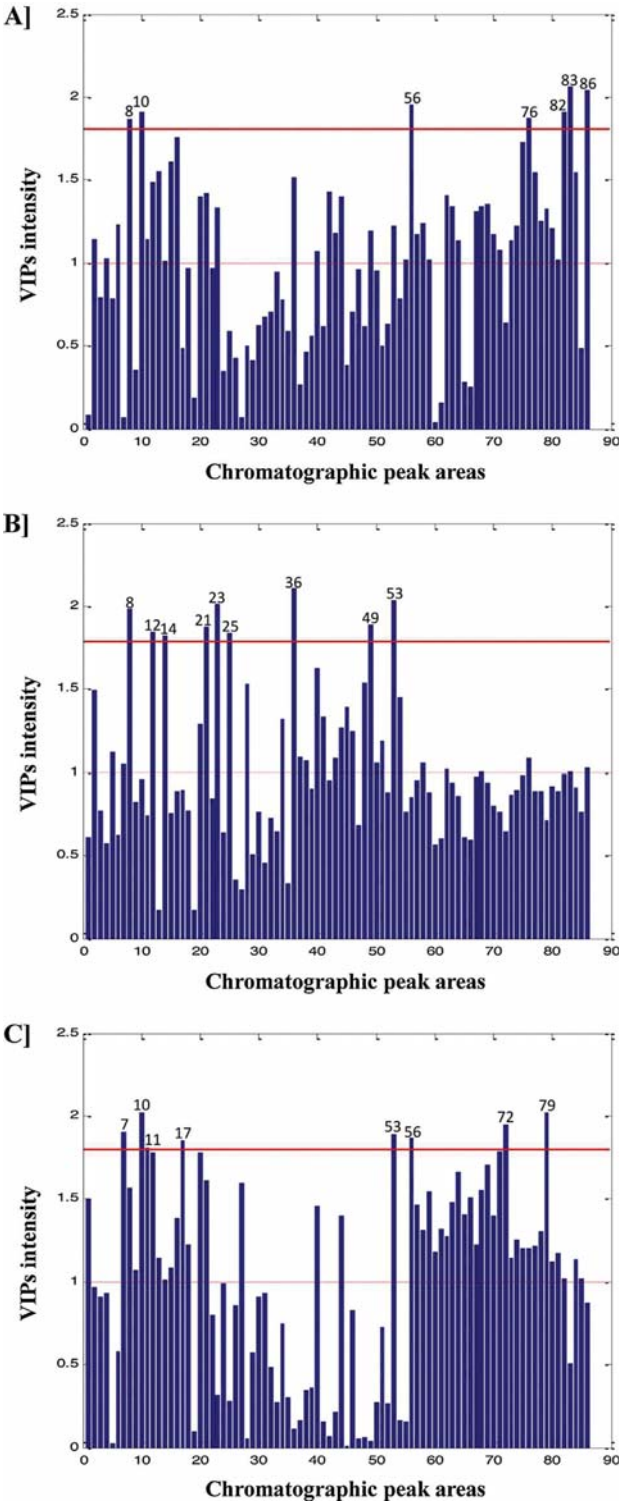

Fig. 6. Variables importance in projection (VIP scores) plot from PLS-DA analysis of the 86 MCR-ALS resolved peak areas, when selecting as groups: (A) controls and treatment A, (B) controls and treatment B and (C) controls and treatment C. Horitzontal red lines show threshold values of 1 (dotted line) and 1.8 (thicker solid line) and numbers inside the plot indicate most important variables according to the highest threshold value.(For interpretation of the references to color in this figure legend, the reader is referred to the web version of this article.)

Table 3
Tentative identification of 24 out of the 33 potential biomarkers calculated by mass accuracy within an error of 5 ppm, with atom constraints C, H, O, N ≥ 1, P ≥ 0 and with −0.5 ≤ DBE ≤ 15.0.

Peak number	MCR-ALS resolved mass (1 amu)	RT (min)	Measured mass (0.0001 amu)	Lipid specie	Elemental composition	Lipid class	Adduct	Calculated mass (Da)	Error (ppm)	DBE
14	511	3.5	510.3912	18:0	$C_{26}H_{57}NO_6P$	Lyso plasmalogen-PC	$[M+H]^+$	510.3918	−1.2	−0.5
23	674	5.0	673.5286	14:1	$C_{37}H_{74}N_2O_6P$	SM	$[M+H]^+$	673.5279	1.0	2.5
25	676	5.5	675.5435	14:0	$C_{37}H_{76}N_2O_6P$	SM	$[M+H]^+$	675.5436	−0.1	1.5
27	703	5.5	702.5069	30:2	$C_{38}H_{73}NO_8P$	PC	$[M+H]^+$	702.5068	0.1	3.5
36	719	7.8	718.5750	32:1	$C_{40}H_{81}NO_7P$	Plasmalogen-PC	$[M+H]^+$	718.5745	0.7	1.5
40	613	9.5	612.5588	34:1	$C_{37}H_{74}NO_5$	DAG	$[M+NH_4]^+$	612.5562	4.2	1.5
44	639	9.9	638.5723	36:2	$C_{39}H_{76}NO_5$	DAG	$[M+NH_4]^+$	638.5718	0.8	2.5
49	775	10.3	774.6365	36:1	$C_{44}H_{89}NO_7P$	Plasmalogen-PC	$[M+H]^+$	774.6371	−0.8	1.5
56	881	15.2–15.4	880.7170	44:4	$C_{52}H_{99}NO_7P$	Plasmalogen-PC	$[M+H]^+$	880.7159	1.2	4.5
57	821	15.0	820.7393	48:2	$C_{51}H_{98}NO_6$	TAG	$[M+NH_4]^+$	820.7389	0.5	3.5
59	847	15.2–15.4	846.7552	50:3	$C_{53}H_{100}NO_6$	TAG	$[M+NH_4]^+$	846.7545	0.8	4.5
63	849	15.6	848.7706	50:2	$C_{53}H_{102}NO_6$	TAG	$[M+NH_4]^+$	848.7702	0.5	3.5
64	875	15.8	874.7863	52:3	$C_{55}H_{104}NO_6$	TAG	$[M+NH_4]^+$	874.7858	0.6	4.5
65	923	15.6	922.7883	56:7	$C_{59}H_{104}NO_6$	TAG	$[M+NH_4]^+$	922.7858	2.7	8.5
66	949	15.7	948.8021	58:8	$C_{61}H_{106}NO_6$	TAG	$[M+NH_4]^+$	948.8015	0.6	9.5
68	877	16.2	876.8029	52:2	$C_{55}H_{106}NO_6$	TAG	$[M+NH_4]^+$	876.8015	1.6	3.5
69	903	16.4	902.8170	54:3	$C_{57}H_{108}NO_6$	TAG	$[M+NH_4]^+$	902.8171	−0.1	4.5
71	901	16.0–16.1	900.8021	54:4	$C_{57}H_{106}NO_6$	TAG	$[M+NH_4]^+$	900.8015	0.7	5.5
72	927	16.2–16.3	926.8185	56:5	$C_{59}H_{108}NO_6$	TAG	$[M+NH_4]^+$	926.8171	1.5	6.5
76	837	16.9	836.8062	50:1	$C_{53}H_{106}NO_5$	DAG	$[M+NH_4]^+$	836.8066	−0.5	1.5
79	955	16.8	954.8480	58:5	$C_{61}H_{112}NO_6$	TAG	$[M+NH_4]^+$	954.8484	−0.4	6.5
82	891	17.8	890.8508	54:2	$C_{57}H_{112}NO_5$	DAG	$[M+NH_4]^+$	890.8535	−3.0	2.5
83	915	17.4	914.8497	56:4	$C_{59}H_{112}NO_5$	DAG	$[M+NH_4]^+$	914.8535	−4.2	4.5
86	865	17.7	864.8375	52:1	$C_{55}H_{110}NO_5$	DAG	$[M+NH_4]^+$	864.8379	−0.5	1.5

DBE: double-bond equivalent.

of PFCs at 0.6 μM produced an increase in the lipid area (Fig. 5B (III b)).

Thus, among the distinct models of disruption, the more common was the one attributed exclusively to the presence of TBT, producing an increment in lipid areas, which occurred in 16 out of the 23 components (Fig. 5B (II a)). The second model with a higher contribution was the one linked to the effects of the mixture of PFCs at the lower dose (0.6 μM), also causing an increase in lipid areas, which was observed in 3 components (Fig. 5B (II a)). Finally, in all other cases, PFC effects at the higher dose, TBT effects producing a diminution in lipid areas and combined effects of both xenobiotics (Fig. 5B (I b), (II b) and III (a and b), respectively), disruption was only noticeable in one MCR-ALS resolved compound each. These results highlighted the important effect of treatment C in the increment of some lipid areas respect to controls and were in accordance to the observed in the first interpretation of raw LC–MS data and MCR-ALS results (see Section 4.3).

4.5. Determination of potential biomarkers for lipid disruption

Potential biomarkers for lipid disruption in JEG-3 cells were determined using two distinct strategies.

First, the same statistical approach used to study the differences produced in elution profiles was utilized. Thus, components showing significant differences in the one-way ANOVA analysis followed by multiple comparisons test were proposed as potential biomarkers.

As a second approach, a PLS-DA analysis was performed in order to obtain the variables importance in projection (VIP) scores [27,38,39], which were used to reveal which variables (lipid compounds) had a greatest influence on the discrimination among controls and exposed samples. VIP scores, defined by Wold et al. [38] as a weighted sum of squares of PLS weights described for each variable which measure the contribution of each predictor variable to the model, is frequently used as a parameter for variable selection [40–42].

For the PLS-DA analysis, calculated areas from all the MCR-ALS resolved components were compiled in a single data matrix which size was 12 × 86 (samples × components). This data matrix was used in three different approaches of classification, all of them considering two group classes; (a) controls and treatment A, (b) controls and treatment B and (c) controls and treatment C. Prior to PLS-DA model calculation, peak areas were autoscaled to give equal relevance to their possible change due to stressing conditions in control and exposed samples. No outlier samples were detected using leave-one-out cross-validation (small number of samples). Therefore, PLS-DA analysis was applied three times, considering one pair of classes each time, categorizing in class 0 control samples and in class 1 the different samples corresponding to the distinct cell stress treatments. In the three analysis, two components were selected to built the model, explaining a cumulative *Y*-variance of 97.66, 99.28 and 96.21%, respectively.

Table 2 shows a summary of the results obtained from one-way ANOVA followed by multiple comparisons test and the three PLS-DA models. For both approaches, biomarkers are indicated separately for the distinct cell stress treatments (A, B and C). With the one-way ANOVA–multiple comparisons test strategy, potential biomarkers where those within a statistical significance level of 5% ($P < 0.05$). The total number of identified biomarkers was 23. Comparison of these results with those of the PLS-DA analysis required a pre-adjustment of the VIP scores threshold value, despite the general criterion for variable selection has been

the "greater than one" rule [40]. As observed in Table 2, the number of potential biomarkers proposed by PLS-DA analysis was higher when reducing VIP scores threshold value. Total number of biomarkers was 39, 21 and 7 for threshold values higher than 1.5, 1.8 and 2, respectively. Thus, conditions at which both approaches resulted in similar number of biomarkers where the second ones, with the VIP scores threshold value higher than 1.8 units. Fig. 6 shows VIPs of the three PLS-DA analysis (A, B and C) for the selected threshold value of 1.8.

When comparing the results of one-way ANOVA–multiple comparisons test and PLS-DA analysis with VIP scores threshold value > 1.8, the number of coincident biomarkers was high (highlighted with a line mark in Table 2). For treatment A, 3 biomarkers coincided, corresponding to compounds 8, 56 and 83. For treatment B, compound 23 was coincident and for treatment C other five biomarkers were common (10, 11, 56, 72 and 79). The combination of the results of both approaches resulted in a total of 8, 10 and 22 biomarkers of lipid disruption for treatments A, B and C, respectively. The sum of these compounds produced a total of 40 biomarkers but since 7 of them were coincident among treatments, final number of biomarkers proposed by the combination of both strategies was 33 (Table 2).

Furthermore, the type of effects (upregulation or downregulation) explained by the biomarkers was separately studied for both approaches. In the first statistical approach, the study of the elution profiles revealed that in only 2 out of the 23 potential biomarkers the xenobiotics caused a diminution in lipid areas. For the rest of biomarkers, the disruption occurred in the inverse way, producing an increase in the area. In the PLS-DA analysis, weight loadings of the different components allowed the determination of the sign of the contribution. All the 21 biomarkers were indicators of an increase in lipid areas caused by the presence of xenobiotics. Only in compounds 40 and 27, potential biomarkers if considering VIP scores > 1.5, the effects were in the inverse way, i.e., decreasing their peak areas.

Thus, within the 33 biomarkers proposed by the combination of both strategies, only two were indicators of a diminution of lipid areas produced by the xenobiotics, whereas all the rest explained an increase. Interestingly, components 49, 63, 64, 68 and 69, observed as altered in the correlation map presented in the first evaluation of MCR-ALS results (see Section 4.3) were within the 33 proposed biomarkers.

These results reasserted that the predominant pattern produced by the presence of PFCs and TBT was an increment in the amount of lipids. Moreover, the higher amount of biomarkers of treatment C respect to treatments A and B highlighted the stronger disruption effects of TBT in comparison to PFCs.

4.6. Tentative identification of potential biomarkers

Information of pure mass spectra ($\mathbf{S^T}$) at 1 amu resolution of the 33 biomarkers was used to find out their exact mass (0.0001 amu resolution) when searching in the original raw full scan UHPLC–TOF-MS chromatograms. Isolated chromatographic peaks corresponding to the 33 unknown compounds were obtained when selecting their mass at low resolution in the raw chromatogram, with a permissible mass error of 0.5 Da. In each case, retention times were used to ensure the correspondence between the isolated chromatographic peaks in the raw chromatogram and their concentration profiles in the MCR-ALS analysis. Exact mass was finally obtained when looking at the spectra of the isolated peaks.

Tentative identification of biomarkers was based on the criteria of low mass error (difference among measurated and calculated mass) using the formula identification tool of Micromass MassLynx software called elemental composition search. The formula constraints were C, H, O ≥ 1, P ≥ 0 and N ≥ 1, following the nitrogen rule. The number of double-bond equivalents (DBEs) was set between −0.5 and 15.0. In addition, information of LC retention times and of a homemade database from a previous study was also used for positive identification (see Section 3.4).

A total number of 24 lipid species were tentatively identified out of the 33 potential biomarkers (Table 3). Identified lipid species included 2 sphingomyelin (SM), 1 phosphatidylcholine (PC), 3 plasmalogen PC, 1 lyso plasmalogen PC, 6 DAG and 11 TAG.

Annotation of lipid species in Table 3: PC and its derivatives with plasmalogens, DAG and TAG are annotated as <lipid subclass><total fatty acyl chain length>:<total number of unsaturated bonds> and SM as <total fatty acyl chain length>:< total number of unsaturated bonds in the acyl chain>.

4.7. Biological interpretation of the changing lipids

Tentative identification of 24 out of the 33 potential biomarkers showed that about 70% of the identified species corresponded to families of DAG and TAG. Moreover, as shown in Table 2, most of them were indicators of the disruption caused by the presence of TBT. These results were in accordance to a previous study [29], in which the effects of the same xenobiotics (PFCs at 0.6 and 6 μM and TBT at 0.1 μM) were evaluated in the same cellular line (JEG-3) but in a classical targeted approach. In that study, effects of TBT were also highly visible in families of TAG and DAG. Even more, 6 of the 24 potential biomarkers tentatively identified here (DAG 34:1, 36:2 and TAG 48:2, 50:3, 50:2, 52:3) also showed significant increments respect to controls in that study. These results confirm the ability of TBT to induce the synthesis of DAG and TAG in the placenta cell line, in agreement with the obesogenic effect reported for TBT in other organisms and cell lines [43,44]. TBT has been reported to induce differentiation of 3T3-L1 cells, increasing the formation of intracellular lipid droplets, mainly formed by TAG and DAG [45].

Apart from DAG and TAG species, other biomarkers tentatively identified corresponded to lyso plasmalogen PC 18:0, PC 30:2, SM 14:0 and 14:1 and plasmalogen-PCs 32:1, 36:1 and 44:4. As shown in Table 2, these biomarkers were indicators of lipid disruption caused by the three treatments. However, special relevance is posed in relation to the mixture of PFCs due to their previous reported effects on membrane lipids [28,46,47] such as plasmalogen-PC species, which has been confirmed in this work. Exposure to TBT and PFCs may promote lipid peroxidation in JEG-3 cells, which will damage cell membrane and stimulate lipid signaling pathways [48]. Although the functions of plasmalogens have not yet been fully elucidated, it has been demonstrated that they can protect mammalian cells against the damaging effects of ROS [49,50], facilitating signaling processes and protecting membrane lipids from oxidation. Thus, the observed increase in lyso plasmalogen and plasmalogen PC species may act as a defense mechanism against PFC and TBT induced oxidative stress.

5. Conclusions

The chemometric strategy proposed in this study based on MCR-ALS analysis of UHPLC–TOF-MS lipidomic data allowed the resolution of a large number of coeluted chromatographic peaks, the calculation of their respective peak areas and the resolution of their corresponding pure mass spectra. Changes in MCR-ALS chromatographic peak areas of the resolved lipid constituent among control and stressed cells were evaluated in order to find out potential biomarkers for lipid disruption. One-way ANOVA followed by a multiple comparisons test and a PLS-DA analysis were the selected strategies for biomarker selection. The combination of the results of both strategies gave rise to a total

of 33 lipids showing differences respect to controls. Identification of 24 out of the 33 potential biomarkers was positively achieved, using the resolved pure MS spectra from MCR-ALS analysis together with the high mass accuracy of the TOF analyzer.

The untargeted methodology proposed in this study noticeably simplifies the interpretation of the lipidome, exclusively focusing the attention on lipids showing important differences among normal and stressing conditions. Thus, the presented chemometric workflow appears as a powerful alternative to the time-demanding extensive screening of LC–MS data required for targeted lipidomics.

Acknowledgments

The research leading to these results has received funding from the European Research Councilunder the European Union's Seventh Framework Programme (FP/2007-2013)/ERC Grant Agreement no. 32073. First author acknowledges the Spanish Government (Ministerio de Educación, Cultura y Deporte) for a predoctoral FPU scholarship. Elisabet Pérez-Albaladejo is acknowledged for cell culture assistance and Dr. R. Chaler, D. Fanjul and Eva Dalmau are acknowledged for TOF-MS support.

References

[1] M. Oresic, V.A. Hänninen, A. Vidal-Puig, Lipidomics: a new window to biomedical frontiers, Trends Biotechnol. 26 (2008) 647–652.
[2] G. Van Meer, Cellular lipidomics, EMBO J. 24 (2005) 3159–3165.
[3] Y. Shi, P. Burn, Lipid metabolic enzymes: emerging drug targets for the treatment of obesity, Nat. Rev. Drug Discov. 3 (2004) 695–710.
[4] B. Blumberg, Obesogens, stem cells and the maternal programming of obesity, J. Dev. Orig. Health Dis. 2 (2011) 3–8.
[5] T. Stahl, D. Mattern, H. Brunn, Toxicology of perfluorinated compounds, Environ. Sci. Eur. 23–38 (2011) 1–52.
[6] T. Buhrke, A. Kibellus, A. Lampen, In vitro toxicological characterization of perfluorinated carboxylic acids with different carbon chain lengths, Toxicol. Lett. 218 (2013) 97–104.
[7] F.D. Gilliland, J.S. Mandel, Serum perfluorooctanoic acid and hepatic enzymes, lipoproteins, and cholesterol: a study of occupationally exposed men, Am. J. Ind. Med. 29 (1996) 560–568.
[8] J.W. Nelson, E.E. Hatch, T.F. Webster, Exposure to polyfluoroalkyl chemicals and cholesterol, body weight, and insulin resistance in the general U.S. population, Environ. Health Perspect. 118 (2010) 197–202.
[9] M.B. Khalil, W. Hou, H. Zhou, F. Elisma, L.A. Swayne, A.P. Blanchard, Z. Yao, S.A.L. Bennett, D. Figeys, Lipidomics era: accomplishments and challenges, Mass Spectrom. Rev. 29 (2009) 877–929.
[10] D. Piomelli, G. Astarita, R. Rapaka, A neuroscientist's guide to lipidomics, Nat. Rev. Neurosci. 8 (2007) 743–754.
[11] X. Han, R.W. Gross, Global analyses of cellular lipidomes directly from crude extracts of biological samples by ESI mass spectrometry: a bridge to lipidomics, J. Lipid. Res. 44 (2003) 1071–1079.
[12] F. Spener, M. Lagarde, A. Géloen, M. Record, Editorial: what is lipidomics? Eur. J. Lipid Sci. Technol. 105 (2003) 481–482.
[13] J.M. Castro-Perez, J. Kamphorst, J. Degroot, F. Lafeber, J. Goshawk, K. Yu, J.P. Shockor, R.J. Vreeken, T. Hankemeier, Comprehensive LC–MSE lipidomic analysis using a shotgun approach and its application to biomarker detection and identification in osteoarthritis patients, J. Proteome Res. 9 (2010) 2377–2389.
[14] L. Yetukuri, M. Katajamaa, G. Medina-Gomez, T. Seppänen-Laakso, A. Vidal-Puig, M. Oresic, Bioinformatics strategies for lipidomics analysis: characterization of obesity related hepatic steatosis, BMC Syst. Biol. 1 (2007) 12.
[15] M. Chadeau-Hyam, G. Campanella, T. Jombart, L. Bottolo, L. Portengen, P. Vineis, B. Liquet, R.C.H. Vermeulen, Deciphering the complex: methodological overview of statistical models to derive OMICS-based biomarkers, Environ. Mol. Mutagen. 54 (2013) 542–557.
[16] J. Boccard, D.N. Rutledge, A consensus orthogonal partial least squares discriminant analysis (OPLS-DA) strategy for multiblock Omics data fusion, Anal. Chim. Acta 769 (2013) 30–39.
[17] M. Farrés, B. Piña, R. Tauler, Chemometric evaluation of *Saccharomyces cerevisiae* metabolic profiles using LC–MS, Metabolomics (2014), doi:http://dx.doi.org/10.1007/s11306–014-0689-z.
[18] G.G. Siano, I. Sánchez Pérez, M.D. Gil García, M. Martínez Galera, H.C. Goicochea, Multivariate curve resolution modeling of liquid chromatography–mass spectrometry data in a comparative study of the different endogenous metabolites behaviour in two tomato cultivars treated with carbofuran pesticide, Talanta 85 (2011) 264–275.
[19] R. Tauler, Multivariate curve resolution applied to second order data, Chemom. Intell. Lab. Syst. 30 (1995) 133–146.
[20] A. de Juan, R. Tauler, Factor analysis of hyphenated chromatographic data. Exploration, resolution and quantification of multicomponent systems, J. Chromatogr. A 1158 (2007) 184–195.
[21] M. Barker, W.S. Rayens, Partial least squares for discrimination, J. Chemom. 17 (2003) 166–173.
[22] S. Wold, M. Sjöström, L. Eriksson, PLS-regression: a basic tool of chemometrics, Chemom. Intell. Lab. Syst. 58 (2001) 109–130.
[23] Y. Hochberg, A.C. Tamhane, Multiple Comparison Procedures, John Wiley & Sons, Hoboken, NJ, 1987.
[24] K. Godfrey, Comparing the means of several groups, N. Engl. J. Med. 311 (1985) 1450–1456.
[25] J.W. Tukey, Some thoughts on clinical trials, especially problems of multiplicity, Science 198 (1977) 679–684.
[26] G.E.P. Box, W.G. Hunter, J. Stuart Hunter, Statistics for Experimenters: An Introduction to Design, Data Analysis, and Model Building, John Wiley & Sons, 1978.
[27] D. Peña Sánchez de Rivera, Estadística. Modelos y métodos. 2. Modelos lineales y series temporales, Alianza Universidad Textos, 1989.
[28] E. Gorrochategui, E. Pérez-Albaladejo, J. Casas, S. Lacorte, C. Porte, Perfluorinated chemicals: differential toxicity, inhibition of aromatase activity and alteration of cellular lipids in human placental cells, Toxicol. Appl. Pharmacol. 277 (2014) 124–130.
[29] E. Gorrochategui, J. Casas, E. Pérez-Albaladejo, O. Jáuregui, C. Porte, S. Lacorte, Characterization of complex lipid mixtures in contaminant exposed JEG-3 cells using liquid chromatography and high-resolution mass spectrometry, Environ. Sci. Pollut. Res. (2014), doi:http://dx.doi.org/10.1007/s11356–014-3172–5.
[30] G.W. Olsen, F.D. Gilliland, M.M. Burlew, J.M. Burris, J.S. Mandel, J.H. Mandel, An epidemologic investigation of reproductive hormones in men with occupational exposure to perfluorooctanoic acid, J. Occup. Environ. Med. 40 (1998) 614–622.
[31] W.W. Christie, Rapid separation and quantification of lipid classes by high-performance liquid chromatography and mass (light-scattering) detection, J. Lipid Res. 26 (1985) 507–512.
[32] A. Garanto, N.A. Mandal, M. Egido-Gabás, G. Marfany, G. Fabriàs, R.E. Anderson, J. Casas, R. González-Duarte, Specific sphingolipid content decrease in Cerkl knockdown mouse retinas, Exp. Eye Res. 110 (2013) 96–106.
[33] J. Jaumot, R. Gargallo, A. de Juan, R. Tauler, A graphical user-friendly interface for MCR-ALS: a new tool for multivariate curve resolution in MATLAB, Chemom. Intell. Lab. Syst. 6 (2005) 101–110.
[34] G. Golub, K. Solna, P. Van Dooren, Computing the SVD of a general matrix product/quotient, SIAM J. Matrix Anal. Appl. 22 (2000) 1–19.
[35] D. Bu, C.W. Brown, Self-modeling mixture analysis by interactive principal component analysis, Appl. Spectrosc. 54 (2000) 1214–1221.
[36] R. Tauler, D. Barceló, Multivariate curve resolution applied to liquid chromatography–diode array detection, Trends Anal. Chem. 12 (1993) 319–327.
[37] R. Tauler, A. Smilde, B. Kowalski, Selectivity local rank, three-way data analysis and ambiguity in multivariate curve resolution, J. Chemom. 9 (1995) 31–58.
[38] PLS-Partial Least Squares Projections to Latent Structures, in: S. Wold, A. Johansson, M. Cochi (Eds.), ESCOM Science Publishers, Leiden, 1993.
[39] S. Wold, PLS for multivariate linear modeling, in: H. van de Waterbeemd (Ed.), QSAR: Chemometric Methods in Molecular Design, Methods and Principles in Medicinal Chemistry, vol. 2, Verlag Chemie, Weinheim, 1995, pp. 195–218.
[40] I.-G. Chong, C.-H. Jun, Performance of some variable selection methods when multicollinearity is present, Chemom. Intell. Lab. Syst. 78 (2005) 103–112.
[41] T. Rajalahti, R. Arneberg, A.C. Kroksveen, M. Berle, K.-M. Myhr, O.M. Kvalheim, Discriminating variable test and selectivity ratio plot: quantitative tools for interpretation and variable (biomarker) selection in complex spectral or chromatographic profiles, Anal. Chem. 81 (2009) 2581–2590.
[42] C.M. Andersen, R. Bro, Variable selection in regression–a tutorial, J. Chemom. 24 (2010) 728–737.
[43] G. Janer, J.C. Navarro, C. Porte, Exposure to TBT increases accumulation of lipids and alters fatty acid homeostasis in the ramshorn snail *Marisa cornuarietis*, Comp. Biochem. Physiol. C 146 (2007) 368–374.
[44] F. Grün, B. Blumberg, Environmental obesogens: organotins and endocrine disruption via nuclear receptor signaling, Endocrinology 147 (2006) S50–S55.
[45] A. Pereira-Fernandes, C. Vanparys, T.L.M. Hectors, L. Vergauwen, D. Knapen, P. G. Jorens, R. Blust, Unraveling the mode of action of an obesogen: mechanistic analysis of the model obesogen tributyltin in the 3T3-L1 cell line, Mol. Cell. Endocrinol. 370 (2013) 52–64.
[46] W. Xie, G. Ludewig, K. Wang, H.J. Lehmler, Model and cell membrane partitioning of perfluorooctanesulfonate is independent of the lipid chain length, Colloids Surf. B 76 (2010) 128–136.
[47] W. Xie, G.D. Bothun, H.J. Lehmler, Partitioning of perfluorooctanoate into phosphatidylcholine bilayers is chain length-independent, Chem. Phys. Lipids 163 (2010) 300–308.
[48] A. Higdon, A.R. Diers, J.Y. Oh, A. Landar, V.M. Darley-Usmar, Cell signaling by reactive lipid species: new concepts and molecular mechanisms, Biochem. J. 442 (2012) 453–464.
[49] B. Engelmann, C. Brautigam, J. Thiery, Plasmalogen phospholipids as potential protectors against lipid-peroxidation of low-density lipoproteins, Biochem. Biophys. Res. Commun. 204 (1994) 1235–1242.
[50] B. Engelman, Plasmalogens: targets for oxidants and major lipophilic antioxidants, Biochem. Soc. Trans. 32 (2004) 147–150.

3.2.4. SCIENTIFIC ARTICLE VII

Chemometric evaluation of glioma cell lipidome in response to proautophagic drugs

E. Gorrochategui, M. Casasampere, R. Tauler, J. Casas

Submitted for publication

Chemometric evaluation of glioma cell lipidome in response to proautophagic drugs

Eva Gorrochategui[1,§], Mireia Casasampere[2,§], Romà Tauler[1], Gemma Fabriàs[2], Josefina Casas[2,*]

[1]Department of Environmental Chemistry, Institute of Environmental Assessment and Water Research (IDAEA), Consejo Superior de Investigaciones Científicas (CSIC), Jordi Girona 18-26, Barcelona, 08034, Catalonia, Spain.

[2]Department of Biomedicinal Chemistry, Institute of Advanced Chemistry of Catalonia (IQAC), Consejo Superior de Investigaciones Científicas (CSIC), Jordi Girona 18-26, Barcelona, 08034, Catalonia, Spain.

[§]Both authors contributed equally
*Corresponding author: Prof. Josefina Casas Brugulat;
E-mail: fina.casas@cid.csic.es

ABSTRACT:

An untargeted lipidomic study was performed in the human glioblastoma T98G cell line exposed to non-lethal doses of celecoxib (CCX), phenoxodiol (PXD), resveratrol (RV), γ-tocotrienol (GTE) and XM462 proautophagic drugs for 24 h. The obtained lipid extracts from exposed and control samples were analysed by ultra-high liquid chromatography coupled to time-of-flight mass spectrometry (UHPLC-HRMS) and the generated data sets were further analysed using chemometric tools. Multivariate Curve Resolution-Alternating Least Squares (MCR-ALS) was used to resolve the elution and spectral profiles of the lipids present in the analysed samples. Lipid species with elution profiles (peak areas) showing more variations between exposed and control groups (*i.e.*, potential biomarkers) were initially estimated by PLS-DA followed by a t-student's test. A relative increase in dihydroshingolipids concentration levels was observed in exposed samples respect to e control samples, confirming the already reported inhibitory effect of the proautophagic drugs on dihydroceramide desaturase 1 (Des1). Moreover, it was also evidenced an increment in the amount of phospholipids, although with a relative decrease of their polyunsaturated species. Overall, the results suggest the capacity of CCX, PXD, RV, GTE and XM462 to inhibit Des1 and also fatty acid desaturases.

Keywords : lipidomics, celecoxib, phenoxodiol, resveratrol, γ-tocotrienol, XM462, chemometrics

1. Introduction

Every year thousands of drugs are synthesized and further consumed by human population. The benefits that these drugs provide to patients are numerous and diverse (*e.g.*, anti-cancer drugs, antibiotics, anti-depressants). However, the increasingly accessible low-cost pharmaceuticals and preventative medication to population leads to higher levels of drugs released in the environment[1]. In fact, environmental contamination by pharmaceuticals is reaching alarming levels nowadays and it is even set to rise. Moreover, some of the effects that these pharmaceuticals and drugs may pose on living organisms are still unknown. Therefore, examining the alterations that these chemicals may cause on organisms appears as a necessary task in environmental-risk assessment. Among the multiple effects that drugs can cause on organisms, the study of the generated alterations on lipid molecules is of crucial importance due to the fact that lipids are involved in most important biological processes. In this sense, the lipidomic assessment of the effects of these chemicals appears as a powerful approach.

Among the numerous drugs released in the environment, a group that is particularly interesting to study due to their reported effects in the inhibition of dihydroceramide desaturase 1 (Des1) is the one of proautophagic drugs, such as celecoxib (CCX), phenoxodiol (PXD), resveratrol (RV), γ-tocotrienol (GTE) and XM462. The chemical structures of these five proatophagic drugs are represented in **Figure S1**. CCX, also commercially named "Celebrex", among others, is a nonsteroidal anti-inflammatory drug (NSAID), specifically inhibitor of the cyclooxygenase isozyme (COX-2), which relieves pain and swelling (inflammation). Celecoxib is used to treat arthritis, acute pain, and menstrual pain and discomfort. The common dose of celecoxib in adult patients varies between 100 and 200 mg once or twice per day. The principal effect of this drug is related with its chemopreventive activity against colon carcinogenesis. Some studies assessing the alterations that this anti-inflamatory drug may pose on lipids are found in the literature. For instance, a study of Mazaleuskaya L.L. *et al*.[2] evaluated the effects of celecoxib in the bioactive eicosanoid lipidome of human blood samples previously exposed to the chemical. On the other hand, phenoxodiol is a synthetic derivative of the naturally occurring plant isoflavone. Some studies have demonstrated the ability of phenoxodiol as a potential future treatment for both hormone sensitive and hormone refractory prostate cancer and also in ovarian cancer. M. Kamsteeg *et al*.[3] showed that phenoxodiol induced apoptosis in ovarian cancer cells by regulating FLICE inhibitory protein (FLIP) and X-linked inhibitor of apoptosis (XIAP). Lately, S. Mahoney *et al*. discovered the ability of phenoxodiol in prostate cancer cells to induce significant cytotoxicity in cells by interacting with p21WAF-1 and inducing cell cycle arrest irrespective of p53 status or caspase pathway interactions[4]. Resveratrol is phytoalexin found in the skin of red grapes, and also in peanuts and berries which is part of a group of compounds called polyphenols. Resveratrol is mainly used for its anti-aging and disease-fighting powers. In particular, most common application is to reduce the lower LDL or "bad" cholesterol, and to make it more difficult for clots to form that can lead to a heart attack. Also, reveratrol helps prevent insulin resistance, which can lead to diabetes. Concerning the effects of resveratrol, some studies demonstrate that this drug activates the SIRT1 gene, which is believed to protect the body against the effects of obesity and the diseases of aging. Also, this drug has shown to present chemopreventive activity. A study of M. Jang *et al*.[4] showed that Resveratrol act as an antioxidant and antimutagen and also induce phase II drug-metabolizing enzymes (anti-initiation activity). In addition, the same authors found that it inhibited the development of preneoplastic lesions in carcinogen-treated mouse mammary glands in culture and inhibited tumorigenesis in a mouse skin cancer model. ɣ-Tocotrienol (or gamma- Tocotrienol) is one of the four types of tocotrienol, a type of vitamin E. Gamma-tocotrienols have been shown to have anticancer effects against a wide range of human cancers. A study oThef S.U. Luk *et al*.[5] reported that treatment with this drug not only inhibits prostate cancer cell invasion but also sensitizes the cells to docetaxel-induced apoptosis, suggesting gamma-tocotrienol as an effective therapeutic agent against advanced stage prostate cancer.

Liquid chromatography coupled to mass spectrometry (LC-MS) methods are highly used in lipidomic procedures since they enable proper analysis of low molecular weight compounds in biological systems, such as complex lipid mixtures or biomolecules[6]. The generated LC-MS data from each chromatogram are arranged in data sets containing information of mass-to-charge (*m/z*), retention times and intensities. Hence, massive amounts of information-rich MS data are obtained in the analysis of every sample, thus requiring specific tools for their analysis and interpretation. Among them, the chemometric tool named Multivariate Curve Resolution-Alternating Least Squares (MCR-ALS)[7], has shown to successfully resolve extensive LC-MS data sets with strongly co-eluted and hidden peaks in recent metabolomic (and lipidomic) studies[8-12]. In addition, other chemometric

tools such as principal component analysis (PCA) and partial least squares-discriminant analysis (PLS-DA) can further explore sample classification/discrimination and allow biomarker discovery[13]. The hypothesis postulated in this work proposes that exposure to dihydroceramide desaturase 1 (Des1) inhibitors also influences the desaturation of other lipid species apart from the well-known effect on dihydroceramides (dhCer). The aim of this study was to elucidate the effect of some Des1 inhibitors such as CCX, PXD, RV, GTE and XM462 in the lipidomic metabolism produced in T98G glioblastoma cell line, using MCR-ALS resolved profiles.

2. Materials and methods

LC-MS analysis

LC-HRMS analysis was performed using an Acquity ultra-high performance liquid chromatography (UHPLC) system (Waters, USA) connected to a Time of Flight (LCT Premier XE) Detector with an Acquity UHPLC BEH C_8 column (1.7 µm particle size, 100 mm x 2.1 mm, Waters, Ireland) at a flow rate of 0.3 mL/min and column temperature of 30 ºC. Full scan spectra from 50 to 1800 Da were acquired, and individual spectra were summed to produce data points each of 0.2 sec. Mass accuracy at a resolving power of 10,000 and reproducibility were maintained by using an independent reference spray *via* the LockSpray interference. The mobile phases were methanol with 2 mM ammonium formiate and 0.2% formic acid (A)/ water with 2 mM ammonium formiate and 0.2% formic acid (B). Phosphatidylcholine (PC), plasmalogen PC, lyso plasmalogen PC, phosphatidylethanolamine (PE), phosphatidylglycerol (PG), triacyl glycerol (TAG), sphingomyelin (SM), dihydrosphingomielin (dhSM), dhCer, lactosylceramide (LacCer), lactosyldihydroceramide (LacdhCer) glucodihydroceramide (GlcdhCer) and sterol lipids (colic acid and cholesterol sulphate) were analysed under positive ESI.

Chemicals and reagents

Dulbecco's Modified Eagle Medium, fetal bovine serum, penicillin/streptomycin, Trypsin-EDTA, RV were purchased from Sigma Aldrich. CCX was purchased from Selleckchem. PXD was a kind gift of Marshall Edwards Pty Ltd. (New South Wales, Australia). GTE was purchased from Cayman Chemical Company. XM462[15] was synthesized in our laboratories. Internal standards for lipidomics were purchased from Avanti Polar Lipids.

Cell culture

Human glioblastoma cell line T98G was cultured at 37 °C in 5% CO_2 in Dulbecco's Modified Eagle Medium supplemented with 10% fetal bovine serum and 100 ng/mL each of penicillin and streptomycin.

Cell treatment and lipid extraction

Cells were seeded at $1x10^5$ cells/mL into 6 well plates (1 mL/well) and allowed to adhere for 24 h in complete medium. Medium was replaced with fresh medium containing CCX (50 µM), PXD (50 µM), RV (100 µM), GTE (35 µM) and XM462 (100 µM) from stock solutions in ethanol at the specified concentrations or EtOH as control. After 24 h, medium was removed; cells were washed with 400 µL PBS and harvested with 400 µL Trypsin-EDTA and 600 µL of complete medium. Sphingolipid extracts, fortified with internal standard (C12-sphingosine, C12-glucosylsphingosine, C12-sphingosylphosphorylcoline and C17-sphinganine, 0.2 nmol each) were prepared and analysed by UHPLC-TOF-MS as previously explained. Six replicates were generated per group, except for CCX and GTE treatments, which contained three and four replicates, respectively. Thus, the current data set included a total of 31 samples, which were pairwise-analysed so that for each treatment the samples (stressed samples) were compared to the control (ethanol as vehicle control).

Peak assignment and identification of lipids

For the identification of the potential biomarkers (*i.e.*, components showing significant differences in control *vs* stressed samples), both a home-made database of lipids built previously[11] using the same chromatographic conditions, and also external databases available on-line such as LipidMaps (http://www.lipidmaps.org) were used. The assigned compound corresponded to the lipid molecule with the minimum mass error value (≤ 10 ppm) respect to the measured *m/z*, considering the possible adducts in positive ionization mode. The lipid annotated also had to fulfill an adequate retention time regarding its polarity. Glycerophospholipids, TAG and DAG species were annotated as <lipid subclass> <total fatty acyl chain length>:<total number of unsaturated bonds> and sphingolipids <total fatty acyl chain length>:<total number of unsaturated bonds in the acyl chain>.

Chemometric analysis of LC-HRMS data

For data analysis, first step was the conversion of the original

UHPLC-HRMS chromatographic run recorded for every sample in a NetCDF file, which was further imported into MATLAB environment. Next, data were loaded into MATLAB workspace and converted to data matrices, with the retention times in the row dimension and the *m/z* values in the column dimension. While constructing these matrices, the size of the original data was simultaneously reduced using in-house written routines which search for the regions of interest (ROI) and construct compressed data matrices containing relevant LC-HRMS features[15], with no loss of spectral mass accuracy. In a further step, five column-wise augmented data matrices containing information of two sample groups each were constructed. Then, the generated augmented matrices were analysed by MCR-ALS[8] in order to resolve co-eluted elution profiles and hidden peaks of the different sample constituents (lipids), together with their corresponding mass spectra. Constraints used in MCR-ALS were non-negativity of elution and spectra profiles. In these analyses, the relative areas of the resolved elution profiles for each of the components in the different sample groups (control and stressed) were also obtained. In order to explore potential biomarkers, the peak areas of the elution profiles of the MCR-ALS resolved components were evaluated using two approaches. First, one PLS-DA model was performed, comparing the control group against all the stressed samples grouped together. Then five more PLS-DA analysis were performed, one for each of the five treatments with the proautophagic drugs (CCX, PXD, RV, GTE and XM462) and MCR-ALS resolved augmented data matrices containing information of the areas of the resolved peaks. The determination of the components (*i.e.*, lipids) showing significant differences was possible by selecting those variables importance in projection (VIP) with a score value higher than one. The second approach was to statistically corroborate the previously found potential biomarkers, by using a two-sample Student's *t*-Test ($P < 0.05$). Changes in lipid areas among the distinct sample classes were visualized by performing five hierarchical cluster analyses (HCA) together with their headmapping display[16] and a Venn diagram, which also allowed examining lipid species showing similar behaviour amongst chemical exposure.

Software for LC-MS data analysis

MATLAB 8.6.0 R2015a and R2015b (The MathWorks, Inc., Natick, MA, USA) were used as the development platforms for LC-MS data analysis and visualization. A graphical interface was used to apply MCR-ALS, which additionally provided detailed information about the implementation of this algorithm. Statistics Toolbox™ for MATLAB, PLS Toolbox 7.3.1 (Eigenvector Research Inc., Wenatchee, WA, USA), Bioinformatics Toolbox™ and other homemade routines[15] were used in this work. Waters/Micromass MassLynx™ V 4.1 software was used for data set conversion from raw into NetCDF format and as one of the formula identification platforms through its elemental composition tool.

3. Results

First evaluation of control and stressed LC-MS lipid profiles

The UHPLC-TOF-MS chromatogram information allowed the classification of the families of lipids according to their retention time. As occurred in a previous study carried out under the same LC and MS conditions[10], lipids corresponding to the families of lyso PC and lyso plasmalogen PC were the first to elute from the chromatographic column. Later, the eluted lipids were PC, plasmalogen PC, PE, plasmalogen PE, PG, Cer, LacCer, dhCer, SM, dhSM, GlcdhCer, LacdhCer and DAG species. Finally, the last lipid species to leave the chromatographic column were TAG. **Figure 1** is a representation of the generated data matrices in MATLAB environment corresponding to the LC-MS lipid profiles of a control sample (see **Figure 1A**) and five stressed samples belonging to the treatments with CCX, PXD, RV, GTE and XM462 (**Figures 1B to 1F**, respectively).

In a first exploratory analysis, the UHPLC-TOF-MS chromatograms of the distinct sample classes were compared. In broad terms, some differences were evidenced when comparing LC-MS profiles of control *vs* exposed samples, being such differences especially noticeable in the lipids eluting at the central region of the chromatogram. However, a deeper study of the LC-MS lipid profiles is needed in order to draw significant conclusions of the potential effects of the proautophagic drugs on the lipidome of T98G cells. First step in that direction was the resolution of LC-MS lipid profiles by MCR-ALS analysis.

MCR-ALS results

From the matrices generated on the basis of UHPLC-TOF-MS chromatograms, new augmented matrices were generated containing information of two group of samples each (control and treated). Specifically, five augmented matrices were generated containing information of controls

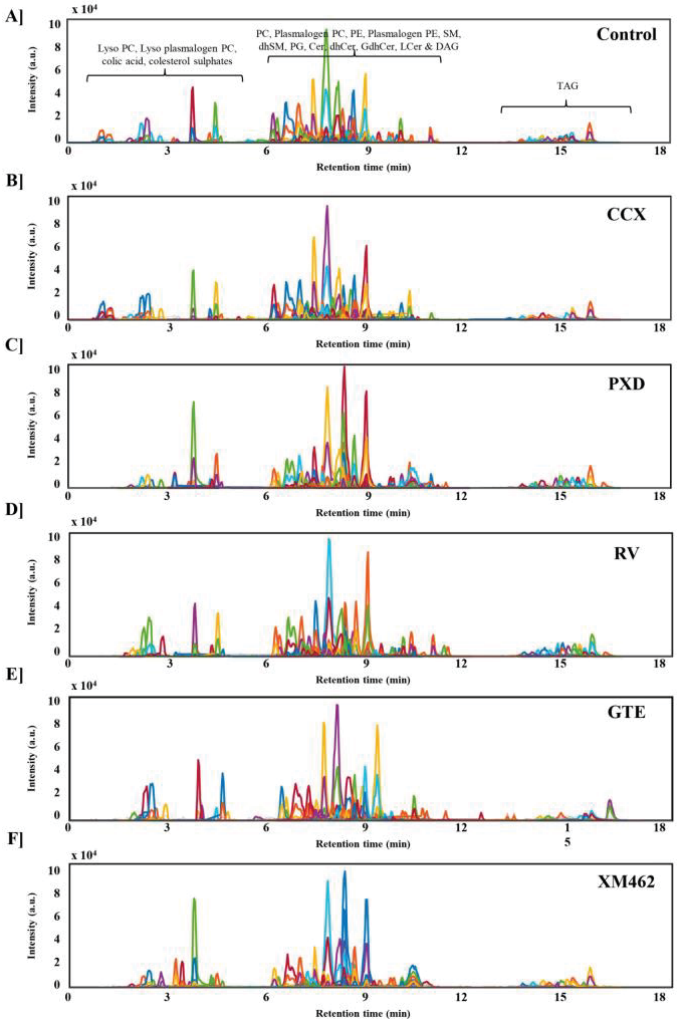

Figure 1. LC-MS profiles obtained after raw data import into MATLAB environment followed by ROI compression and data matrix construction of A) control sample, B) CCX-stressed sample, C) PXD-stressed sample, D) RV-stressed sample, E) GTE-stressed sample and F) XM462-stressed sample.

and CCX, controls and PXD, controls and RV, control and GTE, and controls and XM462; arranging samples one by one, at the top of the other (sample x elution time, *m/z* values) (**see Figure S2**). MCR-ALS allows the resolution of multiple co-eluted chromatographic peaks generated during LC-MS analysis of complex lipid mixtures such as a cell lysate. Moreover, it allows for the evaluation of possible treatment effects in the lipidome of cells by implementing the analysis through the different sample groups (*e.g.*, controls *vs* exposed) simultaneously. For this reason the information extracted from LC-MS data was directly analysed by MCR-ALS in order to resolve the elution and spectra profiles of each of the components (lipids) present in samples (including those coeluting at very similar retention times and other related to solvent, background and spurious instrumental contributions with no chemical meaning). Results of MCR-ALS on the five data sets (*i.e.*, controls and CCX, controls and PXD, controls and RV, controls and GTE and controls and XM462), 150, 120, 120, 100 and 95 components were respectively resolved, each one describing a pure elution and mass spectra profile, and a 98.7, 99.1, 99.0, 98.7 and 98.8% of the total data variance was respectively explained (see **Figure S3**). The elution profiles of the resolved MCR-ALS components in the distinct models were further examined to select those that described reliable chromatographic peak features and filter out the ones explaining background instrumental noise or solvent contribution. Thus, the final number of relevant components of the distinct MCR-ALS models resulted in 105, 82, 80, 65 and 69 for the data sets of CCX, PXD, RV, GTE and XM462, respectively.

Identification of lipid species

In order to identify the corresponding lipid species, the exact mass obtained in the MCR-ALS spectra profiles was used. Using the information of exact mass contained in MCR-ALS resolved spectra profiles the lipid species were successfully identified. Their relative areas were next used to evaluate their relative amounts in each treated sample respect to controls. In this study, 21 PC, 9 plasmalogen PC, 2 lyso PC, 1 lyso plasmalogen PC, 2 PE, 3 plasmalogen PE, 2 PG, 9 TAG, 4 SM, 2 dhSM, 2 dhCer, 2 LacCer, 1 LacdhCer, 1 GlcdhCer lipid, colic acid and cholesterol sulfate species were identified (**Table S2**).

It is worth pointing out that it was possible to identify the presence of some of the metabolites of compounds tested (see **Table S3**). In the samples incubated with GTE, two MCR-ALS components were found, the first describing the GTE monomer and the other corresponding to the GTE dimer. In XM462-stressed samples, XM462 compound itself was detected and also other molecules resulting from its metabolism, such as the oxidation product (O-XM462) and its glycosylation form (GlcXM462). The other compounds tested (*i.e.* CCX, RV and PXD) were not detected since they are expected to elute in the first minute of the chromatogram and would be expected to appear in the chromatographic front (data not analysed). These results illustrate and confirm the adequacy of the proposed approach.

Comparison of MCR-ALS elution and spectra profiles among treatments

In order to draw significant conclusions of the effects caused by the treatments, a comprehensive study of the MCR-ALS results was performed. The elution profiles were compared against sample classes in order to elucidate the possible effects of the different cell treatments. As it can be observed, this is highly useful to evaluate the differences produced in the elution profiles of stressed samples respect to controls. Among the distinct MCR-ALS resolved components corresponding to reliable chromatographic peaks, there was a group of them which presented a significant behaviour. **Figure 2** shows the elution (see **Figures 2A**) and spectra profiles (see **Figures 2B**) of some

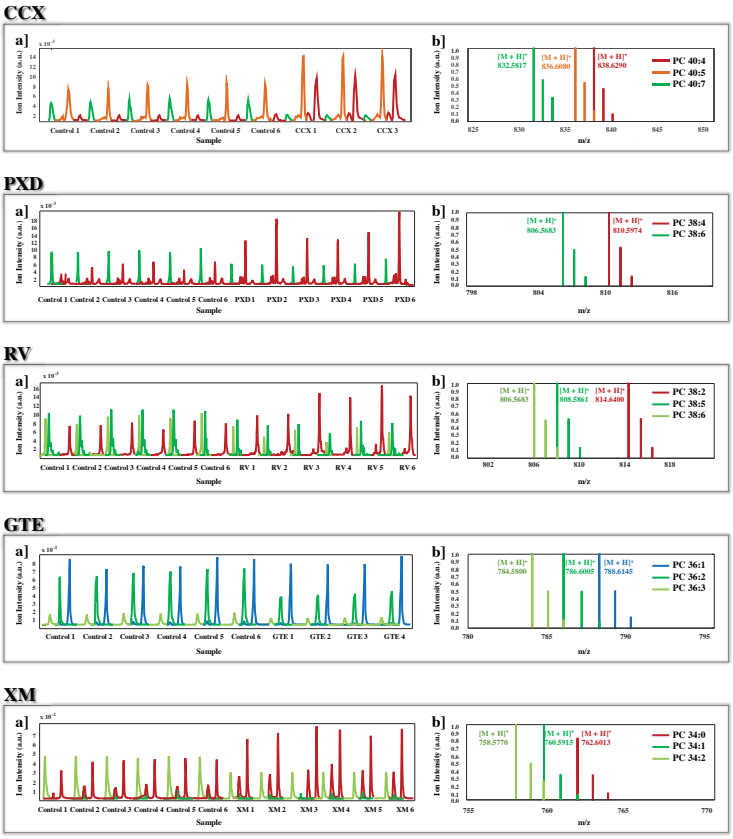

Figure 2. MCR-ALS elution (a) and spectra (b) profiles of some phosphatidylcoline lipid species presenting up-regulation (orange, red), down-regulation (light and dark green) or non-variance (blue) after exposure to CCX, PXD, RV, GTE and XM462. Numbers in the figure correspond to the distinct replicates.

of these lipid species, in concrete distinct PC species. As expected, the findings corroborated the initial hypothesis, since all treatments seemed to block the desaturation of the PC. Thus, treatments produced a decrease in the unsaturated species while an increase or no-change in saturated species in stressed-samples, compared to the control samples. Treatment with CCX, showed a noted increase in PC 40:4, a moderated increase in PC 40:5 and a clear reduction in PC 40:7. PXD also showed the same pattern, increasing the levels of PC 38:4 and decreasing PC 38:6. The same behaviour was observed with RV, in that case the amount of PC 38:2 increased whereas PC 38:5 and PC 38:6 species decreased. However, saturated species did not increase due to desaturation blockade after GTE treatment, since PC 36:1 levels did not vary after treatment, whereas lower levels of PC 36:2 and PC 36:3 were observed. Finally, with XM462 treatment, the amount of PC 34:0 specie raised, while lower levels of PC 34:1 and PC 34:2 were detected. The effects of treatments were not only produced on PC species but also in other lipid families. As mentioned earlier, it is well known that CCX, PXD, RV, GTE and XM462 are inhibitors of the sphingolipid metabolism enzyme Des1. As expected, among the lipids altered by the treatments, sphingolipids were also modified. In particular, an increase in the levels of dihydrosphingolipids (*e.g.* dhCer) and/or a decrease of unsaturated sphingolipids (*e.g.* SM) were detected which confirms their effect on Des1. In the case of TAG metabolism, it was differently affected by the treatments: an exposure to PXD and RV caused an increase in TAG species, both saturated and unsaturated, whereas the treatment with CCX and GTE caused a decrease in the amount of TAG species.

Statistical comparison of elution profiles

Effects of the distinct cell treatments were thoroughly studied by a statistical comparison of the calculated areas of the MCR-ALS resolved chromatographic peaks. Two distinct strategies were used to find components showing significant differences in treated samples compared to controls. PLS-DA is generally performed in order to sharpen the separation between two groups of classes: control and all the treatments. In **Figure 3** the scores of the PLS-DA analysis are represented. Thus, if a sample is represented in the region of the space corresponding to a particular category, it is classified as belonging to that category. Apart from this PLS-DA model considering all treatments simultaneously as a class, five other PLS-DA analyses were performed, considering the same control and one different treatment each time **(see Figure S4)**. All treatments used the same approach of classification, considering two classes and the control samples were clearly distinguished from the stressed samples. PLS-DA analysis was also performed for the purpose of obtaining the variables importance in projection (VIP) scores, which were used to reveal which lipids had a greatest influence on the discrimination between controls and treated samples. Following the general criteria for variable selection, the threshold value was set on one[17]. Consequently, the lipids selected as potential biomarkers were those that were associated with a VIP score greater than one (see **Figure S5**). As a second approach, a two-sample Student's *t*-Test (P<0.05) was performed to corroborate the biomarker selection performed when using the PLS-DA approach. Finally, only those lipid species showing significant alterations in both approaches (VIPs from PLS-DA and Student's *t*-Test) were proposed as potential biomarkers. As it can be observed in **Table S1**, the total number of biomarkers for the different proautophagic ompounds were 34 (CCX and PXD), 33 (RV), 28 (GTE) and 17 (XM462).

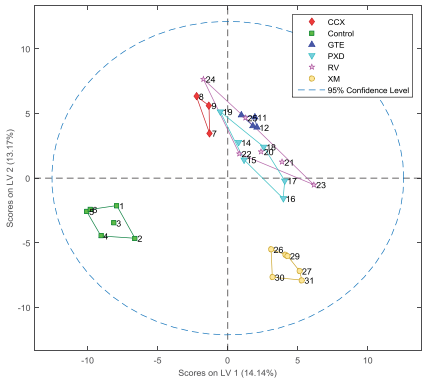

Figure 3. Scores plot of the PLS-DA model performed with the MCR-ALS resolved areas of the augmented data matrix containing information of control (class one) and all the stressed samples (class two).

Representation of significant lipids among treatments

Once the potential biomarkers for lipid disruption were elucidated through chemometric and statistical analyses, the results were evaluated using hierarchical cluster analysis (HCA) and they were represented in a heatmap (see **Figure 4**). This tool allows grouping lipid species that present similar behaviour and thereby provides a visual representation of lipid changes among the distinct sample treatments. As it can be seen in **Figure 4**, in all treatments, the lipid species were organized in two groups. In all cases an opposite pattern of lipid distribution was observed between control and treated samples, being the lipids up-regulated in one group while down-regulated in the other, or vice versa. In any case, the amount of lipid species was similar in control and treated samples.

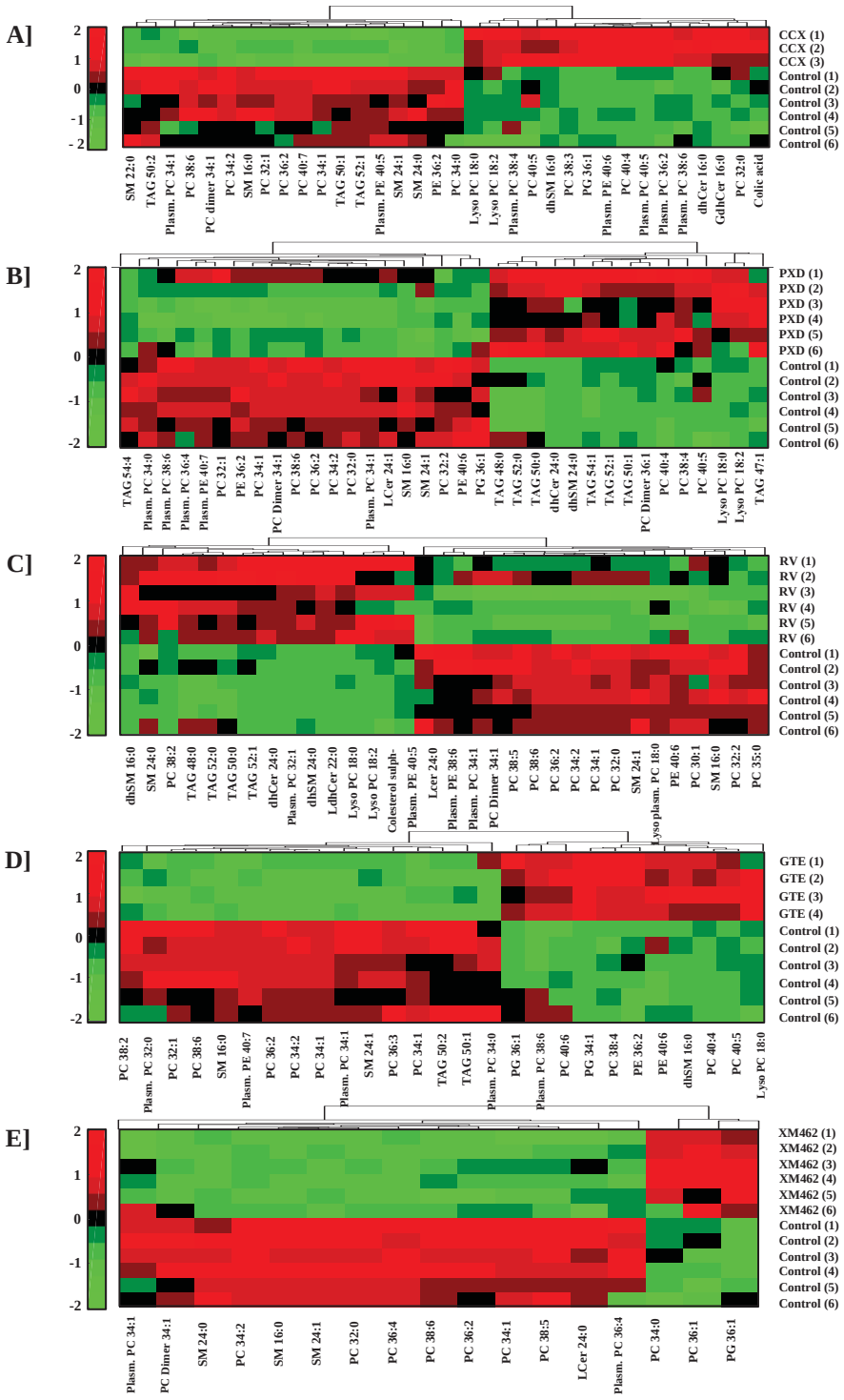

Figure 4. Hierarchical clustering heatmaps of the peak areas of the identified lipid species in T98MG cells (autoescaled data) exposed to A) CCX, B) PXD, C) RV, D) GTE and E) XM462. Degree of change in the stressed groups compared with the control group is marked with colours inside the heatmap indicating up-regulation (red) and down-regulation (green), as indicated by the colour bars. Identified lipids are represented in the horizontal axis, and sample groups in the vertical axis. (1 to 6: replicate number). Numbers in the figure correspond to the distinct replicates.

Subsequently, a Venn diagram was also constructed (see **Figure 5**). A Venn diagram consists of multiple overlapping circles; each representing a group of the different stressed samples. It represents the relations between the lipid biomarkers found for the different treatments. As it can be observed in the central overlapped region of the diagram, 7 lipid species were simultaneously affected by the five drugs. Moreover, the extremes of the diagram indicated the number of lipid species that significantly varied specifically for each single treatment respect to controls. Therefore, CCX (blue extreme) was the treatment producing more specific alterations with 10 potential biomarkers, followed by RV (brown extreme) with 7 biomarkers, then GTE (yellow extreme) and PXD (red extreme), both providing 6 biomarkers and XM462 (green extreme), just contributing with 2 biomarkers for lipid disruption. In **Table 1**, the lipid species corresponding to these potential biomarkers are mentioned. As it is observed in the Table, the potential biomarkers associated to treatments with CCX, PXD and RV all contained sphingolipid species, indicating the capacity of these drugs to inhibit Des1. Contrarily, the biomarkers of GTE and XM462 treatments did not include any sphingolipid specie and mostly included phospholipid species.

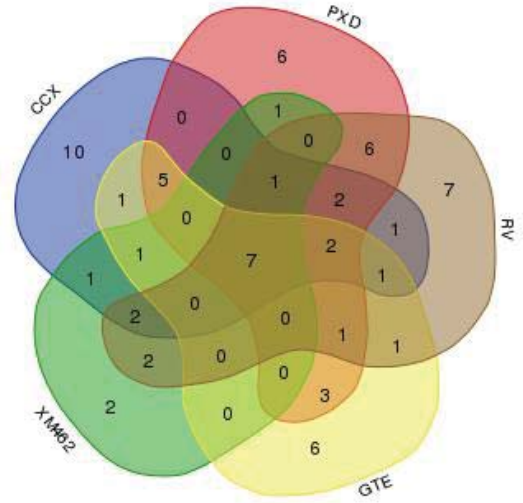

Figure 5. Venn diagram constructed with the information of potential biomarkers for lipid disruption of the distinct treatments (*i.e.*, CCX, PXD, RV, GTE and XM462). Diagram constructed using the Bioinformatics & Evolutionary Genomics webpage (http://bioinformatics.psb.ugent.be/webtools/Venn).

Table 1. List of potential biomarkers of lipid disruption encountered in the Venn diagram.

Drug	Total	Potential biomarkers
CCX	10	Plasmalogen PE 40:6, Colic acid, PC 40:7, GlcdhCer 16:0, dhCer 16:0, PC 38:3, Plasmalogen PC 40:5, Plasmalogen PC 36:2, SM 22:0, Plasmalogen PC 38:4
PXD	6	TAG 54:1, PC dimer 34:1, TAG 54:4, TAG 47:1, LacCer 24:1, PC dimer 36:1
RV	7	Plasmalogen PE 38:6, Lyso plasm PC 18:0, Plasmalogen PC 32:1, Cholesterol sulfate, PC 35:0, PC 30:1, LacdhCer 22:0
GTE	6	PC 40:6, Plasmalogen PC 32:0, PG 34:1, PC 36:3, γ-TE, Dimer γ-TE
XM462	2	PC 36:4, PC 36:1
All treatments	7	PC 38:6, Plasmalogen PC 34:1, PC 36:2, SM 24:1, PC 34:1, SM 16:0, PC 34:2

4. Discussion

The application of MCR-ALS analysis on the UHPLC-HRMS lipidomic data sets followed by the biomarker detection performed by a PLS-DA analysis and further statistical evaluation allowed the elucidation of the effects caused by each treatment compared to control samples. In fact, the differences observed in MCR-ALS resolved elution profiles of treated versus control cells already evidenced an effect on the cell lipidome attributed to the treatments with the tested drugs. The untargeted methodology used in this study allowed the unbiased detection and identification of a large number of lipids showing significant differences among control and treated cells. Moreover, the chemometric methodology used in this study allowed the detection of the alterations produced in minority sphingolipids, including specific dihydroceramides and sphingomielins, indicating that no loss of information was derived from the analysis of data. Such sphingolipid species are associated with the inhibition of Des1, hence deserving attention as potential biomarkers of Des1 inhibition by the drugs.

Des1 is the last enzyme in the *de novo* biosynthesis pathway of Cer and catalyzes the insertion of a double bond in dhCer. Catalytic action of the enzyme Des1 and other desaturases requires NAD(P)H as electron donor, and an electron transport chain with oxygen as the final acceptor[19]. This means that any change in the cellular redox status can modulate the activity of Des1[19]. Several drugs and natural products have been exposed as Des1 inhibitors either acting directly on the enzyme or disrupting the electron transport chain essential for its desaturase activity. Although it has been described that the CCX[21], RV[22]

and GTE[22] increased dhCer levels, its ability to inhibit Des1 had not been examined until recently for our group. In this study, we described CCX and RV along with PXD directly inhibited Des1[23]. Moreover, GTE inhibited the enzyme by altering *DEGS1* gene expression[23], which is the gene that encodes for Des1. XM462 is a synthetic compound specifically designed to inhibit the directly Des1 enzyme[14], based on the enzyme mechanism in desaturation activity.

The hypothesis in this study was that Des1 enzyme inhibitors might also act on other desaturases of the lipid metabolism. Thus, apart from its known effect on the accumulation of dhCer, it could also disturb other lipid species. The aim of this study was to determine the effect of Des1 inhibitors CCX, PXD, RV, GTE and XM462 on the glioblastoma cell line T98G lipidome, through the analysis of MCR-ALS resolved profiles.

As expected, among the lipids altered by the treatments, significant changes in sphingolipid concentrations were also observed. In particular, there was an increase in the levels of dihydrosphingolipids and/or a decrease in unsaturated sphingolipids, confirming the inhibitory effect of the compounds studied on Des1[23]. This effect was observed mainly in dhCer, but also in other more complex dihydrosphingolipids as dhSM, LacdhCer or GlcdhCer. Among these sphingolipids only the most abundant species were identified, specifically the C16, C22 and C24 *N*-acylated.

In the case of GTE and XM462, the identification of their metabolites was also possible. As shown in **Table S3**, the metabolites identified for XM462 included the XM462 compound itself, the 1-glucosyl derivative (Glc-XM462), as well as the oxidation product (O-XM462). The identification of XM462 metabolites indicated that this compound was hydrolysed and metabolised to the 1-glucosyl and 1-oxy derivatives, as described[14]. On the other hand in the samples treated with GTE, the identification of the monomer and the dimer of this drug was also possible. Specifically, most of the product was found as a dimer. Taking into account that XM462 and GTE were not present in control samples, they were overlooked in the further statistical analysis and they were not considered as biomarkers. Regarding CCX, RV and PXD, their identification in the corresponding samples was not possible. Due to their polar nature, they are coeluted in the first minute of the chromatogram and appeared in the chromatographic front. That is why they were not identified in the chemometric MCR-ALS data analysis.

In addition to changes in the cellular content of sphingolipids and the identification of some of the drug metabolites, treatments with CCX, PXD, RV, GTE and XM462, produced an increase in the amount of phospholipids. Among the phospholipids species identified PC, plasmalogen PC, Lyso PC, lyso plasmalogen PC, PE, plasmalogen PE, PG, TAG and some other sterols lipids were detected. A large percentage of the lipids identified correspond to PC, since these lipids are usually find in abundance in eukaryotic cells and therefore they are easily affected by the alteration of cell lipidome. It is important to note that the increased levels of phospholipids are not comparable among different lipid species. A relative decrease of phospholipids containing polyunsaturated acyl groups was observed. These results suggest an inhibition of some fatty acid desaturases by the tested drugs.

In humans there are three fatty acid desaturases, Δ9 or stearoyl-CoA desaturase, Δ6 and Δ52[24]. Results of the chemometric analysis suggest an inhibition of some fatty acid desaturases by CCX, PXD, RV, GTE and XM462. Supporting this hypothesis, it is known that RV[25] and genistein[26] (PXD natural analogue) inhibit the stearoyl-CoA desaturase gene expression. The fatty acid desaturases, such as Des1, depend on the electron transport chain and are modulated by cellular redox state[27]. Therefore these enzymes are susceptible to be affected by the investigated drugs. Thus the results suggest that CCX, PXD, RV, GTE and XM462 might change the redox cell state and hence downregulate desaturase activity, which are associated with NAD(P)H oxidation and oxygen reduction cell processes.

Autophagy is a catabolic pathway involving the lysosomal degradation of proteins and organels to maintain the cellular homeostasis and obtain nutrients and energy under starvation or hypoxia conditions[28,29]. CCX[30], RV[21] and GTE[22] have been described as autophagy inducers in several cell models. In a recent study of our group, dhCer was shown to participate in the induction of the autophagic flux by CCX, PXD, RV, GTE and XM462 in the human glioblastoma cell line T98G[23]. Although autophagy lipid biomarkers species have not been investigated deeply in this work, the fact that all the investigated drugs induced autophagy and that common changes in lipid species were observed for some samples, suggests the possibility that some of the disturbed lipid species detected in this work could be in fact autophagy biomarkers. In summary, we proposed the combined use of LC-MS analytical and MCR-ALS chemometric methodologies to identify those lipids from T98G cells which were significantly altered by CCX, PXD, RV, GTE and XM462 drug treatment. The results, in addition to confirm the effect of the tested compounds on Des1, suggest the inhibition of fatty acid desaturases by the tested compounds with the corresponding relative decrease of unsaturated lipids.

Grant support

The research leading to these results has received funding from the European Research Council under the European Union's Seventh Framework Programme (FP/2007-2013)/ERC Grant Agreement no. 320737. One of the authors (Eva Gorrochategui), acknowledges the Spanish Government (Ministerio de Educación, Cultura y Deporte) for a predoctoral FPU scholarship (FPU13/04384).

References

1. Depledge, M. 2011. Pharmaceuticals: Reduce drug waste in the environment. *Nat. 2011 4787367*.
2. Mazaleuskaya, L. L., J. A. Lawson, X. Li, G. Grant, C. Mesaros, T. Grosser, I. A. Blair, E. Ricciotti, and G. A. FitzGerald. 2016. A broad-spectrum lipidomics screen of antiinflammatory drug combinations in human blood. *JCI Insight*. **1**.
3. Kamsteeg, M., T. Rutherford, E. Sapi, B. Hanczaruk, S. Shahabi, M. Flick, D. Brown, and G. Mor. 2003. Phenoxodiol – an isoflavone analog – induces apoptosis in chemoresistant ovarian cancer cells. *Oncogene*. **22**: 2611–2620.
4. Jang, M., L. Cai, G. O. Udeani, K. V Slowing, C. F. Thomas, C. W. Beecher, H. H. Fong, N. R. Farnsworth, A. D. Kinghorn, R. G. Mehta, R. C. Moon, and J. M. Pezzuto. 1997. Cancer chemopreventive activity of resveratrol, a natural product derived from grapes. *Science*. **275**: 218–20.
5. Luk, S. U., W. N. Yap, Y.-T. Chiu, D. T. Lee, S. Ma, T. K. W. Lee, R. S. Vasireddy, Y.-C. Wong, Y. P. Ching, C. Nelson, Y. L. Yap, and M.-T. Ling. 2011. Gamma-tocotrienol as an effective agent in targeting prostate cancer stem cell-like population. *Int. J. Cancer*. **128**: 2182–2191.
6. Wilson, I. D., R. Plumb, J. Granger, H. Major, R. Williams, and E. M. Lenz. 2005. HPLC-MS-based methods for the study of metabonomics. *J. Chromatogr. B. Analyt. Technol. Biomed. Life Sci.* **817**: 67–76.
7. Tauler, R. 1995. Multivariate curve resolution applied to second order data. *Chemom. Intell. Lab. Syst.* **30**: 133–146.
8. Bedia, C., N. Dalmau, J. Jaumot, and R. Tauler. 2015. Phenotypic malignant changes and untargeted lipidomic analysis of long-term exposed prostate cancer cells to endocrine disruptors. *Environ. Res.* **140**: 18–31.
9. Farrés, M., B. Piña, and R. Tauler. 2014. Chemometric evaluation of Saccharomyces cerevisiae metabolic profiles using LC–MS. *Metabolomics*. **11**: 210–224.
10. Gorrochategui, E., J. Casas, E. Pérez-Albaladejo, O. Jáuregui, C. Porte, and S. Lacorte. 2014. Characterization of complex lipid mixtures in contaminant exposed JEG-3 cells using liquid chromatography and high-resolution mass spectrometry. *Environ. Sci. Pollut. Res. Int.* **21**: 11907–16.
11. Navarro-Reig, M., J. Jaumot, A. García-Reiriz, and R. Tauler. 2015. Evaluation of changes induced in rice metabolome by Cd and Cu exposure using LC-MS with XCMS and MCR-ALS data analysis strategies. *Anal. Bioanal. Chem.* **407**: 8835–47.
12. Ortiz-Villanueva, E., J. Jaumot, F. Benavente, B. Piña, V. Sanz-Nebot, and R. Tauler. 2015. Combination of CE-MS and advanced chemometric methods for high-throughput metabolic profiling. *Electrophoresis*. **36**: 2324–2335.
13. L. Yi, N. Dong, Y. Yun, B. Deng, D. Ren, S. Liu, Y. L. Chemometric methods in data processing of mass spectrometry-based metabolomics: A review. *Anal. Chim. Acta*. **In press**.
14. Munoz-Olaya, J. M., X. Matabosch, C. Bedia, M. Egido-Gabás, J. Casas, A. Llebaria, A. Delgado, and G. Fabriàs. 2008. Synthesis and biological activity of a novel inhibitor of dihydroceramide desaturase. **3**: 946–953.
15. Gorrochategui, E., J. Jaumot, and R. Tauler. 2015. A protocol for LC-MS metabolomic data processing using chemometric tools. *Protoc. Exch.* doi:10.1038/protex.2015.102.
16. Schonlau, M. 2004. Visualizing non-hierarchical and hierarchical cluster analyses with clustergrams. *Comput. Stat.* **19**: 95–111.
17. Palermo, G., P. Piraino, and H.-D. Zucht. 2009. Performance of PLS regression coefficients in selecting variables for each response of a multivariate PLS for omics-type data. *Adv. Appl. Bioinform. Chem.* **2**: 57–70.
18. Geeraert L., G.P. Mannaerts and P.P. van Veldhoven. 1997. Conversion of dihydroceramide into ceramide involvement of a desaturase. *Biochem. J.* **327**: 125–32.
19. Idkowiak-Baldys J., A. Apraiz, L. Li, M. Rahmaniyan, C.J. Clarke, J.M. Kraveka, A. Asumendi, Y.A. Hannun. 2010. Dihydroceramide desaturase activity is modulated by oxidative stress. *Biochem. J.* **427**: 265–74.
20. Schiffmann S., J. Sandner, R. Schmidt, K. Birod, I. Wobst, H. Schmidt, C. Angioni, G. Geisslinger, S. Grösch. 2009. The selective COX-2 inhibitor celecoxib modulates sphingolipid synthesis. *J. Lipid. Res.* **50**: 32–40.
21. Signorelli P., J.M. Munoz-Olaya, V. Gagliostro, J. Casas, R. Ghidoni, G. Fabriàs. 2009. Dihydroceramide intracellular increase in response to resveratrol treatment mediates autophagy in gastric cancer cells. *Cancer. Lett.* **282**: 238–43.
22. Jiang Q., X. Rao, C.Y. Kim, H. Freiser, Q. Zhang, Z. Jiang, G. Li. 2012. Gamma-tocotrienol induces apoptosis and autophagy in prostate cancer cells by increasing intracellular dihydrosphingosine and dihydroceramide. *Int. J. Cancer.* **130**: 685–93.
23. Casasampere M., Y.F Ordoñez, J. Casas, G. Fabrias. 2017. Dihydroceramide desaturase inhibitors induce autophagy via dihydroceramide-dependent and independent mechanisms. *Biochim. Biophys. Acta.* **1861**: 264-75.
24. Nakamura M.T., T.Y. Nara. 2004. Structure, Function and Dietary Regulation of Δ6, Δ5, and Δ9 Desaturases. *Annu. Rev. Nutr.* **24**: 345–76.
25. Zhang X.H., B. Huang, S.K. Choi, J.S. Seo. 2012. Anti-obesity effect of resveratrol-amplified grape skin extracts on 3T3-L1 adipocytes differentiation. *Nutr. Res. Pract.* **6**: 286–93.
26. Shin E.S., H.H Lee, S.Y Cho, H.W Park, S.J. Lee, T.R. Lee. 2007. Genistein downregulates SREBP-1 regulated gene expression by inhibiting site-1 protease expression in HepG2 cells. *J. Nutr.* **137**: 1127–31.
27. Fabrias G., J. Muñoz-Olaya, F. Cingolani, P. Signorelli, J. Casas, V. Gagliostro, R. Ghidoni. 2012. Dihydroceramide

desaturase and dihydrosphingolipids: Debutant players in the sphingolipid arena. *Prog. Lipid. Res.* **51**: 82–94.

28. Ryter S.W., S.M. Cloonan, A.M.K. Choi. 2013. Autophagy: a critical regulator of cellular metabolism and homeostasis. *Mol. Cell.* **36**: 7-16
29. Rohwer N., T. Cramer. 2011. Hypoxia-mediated drug resistance: novel insights on the functional interaction of HIFs and cell death pathways. *Drug. Resist.* **14**: 191-201
30. Huang S., F.A. Sinicrope. 2010. Celecoxib-induced apoptosis is enhanced by ABT-737 and by inhibition of autophagy in human colorectal cancer cells. *Autophagy* **6**: 256–69.

SUPPLEMENTARY MATERIAL OF SCIENTIFIC ARTICLE VII

Chemometric evaluation of glioma cell lipidome in response to proautophagic drugs

E. Gorrochategui, M. Casasampere, R. Tauler, J. Casas

Submitted for publication

Figure S1. Chemical structures of the target proautophagic drugs: CCX, PXD, RV, GTE and XM462.

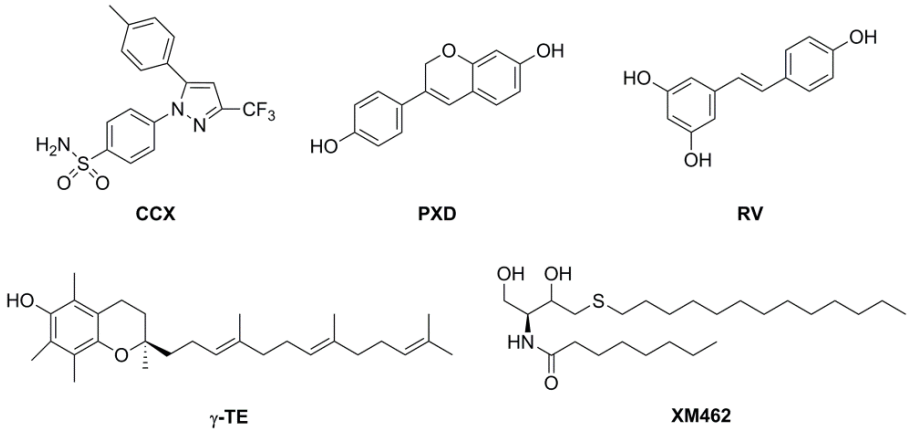

Figure S2. Plot of augmented LC-MS data matrices of control, CCX-exposed, PXD-exposed, RV exposed, GTE-exposed and XM462-exposed cell samples.

Control and CCX:

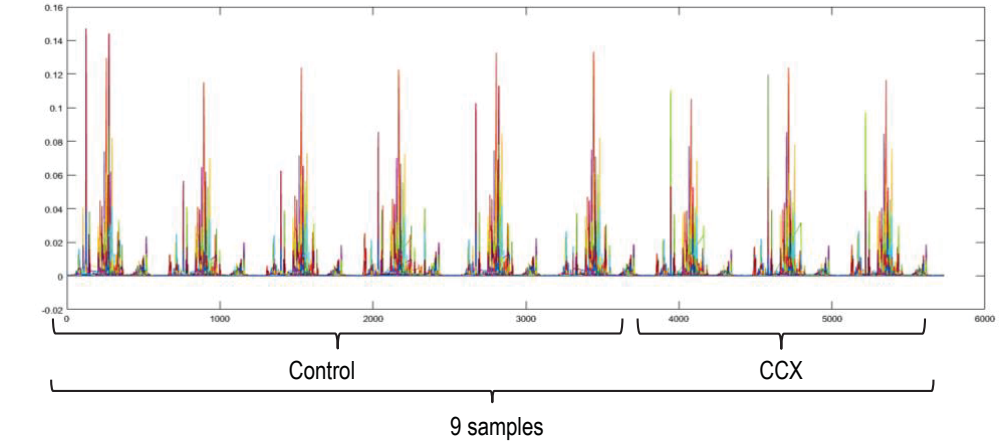

Control and PXD:

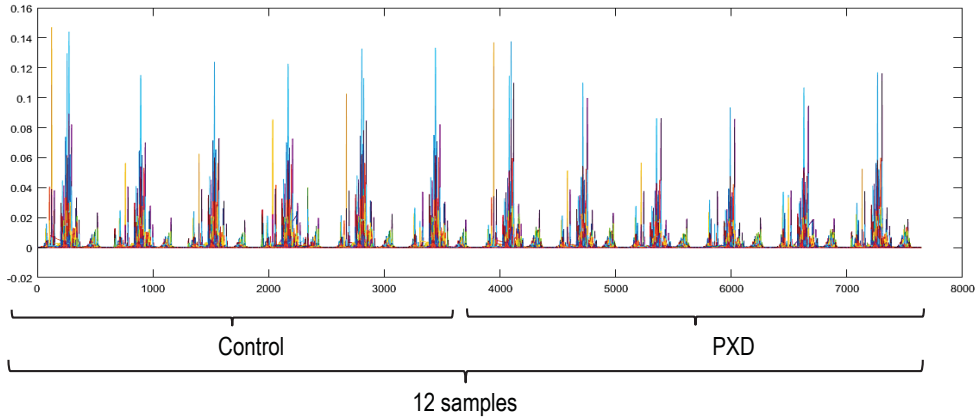

Control and RV:

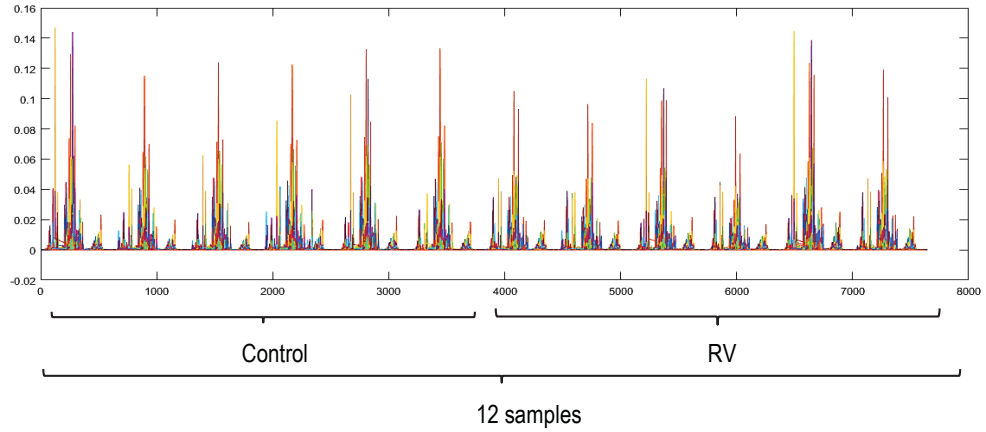

Control and GTE:

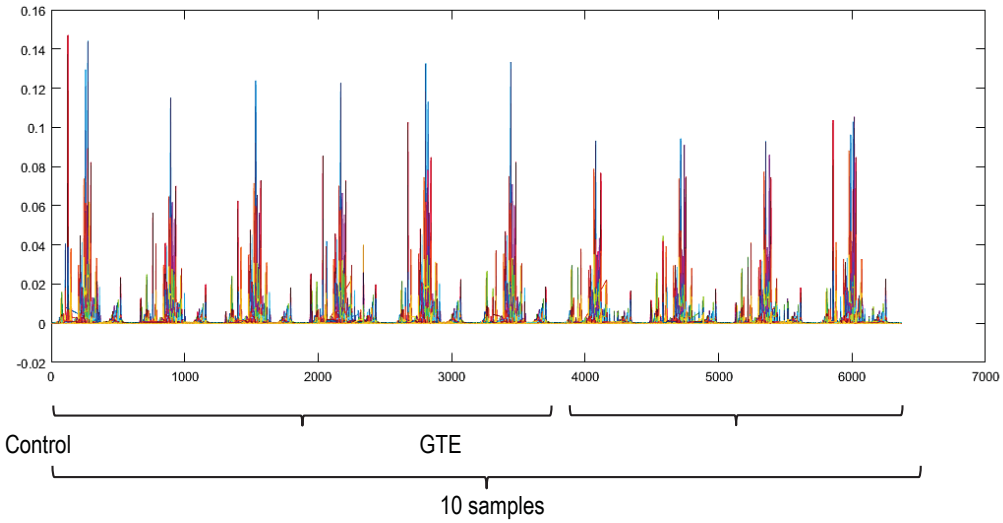

Control and XM462:

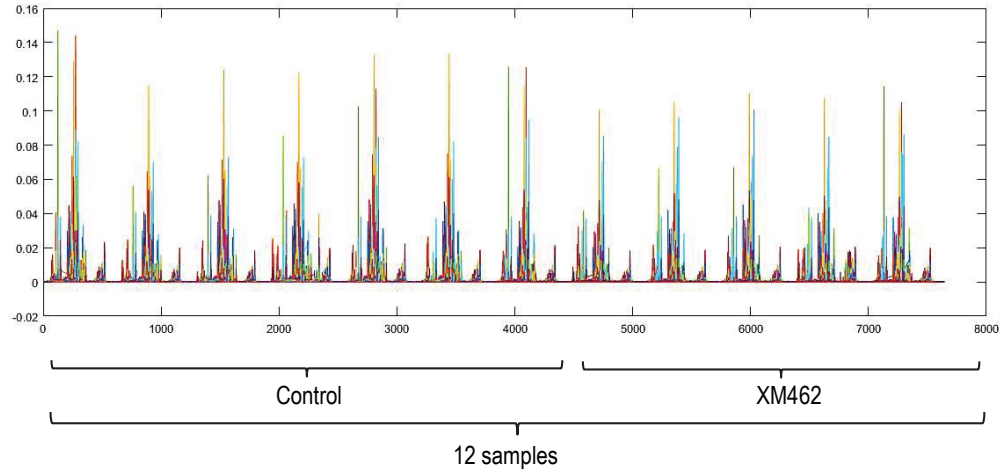

Figure S3. Elution and mass spectra profiles resolved by MCR-ALS showing in the analysis of:

a) Control and CCX exposed cell samples using **150 components** (98.6933% of variance explained).

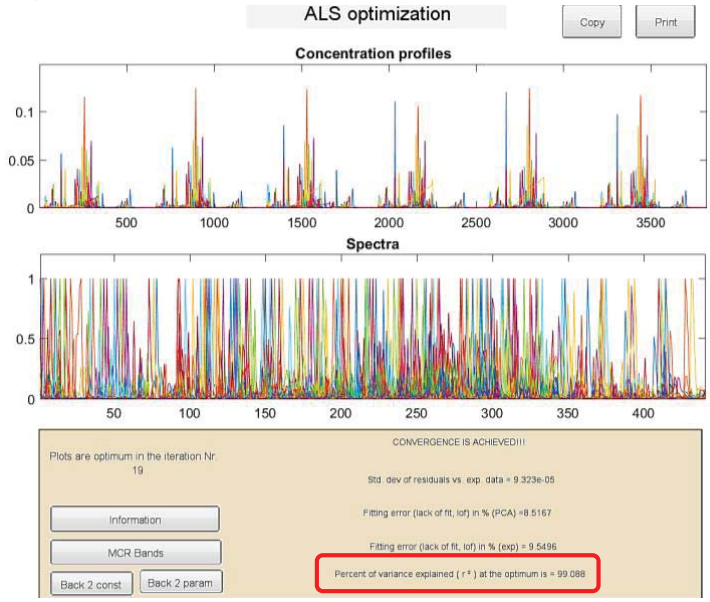

b) Control and PXD exposed cell samples using **120 components** (99.0664% of variance explained).

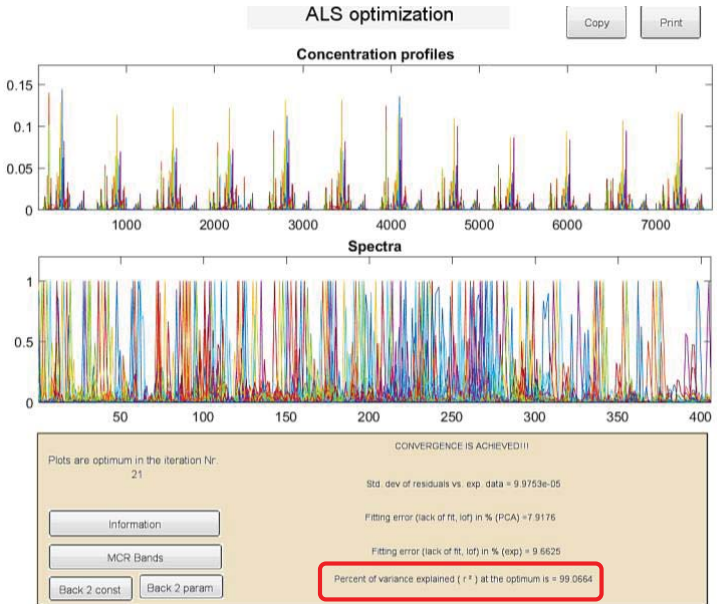

c) Control and RV exposed samples using **120 components** (98.9583% of variance explained).

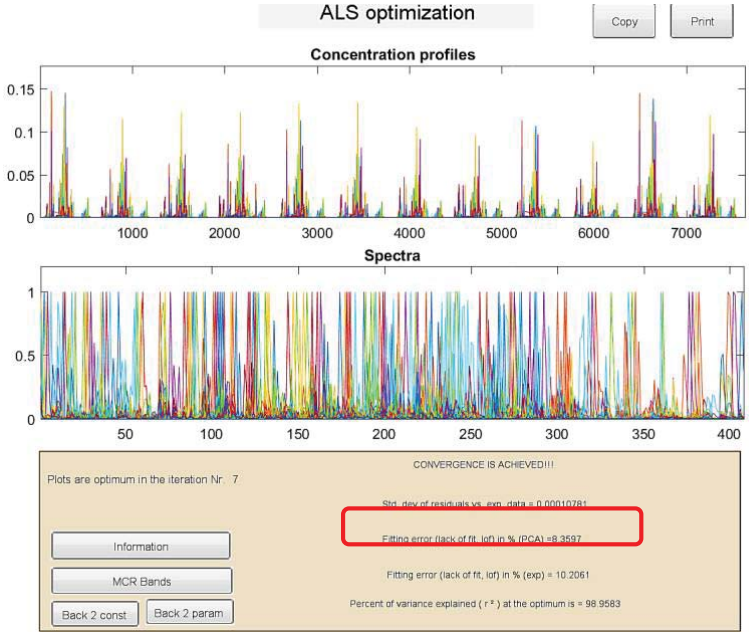

d) Control and GTE exposed cell samples using **100 components** (98.7343% of variance explained).

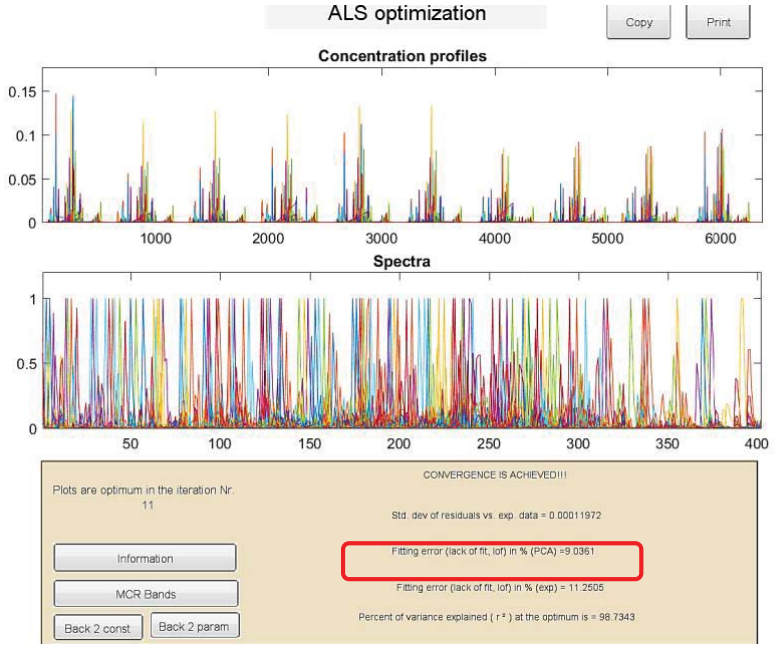

e) Control and XM462 exposed cell samples using **95 components** (98.8064% of variance explained).

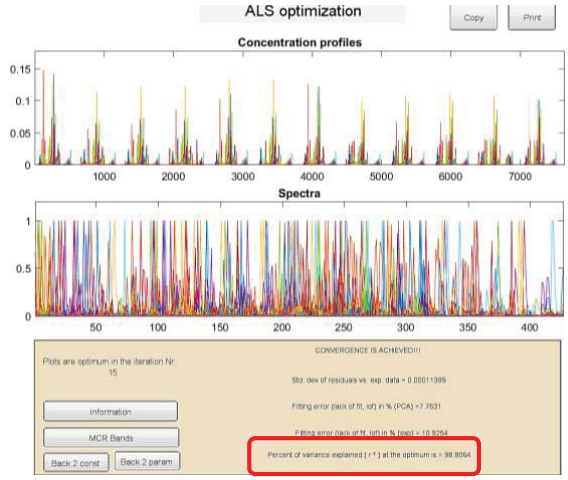

Figure S4. PLS-DA sample scores of the five models performed on the peak areas of the MCR-ALS resolved elution profiles in the analysis of the five data sets containing information of A) controls and CCX samples, B) controls and PXD samples, C) controls and RV samples, D) controls and GTE samples and E) controls and XM462 samples.

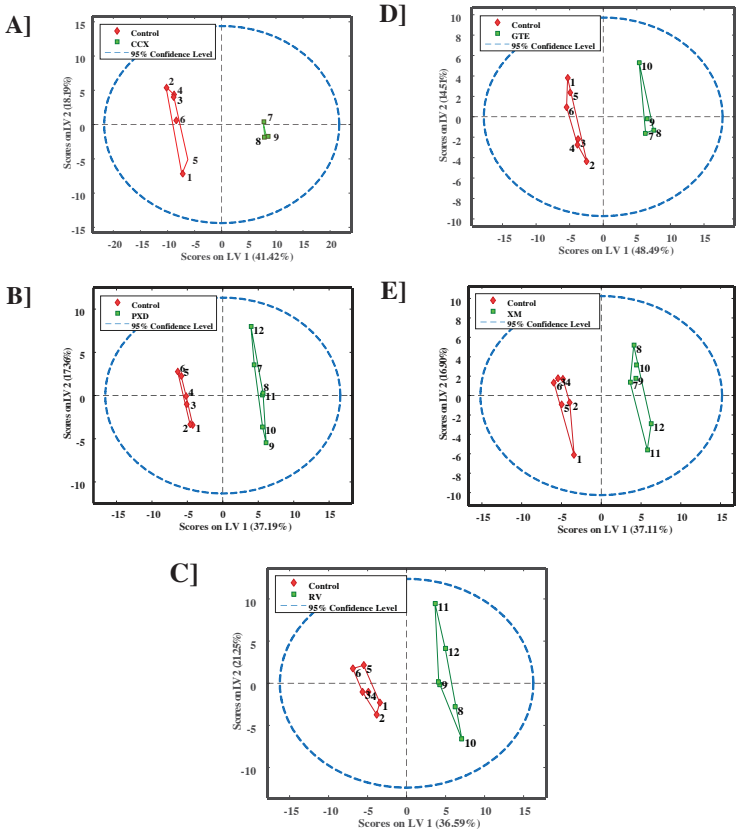

Figure S5. Variables importance in projection (VIP scores) obtained from the five PLS-DA models given in Figure 3 of the manuscript). Horizontal red line in VIP plots indicate a threshold value of 1.

Control and CCX:

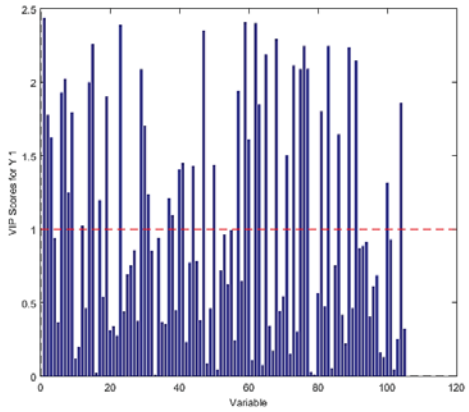

Control and PXD:

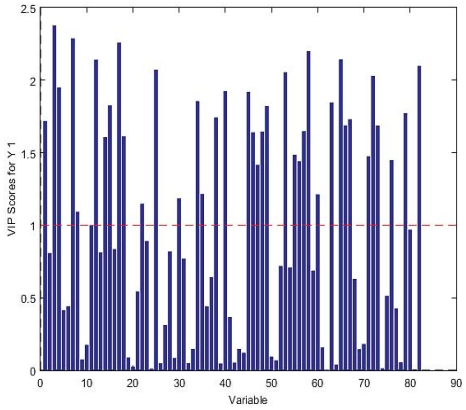

Control and RV:

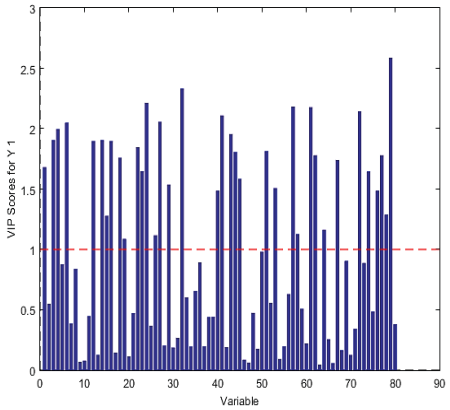

Control and GTE:

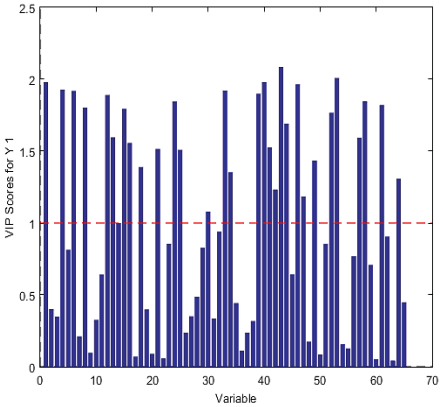

Control and XM462:

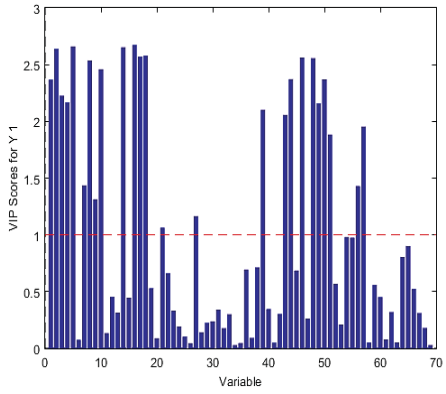

Table S1. Potential biomarkers for lipid disruption in T98G cells exposed to CCX, PXD, RV, GTE and XM462. Significant down- or up- regulation of lipid species respect to controls were determined by PLS-DA analyses (VIP > 1) and further tested using two-sample Student's *t*-Test ($P < 0.05$).

Lipid specie	Lipid classification	Fold change	*p*-values	Up (+) or down (-) regulation
CCX				
PC 32:0	Glycerophospholipid	1.15	0.00832	+
PC 32:1	Glycerophospholipid	1.24	0.00311	-
PC 34:0	Glycerophospholipid	1.28	0.00318	-
PC 34:1	Glycerophospholipid	1.16	0.00349	-
PC 34:2	Glycerophospholipid	1.32	0.00065	-
PC 36:2	Glycerophospholipid	1.26	0.00139	-
PC 38:3	Glycerophospholipid	2.16	0.00002	+
PC 38:6	Glycerophospholipid	1.30	0.01540	-
PC 40:4	Glycerophospholipid	4.93	0.000003	+
PC 40:5	Glycerophospholipid	1.47	0.01700	+
PC 40:7	Glycerophospholipid	1.94	0.00035	-
Dimer of PC 34:1	Glycerophospholipid	1.57	0.00235	-
Plasmalogen PC 34:1	Glycerophospholipid	1.14	0.04040	-
Plasmalogen PC 36:2	Glycerophospholipid	1.72	0.00004	-
Plasmalogen PC 38:4	Glycerophospholipid	2.13	0.00505	+
Plasmalogen PC 38:6	Glycerophospholipid	1.57	0.00033	+
Plasmalogen PC 40:5	Glycerophospholipid	3.31	0.00310	+
Lyso PC 18:0	Glycerophospholipid	1.37	0.0314	+
Lyso PC 18:2	Glycerophospholipid	1.40	0.00668	+
PE 36:2	Glycerophospholipid	1.51	0.00309	+
Plasmalogen PE 40:5	Glycerophospholipid	1.55	0.00034	-
Plasmalogen PE 40:6	Glycerophospholipid	2.08	$3 \cdot 10^{-7}$	-
PG 36:1	Glycerophospholipid	2.09	$8 \cdot 10^{-7}$	+
TAG 50:1	Glycerolipid	1.44	0.00034	+
TAG 50:2	Glycerolipid	1.26	0.01680	-
TAG 52:1	Glycerolipid	1.66	0.00011	-
SM 16:0	Sphingolipid	1.38	0.00079	-
SM 22:0	Sphingolipid	1.55	0.01280	-
SM 24:0	Sphingolipid	1.87	0.00168	-
SM 24:1	Sphingolipid	1.34	0.00003	-
dhSM 16:0	Sphingolipid	1.73	0.00135	-
dhCer 16:0	Sphingolipid	2.37	0.00006	+
GlcdhCer 16:0	Sphingolipid	1.62	0.00211	+
Colic acid	Sterol lipids	1.20	0.01070	+
PXD				
PC 32:0	Glycerophospholipid	1.54	0.000007	-
PC 32:1	Glycerophospholipid	1.22	0.02930	-
PC 32:2	Glycerophospholipid	1.34	0.00096	-
PC 34:1	Glycerophospholipid	1.25	0.00207	-
PC 34:2	Glycerophospholipid	1.67	0.00002	-
PC 36:2	Glycerophospholipid	1.42	0.00051	-
PC 38:4	Glycerophospholipid	1.97	0.00065	+
PC 38:6	Glycerophospholipid	1.52	0.00061	-
PC 40:4	Glycerophospholipid	2.34	0.00008	+
PC 40:5	Glycerophospholipid	1.45	0.02580	+

PC dimer 34:1	Glycerophospholipid	1.80	0.00195	-
PC dimer 36:1	Glycerophospholipid	2.16	0.00737	+
Plasmalogen PC 34:0	Glycerophospholipid	1.53	0.00173	-
Plasmalogen PC 34:1	Glycerophospholipid	1.55	0.00003	-
Plasmalogen PC 36:4	Glycerophospholipid	1.19	0.01920	-
Plasmalogen PC 38:6	Glycerophospholipid	1.40	0.00300	-
Lyso PC 18:0	Glycerophospholipid	2.24	0.00107	+
Lyso PC 18:2	Glycerophospholipid	1.62	0.00289	+
PE 36:2	Glycerophospholipid	1.42	0.00152	-
PE 40:6	Glycerophospholipid	1.77	0.00011	-
Plasmalogen PE 40:7	Glycerophospholipid	1.26	0.00755	-
TAG 47:1	Glycerolipid	1.40	0.00232	+
TAG 48:0	Glycerolipid	1.56	0.02010	+
TAG 50:0	Glycerolipid	2.67	0.00022	+
TAG 50:1	Glycerolipid	1.38	0.00410	+
TAG 52:0	Glycerolipid	2.19	0.00848	+
TAG 52:1	Glycerolipid	2.04	0.00102	+
TAG 54:1	Glycerolipid	1.24	0.00018	+
TAG 54:4	Glycerolipid	3.36	0.00235	+
SM 16:0	Sphingolipid	1.34	0.00011	-
SM 24:1	Sphingolipid	1.31	0.00340	-
dhSM 24:0	Sphingolipid	3.82	0.00303	+
LacCer 24:1	Sphingolipid	1.46	0.00120	-
dhCer 24:0	Sphingolipid	3.56	0.00026	+
RV				
PC 30:1	Glycerophospholipid	1.42	0.00368	-
PC 32:0	Glycerophospholipid	1.41	0.00091	-
PC 32:2	Glycerophospholipid	1.66	0.00237	-
PC 34:1	Glycerophospholipid	1.27	0.00315	-
PC 34:2	Glycerophospholipid	1.57	0.00036	-
PC 35:0	Glycerophospholipid	1.94	0.00184	-
PC 36:2	Glycerophospholipid	1.48	0.00053	-
PC 38:2	Glycerophospholipid	1.90	0.00427	+
PC 38:5	Glycerophospholipid	1.37	0.00510	-
PC 38:6	Glycerophospholipid	1.59	0.00071	-
Plasmalogen PC 32:1	Glycerophospholipid	1.73	0.00021	+
Plasmalogen PC 34:1	Glycerophospholipid	1.19	0.03340	-
Lyso plasm PC 18:0	Glycerophospholipid	1.20	0.00148	-
Lyso PC 18:0	Glycerophospholipid	2.35	0.00097	+
Lyso PC 18:2	Glycerophospholipid	1.78	0.00165	+
PE 40:6	Glycerophospholipid	1.48	0.00182	-
Plasmalogen PE 38:6	Glycerophospholipid	1.52	0.02880	-
Plasmalogen PE 40:5	Glycerophospholipid	1.56	0.00781	-
Dimer of PC 34:1	Glycerophospholipid	1.51	0.01580	-
TAG 48:0	Glycerolipid	1.49	0.00635	+
TAG 50:0	Glycerolipid	2.63	0.00049	+
TAG 50:1	Glycerolipid	1.30	0.00340	+
TAG 52:0	Glycerolipid	1.89	0.00745	+
TAG 52:1	Glycerolipid	1.57	0.00051	+
SM 16:0	Sphingolipid	1.30	0.01020	-
SM 24:0	Sphingolipid	1.33	0.00096	-
SM 24:1	Sphingolipid	1.61	0.01620	+
dhSM 16:0	Sphingolipid	2.00	0.00178	+
dhSM 24:0	Sphingolipid	4.93	0.00003	+

LacCer 24:0	Sphingolipid	1.27	0.00694	-
dhCer 24:0	Sphingolipid	3.84	0.00016	+
LacdhCer 22:0	Sphingolipid	3.13	0.00031	+
Cholesterol sulfate	Sterol lipids	1.56	0.02430	+
GTE				
PC 32:1	Glycerophospholipid	1.39	0.00009	-
PC 34:1	Glycerophospholipid	2.44	0.00004	-
PC 34:2	Glycerophospholipid	1.58	0.000009	-
PC 36:2	Glycerophospholipid	1.54	0.000007	-
PC 36:3	Glycerophospholipid	1.39	0.00005	-
PC 38:2	Glycerophospholipid	1.25	0.00494	-
PC 38:4	Glycerophospholipid	1.60	0.000003	+
PC 38:6	Glycerophospholipid	1.47	0.00035	-
PC 40:4	Glycerophospholipid	6.23	0.00089	+
PC 40:5	Glycerophospholipid	4.98	0.00166	+
PC 40:6	Glycerophospholipid	1.22	0.00680	+
Plasmalogen PC 32:0	Glycerophospholipid	1.41	0.00132	-
Plasmalogen PC 34:0	Glycerophospholipid	1.46	0.02030	-
Plasmalogen PC 34:1	Glycerophospholipid	1.45	0.00009	-
Plasmalogen PC 38:6	Glycerophospholipid	1.72	0.01180	+
Lyso PC 18:0	Glycerophospholipid	1.60	0.00399	+
PE 36:2	Glycerophospholipid	1.71	0.00009	+
PE 40:6	Glycerophospholipid	1.44	0.00347	+
Plasmalogen PE 40:7	Glycerophospholipid	1.60	0.000002	-
γ-TE	Glycerophospholipid	1.93	0.00001	+
Dimer γ-TE	Glycerophospholipid	20.62	$6 \cdot 10^{-7}$	+
PG 34:1	Glycerophospholipid	2.89	$8 \cdot 10^{-12}$	+
PG 36:1	Glycerophospholipid	1.72	0.01070	+
TAG 50:1	Glycerolipid	1.35	0.00174	-
TAG 50:2	Glycerolipid	1.21	0.00169	-
SM 16:0	Sphingolipid	1.57	0.00002	-
SM 24:1	Sphingolipid	1.18	0.00091	-
dhSM 16:0	Sphingolipid	2.03	0.00020	+
XM462				
PC 32:0	Glycerophospholipid	1.96	$7 \cdot 10^{-9}$	-
PC 34:0	Glycerophospholipid	1.69	0.00815	+
PC 34:1	Glycerophospholipid	1.26	0.00001	-
PC 34:2	Glycerophospholipid	1.62	$4 \cdot 10^{-7}$	-
PC 36:1	Glycerophospholipid	1.30	0.00009	+
PC 36:2	Glycerophospholipid	1.28	0.00010	-
PC 36:4	Glycerophospholipid	1.57	$2 \cdot 10^{-7}$	-
PC 38:5	Glycerophospholipid	1.61	$9 \cdot 10^{-6}$	-
PC 38:6	Glycerophospholipid	1.49	$9 \cdot 10^{-6}$	-
Plasmalogen PC 34:1	Glycerophospholipid	1.14	0.03840	+
Plasmalogen PC 36:4	Glycerophospholipid	1.26	0.08800	-
Dimer of PC 34:1	Glycerophospholipid	1.63	0.00056	-
PG 36:1	Glycerophospholipid	2.35	0.00011	+
SM 16:0	Sphingolipid	2.62	$3 \cdot 10^{-9}$	-
SM 24:0	Sphingolipid	2.02	$2 \cdot 10^{-10}$	-
SM 24:1	Sphingolipid	8.07	$2 \cdot 10^{-7}$	-
LacCer 24:0	Sphingolipid	1.76	0.00024	-

Fold change- mean of stressed-samples/mean of control samples.
***p*-value- Significance levels for the two-**sample Student's ***t*-Test were computed for assessing the significance between stressed and control samples.**

Table S2. Elemental composition of glycerophospholipid and glycerolipid species found in T98G cells, calculated by mass accuracy within error of 10 ppm, with atom constraints and with -0.5 ≤ DBE ≤ 15.0. DBE: double-bond equivalent. Elemental composition of PC, Plasmalogen PC, Lyso PC, Lyso Plasmalogen PC, PE, SM, dhSM, Cer, dhCer, LacCer, LacdhCer, GdhCer and sterol species refer to the $[M+H]^+$ ions whereas PG and TAG species refer to ammonium adducts $[M + NH_4]^+$. Lipid species were detected under ESI (+) using an UHPLC system coupled to a TOF analyzer with an Acquity UPLC BEH C_8 column (1.7 µm particle size, 100 mm x 2.1 mm).

GLYCEROPHOSPHOLIPIDS						
Lipid subclass	**Lipid specie**	**Measured mass (Da)**	**Elemental composition**	**Calculated mass (Da)**	**Error (ppm)**	**DBE**
PC						
	30:1	704.5230	$C_{38}H_{75}NO_8P$	704.5230	0.0	2.5
	32:0	734.5734	$C_{40}H_{81}NO_8P$	734.5694	5.4	1.5
	32:1	732.5600	$C_{40}H_{79}NO_8P$	732.5538	8.5	2.5
	32:2	730.5451	$C_{40}H_{77}NO_8P$	730.5387	8.8	3.5
	34:0	762.6013	$C_{42}H_{85}NO_8P$	762.6007	0.8	1.5
	34:1	760.5915	$C_{42}H_{83}NO_8P$	760.5851	8.4	2.5
	34:2	758.5770	$C_{42}H_{81}NO_8P$	758.5694	10.0	3.5
	35:0	776.6090	$C_{43}H_{87}NO_8P$	776.6169	10.0	1.5
	36:1	788.6145	$C_{44}H_{87}NO_8P$	788.6164	-2.4	2.5
	36:2	786.6005	$C_{44}H_{85}NO_8P$	786.6007	-0.3	3.5
	36:3	784.5800	$C_{44}H_{83}NO_8P$	784.5851	-6.5	4.5
	36:4	782.5711	$C_{44}H_{81}NO_8P$	782.5694	2.2	5.5
	38:2	814.6400	$C_{46}H_{89}NO_8P$	814.6320	9.8	3.5
	38:3	812.6177	$C_{46}H_{87}NO_8P$	812.6164	-5.8	4.5
	38:4	810.5974	$C_{46}H_{85}NO_8P$	810.6007	-4.1	5.5
	38:5	808.5861	$C_{46}H_{83}NO_8P$	808.5851	1.2	6.5
	38:6	806.5683	$C_{46}H_{81}NO_8P$	806.5694	-1.4	7.5
	40:4	838.6290	$C_{48}H_{89}NO_8P$	838.6320	-3.6	5.5
	40:5	836.6080	$C_{48}H_{87}NO_8P$	836.6164	-10.0	6.5
	40:6	834.5975	$C_{48}H_{85}NO_8P$	834.6013	-4.6	7.5
	40:7	832.5817	$C_{48}H_{83}NO_8P$	832.5856	-4.7	8.5
Plasmalogen PC						
	32:0	720.5840	$C_{40}H_{83}NO_7P$	720.5907	-9.3	0.5
	32:1	718.5771	$C_{40}H_{81}NO_7P$	718.5751	2.8	1.5
	34:0	748.6150	$C_{42}H_{87}NO_7P$	748.6220	-9.4	0.5
	34:1	746.5993	$C_{42}H_{85}NO_7P$	746.6064	-9.5	1.5
	36:2	772.6140	$C_{44}H_{87}NO_7P$	772.6215	-9.7	2.5
	36:4	768.5833	$C_{44}H_{83}NO_7P$	768.5907	-9.6	4.5

	38:4	796.6140	$C_{46}H_{87}NO_7P$	796.6220	-10.0	4.5
	38:6	792.5850	$C_{46}H_{83}NO_7P$	792.5907	-7.2	6.5
	40:5	822.6295	$C_{48}H_{89}NO_7P$	822.6377	-10.0	5.5
Lyso PC						
	18:0	524.3671	$C_{26}H_{55}NO_7P$	524.3711	7.6	0.5
	18:2	520.3394	$C_{26}H_{51}NO_7P$	520.3403	-1.7	2.5
Lyso plasmalogen PC						
	18:0	510.3868	$C_{26}H_{57}NO_6P$	510.3918	-9.8	-0.5
PE						
	36:2	744.5600	$C_{41}H_{79}NO_8P$	744.5543	7.7	3.5
	40:6	790.5441	$C_{45}H_{77}NO_8P$	790.5387	6.8	8.5
Plasmalogen PE						
	38:6	750.6057	$C_{43}H_{77}NO_7P$	750.5436	0.3	6.5
	40:5	778.5699	$C_{45}H_{81}NO_7P$	778.5747	-6.2	5.5
	40:7	774.5497	$C_{45}H_{77}NO_7P$	774.5438	7.6	7.5
PG						
	34:1	766.5634	$C_{40}H_{81}NO_{10}P$	766.5598	9.8	1.5
	36:1	794.5949	$C_{42}H_{85}NO_{10}P$	794.5949	0.6	6.5
GLYCEROLIPIDS						
TAG						
	47:1	796.7382	$C_{49}H_{98}NO_6$	796.7394	-1.5	2.5
	48:0	824.7682	$C_{51}H_{102}NO_6$	824.7707	-3.0	1.5
	50:0	852.7984	$C_{53}H_{106}NO_6$	852.8020	-4.2	1.5
	50:1	850.7836	$C_{53}H_{104}NO_6$	850.7858	-2.6	2.5
	50:2	848.7687	$C_{53}H_{102}NO_6$	848.7702	-1.8	3.5
	52:0	880.8301	$C_{55}H_{110}NO_6$	880.8333	-3.6	1.5
	52:1	878.8143	$C_{55}H_{108}NO_6$	878.8171	-3.2	2.5
	54:1	906.8446	$C_{57}H_{112}NO_6$	906.8489	-4.7	2.5
	54:4	900.7956	$C_{57}H_{106}NO_6$	900.8015	-6.5	5.5
SPHINGOLIPIDS						
SM						
	16:0	703.5699	$C_{39}H_{80}N_2O_6P$	703.5749	-7.1	1.5
	22:0	787.6668	$C_{45}H_{92}N_2O_6P$	787.6688	-2.5	1.5
	24:0	815.6940	$C_{47}H_{96}N_2O_6P$	815.7001	-7.5	1.5
	24:1	813.6824	$C_{47}H_{94}N_2O_6P$	813.6844	-2.5	2.5
dhSM						
	16:0	705.5859	$C_{39}H_{82}N_2O_6P$	705.5911	-7.4	0.5
	24:0	817.7094	$C_{47}H_{98}N_2O_6P$	817.7162	-8.3	0.5
dhCer						

	16:0	540.5334	$C_{34}H_{70}NO_3$	540.5356	-4.1	0.5
	24:0	652.6566	$C_{42}H_{86}NO_3$	652.6608	-6.4	0.5
LacCer						
	24:0	974.7430	$C_{54}H_{104}NO_{13}$	974.7508	-8.0	3.5
	24:1	972.7320	$C_{54}H_{102}NO_{13}$	972.7351	-3.2	4.5
LacdhCer						
	22:0	976.7572	$C_{54}H_{106}NO_{13}$	976.7659	-8.9	2.5
GlcdhCer						
	16:0	700.5728	$C_{40}H_{80}NO_8$	700.5727	-7.6	2.5
STEROL LIPIDS						
	Colic acid	391.2822	$C_{24}H_{39}O_4$	391.2848	0.3	5.5
	Cholesterol sulphate	465.3057	$C_{28}H_{46}ClO_3$	465.3034	0.4	8.5

[a]Fold change- mean of stressed-samples/mean of control samples.
[b]*p*-value- Significance levels for the two-sample Student's *t*-Test were computed for assessing the significance between stressed and control samples.

Table S3. Elemental composition of XM462 and γ-tocotrienol drugs and of some of their metabolic forms found in T98MG cells, calculated by mass accuracy within error of 10 ppm, with atom constraints and with -0.5 ≤ DBE ≤ 15.0. DBE: double-bond equivalent. Elemental composition of these species refer to the $[M+H]^+$ ions.

GLYCEROPHOSPHOLIPIDS					
Compound	**Measured mass (Da)**	**Elemental composition**	**Calculated mass (Da)**	**Error (ppm)**	**DBE**
γ-TE	411.3232	$C_{28}H_{42}O_2$	411.3241	-7.3	4.5
γ-TE Dimer	819.6128	$C_{56}H_{83}O_4$	819.6147	2.6	6.1
XM462	446.3656	$C_{25}H_{51}NO_3S$	446.3668	-2.4	1.8
O-XM462	462.3597	$C_{25}H_{51}NO_{23}S$	462.3602	-1.4	2.3
GlcXM462	608.4172	$C_{31}H_{61}NO_8S$	608.4196	1.6	7.2

[a]Fold change- mean of stressed-samples/mean of control samples.
[b]*p*-value- Significance levels for the two-sample Student's *t*-Test were computed for assessing the significance between stressed and control samples.

3.3. DISCUSSION OF RESULTS

In this Section of the discussion of results, the findings obtained in the study of the effects of TBT, of a mixture of eight PFASs and of five proautophagic drugs in the lipidome of two distinct human cell lines are presented. Moreover, the cytotoxicity assays of the chemicals, performed previous to the lipidomic analysis, and the analytical evaluation of the LC-MS methodology used to analyse the lipids are also exposed.

Cytotoxicity of PFASs increases with the elongation of the fluorocarbon chain

The study of the alterations that environmental chemicals (*e.g.*, TBT, PFASs and proautophagic drugs) can pose on the lipidome of cells requires previous evaluation of the cytotoxicity of the chemicals in the cell lines. Such evaluation is necessary in order to find out the non-lethal doses that will further be utilized to perform lipidomic studies. Oppositely, the selection of lethal doses of exposure would lead to the elucidation of the effects of the chemicals in the lipids strongly associated with cell death.

In this Thesis, the determination of the non-lethal doses of proautophagic drugs in T98G cells was not necessary, since information of the cytotoxicity of these compounds in the same cell line was available from a previous study of the authors Casasampere M. *et al.*[127] According to the results of the latter study, the doses of exposure selected in this Thesis to perform lipidomics of proautophagic drugs (Scientific article VII) were 35 μM (GTE), 50 μM (CCX and PXD) and 100 μM (RV and XM462). Also, no cytotoxic evaluation of TBT on JEG-3 cells was required in this Thesis since the selected dose of exposure (*i.e.*, 0.1 μM, as stated in Scientific articles V and VI) was the one previously reported to promote adipogenesis in vertebrates[163]. However, the lack of cytotoxic data of PFASs on JEG-3 cells made necessary the determination of their cell viability in this cell line (Scientific article IV).

The obtained EC_{50}-values of PFASs, concerning cell membrane integrity (**FIGURE 3.1**) and metabolic impairment (**FIGURE 3.2**), evidenced that the cytotoxicity of PFASs was to a great extent related with the length of their fluorinated carbon chain. While short-chain PFASs (*i.e.*, PFBA, PFBS, PFHxA and PFHxS) showed no cytotoxicity at the highest concentration tested (500 μM), the longer ones (*i.e.*, PFDoA, PFNA, PFOA and PFOS) showed significant cytotoxicity. Among them, PFOS showed the highest cytotoxicity with an EC_{50} in the range of

107-125 µM, followed by PFDoA and PFNA (181-220 µM) and PFOA (594-647 µM). Moreover, it was evidenced that the cytotoxicity of perfluorosulfonate compounds was comparatively higher to that of perfluorocarboxylic acids. This was particularly evident for PFOS, with an EC_{50} 5-fold lower than that of PFOA.

The correlation among the cytotoxicity of PFASs and the elongation of their flurorocarbon chain found in this Thesis was in accordance to other studies found in the literature[466–468]. In this line, a study of the authors Mahapatra C.T., *et al.*[466] evidenced a higher cytotoxicity of PFOA and a lower cytotoxicity of the shorter carbon chain homologues PFHxA and PFBA on a zebrafish liver cell line. Similarly, Kleszczynski, K. *et al.*[467] measured EC_{50}-values of different PFASs in human colon carcinoma HCT116 cells evidencing that cytotoxicity incremented for longer fluorocarbon chain PFAS. The determined EC_{50}-values in this Thesis together with those obtained in the studies of Mahapatra, C.T. *et al.*[466] and Kleszczynski, K. *et al.*[467] are summarized in **TABLE 3.3.** Overall, these results support the recently adopted decision of using shorter PFAS as substitutes of highly bioaccumulative and persistent long PFAS.

TABLE 3.3. Estimated EC_{50}-values of PFASs obtained in three distinct studies.

PFAS	Gorrochategui, E. et al.[469] Human placental JEG-3 cells		Mahapatra, C.T. et al.[466] Zebrafish liver cells	Kleszczynski, K. et al.[467] Human colon HCT116 cells
	Alamar Blue	CFDA-AM	MTT assay	MTT assay
PFBA	-	-	563 ppm	n.d.
PFBS	-	-	n.d.	n.d.
PFHxA	-	-	500 ppm	4153.9 ± 14.6 µM
PFHxS	-	-	n.d.	n.d.
PFOA	594 ± 19 µM	647 ± 22 µM	90 ppm	937.1 ± 67.9 µM
PFOS	213 ± 3 µM	220 ± 3 µM	n.d.	n.d.
PFNA	181 ± 10 µM	219 ± 16 µM	n.d.	707.7 ± 10.8 µM
PFDoA	107 ± 9 µM	125 ± 6 µM	n.d.	136.4 ± 10.7 µM

-: No significant cytotoxicity at the highest concentration tested (500 µM)

n.d.; Not determined

PFASs bioaccumulation in cells is strongly related to their cytotoxicity

In order to operate in a more realistic concentration-effect scenario, the fraction of PFASs retained in the cells after the exposure at different times was evaluated in this Thesis

(Scientific article IV). The analytical considerations to perform such analysis have been previously described in Section 3.1 and the most common precursor > product transitions used in their LC-MS/MS analysis are mentioned in **TABLE 3.1**.

In this Thesis, the differential bioavailability of PFASs in the in-vitro system was assessed after 0, 1, 3, 5, 8 and 24 h of exposure of JEG-3 cells to the mixture of eight PFASs at 6 µM. Our findings showed that PFASs residues detected in JEG-3 cells after 24 h exposure followed this trend: PFDoA > PFOS >> PFNA > PFOA ~ PFHxA, being shorter chain PFASs (*i.e.*, PFBA, PFBS and PFHxS) below the detection limit. These results evidenced an interesting connection between the bioavailability of PFASs and their cytotoxicity and the length of their fluorocarbon chain. Concerning the linkage between bioavailability and cytotoxicity of the compounds, it was evidenced that less cytotoxic PFASs (*i.e.*, PFBA, PFBS and PFHxS) were the ones with lower fractions retained in cells. Regarding the relation of bioavailability and the elongation of PFASs, it was shown that in general terms, longer PFASs were the ones presenting higher uptake by cells. This was the case of PFDoA and PFOS, which showed the highest intracellular concentration (1190 and 470 pmol/mg protein after 24 h exposure, respectively), but not the case of the also long PFNA, which showed an intracellular concentration 10- to 30-fold lower.

The results of the uptake study of PFASs by JEG-3 cells, expressed as the percentage of compound found inside the cells after 24 h of exposure, are shown in **FIGURE 3.4**. Moreover, the fractions of PFASs remaining in the culture media (at times 0, 5 and 24 h after exposure) were also analysed (despite not published in the Scientific article IV), and are represented in **FIGURE 3.5**, again as a percentage (being 100% the initial dose of exposure).

Interestingly, the fractions of PFASs detected in the culture medium were in agreement to the ratios of PFASs found inside cells. Thus, the highest percentages of PFASs (around 100%) in culture medium corresponded to those PFASs that were below detection limit in the analysis inside cells (*i.e.*, PFBA, PFBS, PFHxS), followed by PFHxA, PFOA and PFNA, with a percentage slightly below 100% in the growth medium. Finally, PFOS (~1.5% inside cells and ~95% in culture medium) and PFDoA (~5% inside cells and ~90% in culture medium) were the PFASs with highest bioaccumulation potential.

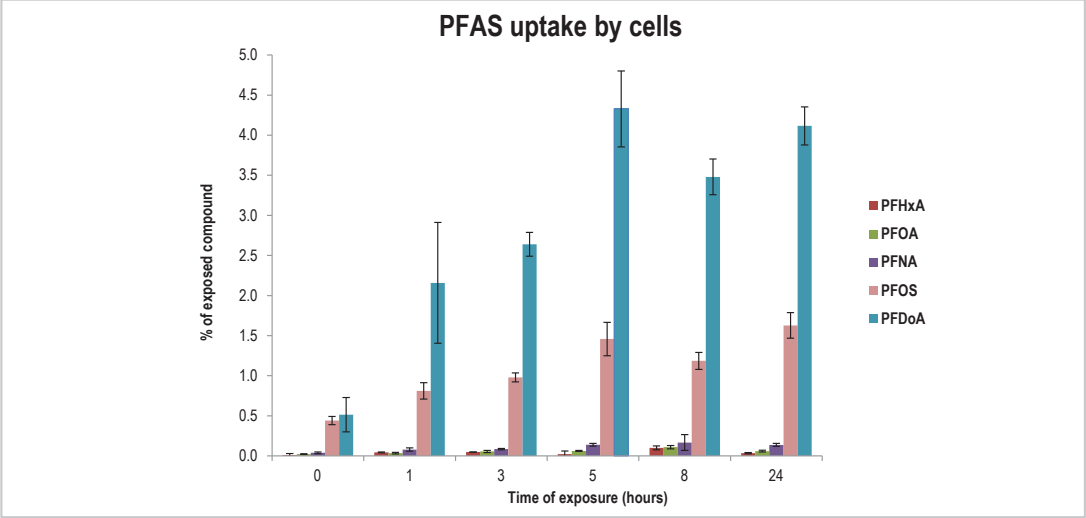

FIGURE 3.4

Time-dependent concentration of PFHxA, PFOA, PFNA, PFDoA and PFOS in JEG-3 cells exposed to a mixture of eight PFASs at a nominal concentration of 6 μM. Values are expressed as a percentage of PFASs that has entered to the cells (being 100% the initial dose of exposure). Concentrations of PFBA, PFBS and PFHxS were below detection limit.

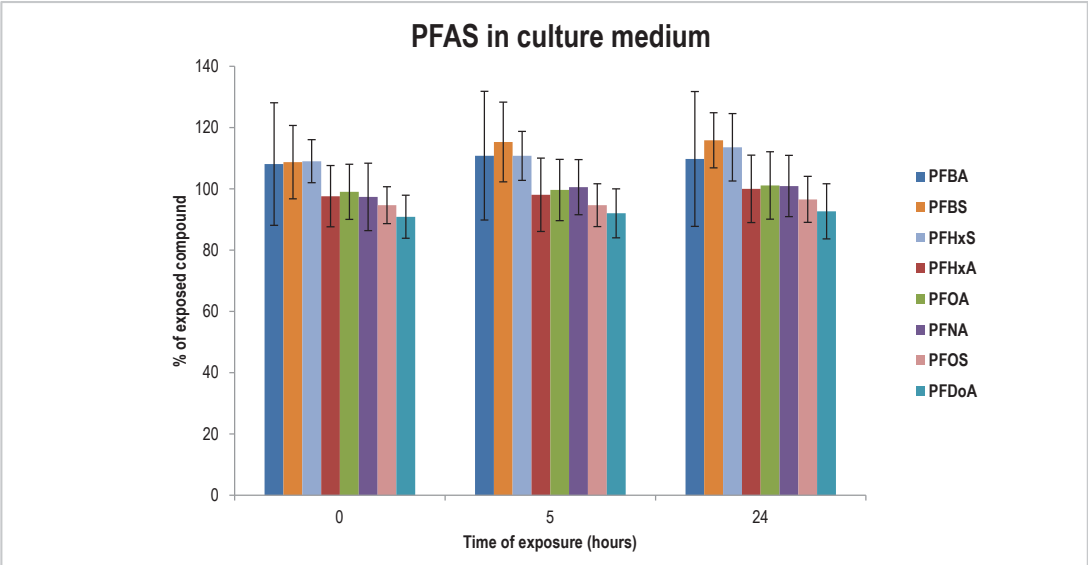

FIGURE 3.5

Time-dependent concentration of PFBA, PFBS, PFHxS, PFHxA, PFOA, PFNA, PFOS and PFDoA in culture media of JEG-3 cells exposed to the mixture of eight PFASs at a nominal concentration of 6 μM. Values are expressed as a percentage of PFASs that remains in the media (being 100% the initial dose of exposure). *Not-published data*.

These results were in accordance to the findings of the authors Pi N. *et al*.[470], who studied the uptake, elimination and translocation behaviour of PFASs in *Echinodorus horemanii* (submerged species) and *Eichhornia crassipes* (free-floating species), two common aquatic macrophyte species. In that study, the authors found that the accumulation of the chemicals augmented with increasing perfluoroalkyl chain length, being the shorter PFASs (*i.e.*, PFBS, PFPeA and PFHxA) the ones with less accumulation tendency. Also, Nouhi S. *et al*.[471] demonstrated the capacity of PFASs to interact with the phospholipid bilayer by incorporation, indicating PFAS ability to accumulate once ingested or taken up by organisms.

PFOS, PFOA and short-chain PFBS and PFHxS: strong inhibitors of CYP19 aromatase activity in JEG-3 cells

Following the study of the cytotoxicity and uptake of PFASs, further toxicological assessment of the effects of these pollutants on JEG-3 cells consisted on the evaluation of their capacity to inhibit CYP19 aromatase activity. Such evaluation was crucial due to the already reported ability of PFASs to affect steroidogenesis through increase of CYP19 gene expression[472]. Moreover, the adequacy of JEG-3 cell line to assess aromatase activity (Section 3.2 of this Chapter) previously reported by Huang H. *et al*.[473], made such determination appropriate, and was the reason why in this Thesis it was determined on this cell line (Scientific article IV) but not on T98G cell line (Scientific article VII).

The differential capability of PFASs to inhibit aromatase activity in JEG-3 cells was assessed at a wide range of doses (3 nM- 500 μM) following 24 h exposure (Scientific article IV). The obtained concentrations causing a 50% decline on enzyme activity (IC_{50}) evidenced the higher capacity of PFOS, PFOA and PFBS to inhibit CYP19 aromatase activity in JEG-3 cells respect to the other PFASs. In the case of PFOS it was also evidenced a close relation between its cytotoxicity and its inhibitory capacity, observing 48% of cell death and 80% of inhibition of aromatase activity for 100 μM PFOS, and IC_{50} (57 ± 4 μM) and EC_{50} (107-125 μM) differing only by a factor of 2. When considering the ability of PFASs to inhibit CYP19 together with their bioavailability, it was stressed out the capacity of PFBS and PFHxS to inhibit aromatase activity despite being the measured uptake of these compounds below the detection limit. Overall, the initial *toxicomic* evaluation of PFASs effects on the human

placental choriocarcinoma JEG-3 cells evidenced higher capacity of longer PFASs to induce toxicological alterations in cells respect to the shorter ones. These findings are particularly determining since ultimately, producers of PFASs are substituting long-chain for short-chain PFASs, which are expected to be more eco-friendly chemicals.

Targeted LC-MS analysis of lipids using both TOF and Orbitrap instrumentation allows successful characterization of JEG-3 lipidome

First targeted lipidomic evaluation of JEG-3 lipidome was performed using a TOF mass spectrometer, obtaining successful results (Scientific article IV). However, in order to take the maximum profit of such lipidomic evaluation, the conditions of the analytical methodology to perform LC-MS lipid analysis were optimized (Scientific article V). In this context, two distinct high-resolution mass spectrometers (*i.e.*, TOF and Orbitrap) both coupled to liquid chromatography, were used to characterize the lipidomic composition of JEG-3 cells, before and after exposure to chemicals. The comparative evaluation of the performance of the two instruments required previous determination of the optimum UHPLC and MS conditions to perform lipid analysis (Scientific article V, Table 1). In both cases, successful UHPLC separation of lipids was achieved using a C_8-bonded silica column of 100-mm length, at a column temperature of 30 ºC and a mobile phase consisting of methanol with 1 mM ammonium formate and 0.2% formic acid (A) combined with water with 2 mM ammonium formate and 0.2% formic acid (B). However, with TOF instrumentation, 10 µL of injection of the sample allowed proper resolution and sensitivity whereas 5 µL were required to improve the chromatographic peak shape when working with Orbitrap spectrometer. Also, slight differences in the gradient elution program were required for proper lipid separation, causing that the UHPLC-Orbitrap chromatogram was longer than the one of UHPLC-TOF-MS. Concerning the MS conditions, the analysis with Orbitrap required the acquisition in a shorter MS range in order to supress high contribution of background ions in the system.

Overall, the characterization of the lipidome of JEG-3 cells using both instrumentation allowed the identification of 178 lipid species; 88% of them detected by both spectrometers, 4% only detected by TOF, and 8% only found with Orbitrap. These results evidenced that both UHPLC-TOF/Orbitrap approaches allowed successful lipid profiling of JEG-3 cells. The adequacy of these two instruments to perform lipidomic analysis is also evidenced in the

literature. For instance, Zhou J. *et al.*[474] investigated the applicability of a large-scale targeted lipidomic assay using a UHPLC-Q-TOF-MS system in serum samples, working under parallel reaction monitoring (PRM) mode, demonstrating the robustness and wide applicability of the method. In that study, lipid separation was performed using a C_{18} column working at 40 ºC, injecting a volume of 10 µL, and lipid identification was based on the performance of MS/MS acquisitions. Another study of Li Q. *et al.*[475] used an UPLC-Q-Exactive Orbitrap-MS method for comprehensive lipidomic analysis of bee pollen (BP). In the latter study, lipid separation was performed using a C_{18} column at a temperature of 45 ºC; very similar conditions to the ones used by Zhou J. *et al.*[474] The use of Orbitrap instrumentation allowed the identification of nine lipid classes consisting on a total of 334 lipid species in the lipid extracts of three BPs. It is important to stress out that in these two studies[474,475], in order to perform lipid identification, previous generation of a list of target lipids containing information of their properties such as their precursor *m/z*, retention time and ion polarity was required. In the same way, in this Thesis we evaluated the performance of UHPLC-TOF/Orbitrap instrumentation when working under a targeted lipidomic approach. Therefore, an inventory of 225 lipids, containing 45 PC, 36 plasmalogen PC, 18 lyso PC, 4 lyso plasmalogen PC, 39 TAG, 26 DAG, 7 CE, 35 PE and 15 SM, was first generated including information of their relative retention times in UHPLC, compared to that of some standards used in a previous study[476], and of their theoretical exact masses determined with a spectrum simulation tool. Similarly, the authors Zhou J. *et al.*[474] elaborated an initial list of 222 lipids to be further analysed, but in this case, information of their MS/MS transitions was also included. Also, in the study of Li Q. *et al.*[475], the information of retention time and characteristic product ions was used to elaborate the referential list of lipids.

Once elaborated the list of target lipids and optimized the UHPLC and MS conditions, the LC-MS methodologies developed in this Thesis were used to study the effects of the mixture of eight PFASs at the same two doses tested previously (0.6 and 6 µM) and of a well-known reported obesogen; TBT at 0.1 µM. The differential resolution of TOF and Orbitrap, 11.500 and 30.000 FWHM at m/z 556 and 400, respectively, gave rise to a high lipid identification power. In **FIGURE 3.6** the percentage of lipids identified by both instruments, together with the fractions only identified by TOF and Orbitrap, independently.

As it is shown in the figure, 88% of the total lipids were detected by both mass spectrometers, 4% were only detected by TOF, and 8% were exclusively found with Orbitrap.

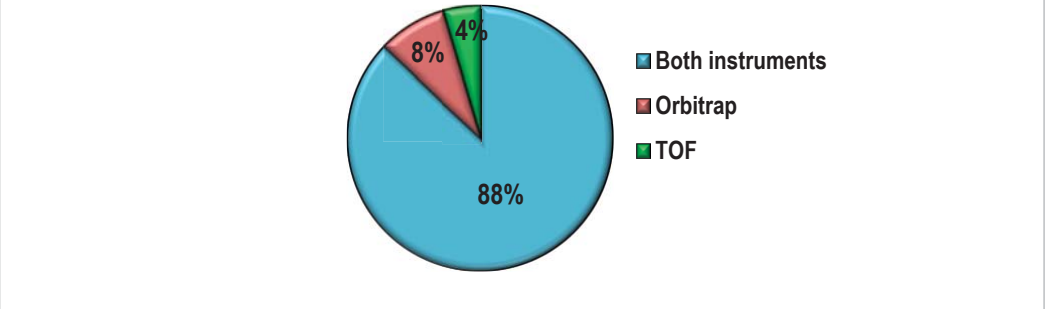

FIGURE 3.6

Percentage of identified lipid species when using TOF and Orbitrap spectrometers.

Chemometric tools allow powerful untargeted lipidomic analysis

Apart from the targeted lipidomic approach, which consists on processing a subset of the lipidome initially defined in a referential database, another approach that can be used in the lipidomic research is the untargeted strategy. In this Thesis, initial lipidomic evaluation was based on the targeted approach (Scientific articles IV and V), but untargeted lipidomic evaluation was further pursued (Scientific articles VI and VII). The latter approach attempts the comprehensive analysis of all measurable analytes in a sample, including the uncharacterized ones, without the requirement of a referential database. However, the comprehensive nature of the untargeted approach demands the evaluation of whole data sets, which difficult their analysis. The complex nature of LC-MS data sets, and the vast amount of information that they contain make necessary the use of chemometric tools to facilitate the analysis, as previously stated in Chapter 2 of this Thesis. However, the difficulty of data analysis associated to the untargeted lipidomic approach (Scientific articles VI and VII) is compensated by the fact that no previous elaboration of a referential lipid database is required, as opposed to the untargeted lipidomic approach (Scientific articles IV and V). One of the first steps required for data processing is the reduction of their dimensions into more computationally manageable formats. In this Thesis, three distinct data compression

strategies were used. First, binning compression of the data (using a bin size of 1 amu) followed by time windowing (dividing the chromatogram in 20 time windows) was used to reduce the size of LC-MS data sets containing information of lipid extracts from JEG-3 cells after the exposure to the mixture of PFASs at two doses (0.6 and 6 μM) and to TBT at 0.1 μM (Scientific article VI). However, the drawbacks associated with that type of compression (mainly related to a loss of spectral accuracy) made necessary to utilize an alternative compression strategy based on the search of ROIs to study the effects of some proautophagic drugs on human glioblastoma T98G cells (Scientific article VII).

MCR-ALS enables successful LC-MS data resolution of multiple samples simultaneously

Next step following data compression was data resolution, in order to resolve chromatographic coelutions. In this Thesis, the MCR-ALS was used to obtain the purest concentration and mass spectra profiles of the chemical constituents present in a sample or in a group of samples simultaneously. In order to analyse all samples simultaneously, column-wise augmented data matrices were constructed. In the data sets compressed by binning and time windowing (Scientific article VI), 20 augmented column-wise data matrices were constructed; one for each time window, containing information of the 12 samples simultaneously (*i.e.*, three replicates of controls, three replicates of samples exposed to the mixture of PFASs at 0.6 μM, three replicates of samples exposed to the mixture of PFASs at 6 μM and three replicates of samples exposed to TBT at 0.1 μM). The total number of components used in the 20 MCR-ALS analyses was 86, and in most of these analyses the percentage of lack of fit was lower than 20% and the explained variance was higher than 96%. Differently, in the data sets compressed by ROI strategy (Scientific article VII), only one column-wise augmented matrix was constructed per chromatogram, since no previous division of the chromatogram in distinct time windows was performed. However, in these data sets, five independent MCR-ALS analyses were performed, considering in each case the control samples and one of the proautophagic drugs. The number of MCR-ALS components selected for the analysis of control and CCX, control and PXD, control and RV, control and

GTE and control and XM462 were 150, 120, 120, 100 and 95, respectively, and in all cases the variance explained was higher than the 98%.

ANOVA followed by multcompare test *vs.* PLS-DA (and VIPSs): two alternative strategies to find out potential biomarkers of lipid disruption

Following data resolution, next step was the statistical evaluation of the MCR-ALS elution profiles in order to find out potential biomarkers of lipid disruption. In this Thesis, two distinct strategies were used to detect lipids showing significant differences between controls and exposed samples. First strategy consisted on the application of one-way ANOVA (lipid by lipid) followed by a multiple comparisons test to avoid false positives[477] (Scientific article VI) and second strategy was based on the performance of a PLS-DA analysis to obtain the variables importance in projection (VIP) scores, which revealed those variables having a greatest influence on the discrimination among controls and exposed samples (Scientific articles VI and VII). In order to compare the performance of these two strategies, the lipid disruption caused by the mixture of PFASs at two doses and of TBT were examined with the two approaches (Scientific article VI).

The evaluation with ANOVA followed by *multcompare* test evidenced that 23 out of the 86 MCR-ALS components showed significant differences (P < 0.05) respect to controls. Moreover, more exhaustive evaluation of those 23 potential biomarkers indicated three differential patterns of lipid disruption. First type of disruption was related to effects produced by PFASs at the two doses tested but no significant effects associated to TBT exposure. Second type of disruption accounted for effects exclusively related to the exposure to TBT and third type of disruption detailed effects related to the presence of both xenobiotics. On the other hand, three PLS-DA analyses were performed with the resolved MCR-ALS peak (elution profile) areas, each one considering two categories of samples (*i.e.*, controls *vs* the mixture of PFASs at 0.6 μM, controls *vs* the mixture of PFASs at 6 μM and controls *vs* TBT). The total number of potential biomarkers elucidated with the latter strategy depended on the VIP scores threshold selected, despite being the general criterion for variable selection the "greater than one" (*i.e.* higher than the averaged effect) rule. Three different VIP scores threshold were selected (1.5, 1.8 and 2), which lead to the obtainment of 39, 21 and 7 potential biomarkers,

respectively. Therefore, the conditions at which both approaches resulted in comparable number of biomarkers were the use of a threshold value of 1.8 units. The combination of both common and uncommon biomarkers detected by the two strategies resulted in a total of 33 biomarkers. Moreover, the type of effects (*i.e.*, up- or down-regulation) in the distinct biomarkers was elucidated for both strategies. The results of ANOVA followed by *multcompare* test indicated that 21 out of the 23 biomarkers suggested by this strategy showed up-regulation, whereas the remaining two showed downregulation. In contrast, all the 21 biomarkers suggested by the PLS-DA and VIP strategy showed up-regulation after the exposure to the xenobiotics, indicated by the weight loadings of the different components.

Once compared the performance of the two strategies to elucidate biomarkers of lipid disruption and having observed that both lead to similar results (Scientific article VI), the second alternative (*i.e.*, PLS-DA with VIPs) was used to identify the potential biomarkers of lipid disruption caused by five proautophagic drugs in T98G cells (Scientific article VII). In order to find out the potential biomarkers, five PLS-DA analyses were performed, each one considering two categories of samples (*i.e.*, controls *vs* CCX, controls *vs* PXD, controls *vs* RV, controls *vs* GTE and controls *vs* XM462). The selected biomarkers where those variables having a VIP score higher than one that showed significant differences when further tested with a *t*-student test ($P < 0.05$). Resulting from that strategy, the number of biomarkers associated to the exposure to the distinct proatophagic drugs were: 34 for CCX, 34 for PXD, 33 for RV, 28 for GTE and 17 for XM462 (Table S1, supplementary material of scientific article VII).

PFASs produce an increase on membrane lipids whereas TBT causes an increment of TAG and DAG lipid species

The capacity of lipid disruption of the mixture of eight PFASs at 0.6 and 6 μM and of TBT at 0.1 μM was assessed in this Thesis following two distinct lipidomic approaches: targeted (Scientific articles IV and V) and untargeted (Scientific article VI).

Targeted evaluation was performed in two different stages. In a first stage, an exploratory evaluation of global changes on lipid classes was performed to obtain a general idea of the lipid disruption potential of PFASs (Scientific article IV). In a second stage, an in-depth

evaluation of the effects of PFASs and also of the well-known obesogen TBT was performed by studying the changes produced in individual lipid species (Scientific article V). The results of the preliminary targeted evaluation evidenced a notable increase (2- to 3-fold change) of membrane lipids (*i.e.*, PC, plasmalogen and lyso plasmalogen PC) and a minor increase of non-membrane lipids (*e.g.*, TAG) in JEG-3 cells exposed to PFASs. Moreover, the findings of the preliminary targeted evaluation evidenced a higher capacity of of the mixture of PFASs at the lower dose tested to cause lipid disruption. The confirmation of the capacity of PFASs to interact with cellular lipids obtained in this targeted preliminary evaluation, together with the capacity of PFASs to induce lipid alterations already reported in the literature[478–480], awoke the interest on further in-depth evaluation of PFASs lipidomic effects. The findings obtained in the detailed targeted evaluation of JEG-3 lipidome (Scientific article V) were in agreement to those obtained in the preliminary targeted evaluation (Scientific article IV). Thus, the in-depth targeted study of PFASs lipidomic effects on JEG-3 cells confirmed the capacity of these chemicals to produce an increment of membrane lipids: up to 3-fold change in some GP lipid species, such as PC, plasmalogen PC, lyso PC, and lyso plasmalogen PC. Also, in the latter detailed targeted lipidomic approach, the effects of TBT were evaluated, evidencing the already reported capacity of TBT to produce a significant increase in families of TAG and DAG (up to 8- and 4-fold change, respectively, in the data generated in this Thesis).

In a next step, the untargeted lipidomic evaluation was performed using chemometric tools (Scientific article VI). The results of the latter approach were again in agreement to the previous findings of targeted lipidomics (Scientific articles IV and V). Therefore, once more it was proved the capacity of TBT to produce a dramatic arise in the amount of TAG and DAG lipid species and the ability of PFASs to cause an increment on membrane lipids (particularly on plasmalogen-PC species). The increment of the latter lipid species, which have been reported to have functions of protection of mammalian cells against ROS[481,482], may indicate a defence mechanism of cells against the oxidative stress produced by the xenobiotics. The suggested capacity of PFASs to induce oxidative stress on JEG-3 cells is also confirmed in some other studies. For instance, the authors Qian Y. *et al.*[483] found that exposure of human microvascular endothelial cells (HMVEC) to PFOS induced the production of ROS and caused actin filament remodelling and endothelial permeability changes. Furthermore, it was

demonstrated that the production of ROS plays a regulatory role in PFOS-induced actin filament remodelling and the increase of endothelial permeability, indicating that the generation of ROS may play a role in PFOS-induced aberrations of the endothelial permeability barrier. Some other evidences of the capacity of PFAS to interact and alter cellular membranes are reported in the literature. For instance, a study performed on *Escherichia coli* exposed to PFOA[484], demonstrated the capacity of this chemical to increase membrane permeability while decreasing membrane potential. Also, as previously stated, a study based on neutron reflectometry of the authors Nouhi S. *et al*.[471] evidenced the capacity of six PFASs (*i.e.*, PFBS, PFHxA, PFHxS, PFNA, PFOS and perfluorooctane sulphonamide) to interact with phospholipid bilayers. In the same way, the effects of TBT on lipids have been reported in numerous studies. In one of the most recent studies[485], the effects of TBT in muscle tissues of rare minnow (*Gobiocypris rarus*) were evaluated after 60 days of exposure, observing that TBT disrupted fatty acid composition and increased contents of unsaturated fatty acids as well as muscle lipid peroxidation.

Five proautophagic drugs (CCX, PXD, RV, GTE and XM462) appear as potential inhibitors of Des1 and fatty acid desatyurases in T98G cells

The untargeted lipidomic evaluation of five proautophagic drugs (CCX, PXD, RV, GTE and XM462) using chemometric tools evidenced the capacity of these chemicals to inhibit Des1 on T98G cells (Scientific article VII). This effect was observed mainly in dhCer, but also in other more complex dihydrosphingolipids such as dhSM, LacdhCer or GlcdhCer. Moreover, it was found that resulting from the exposure to T98G cells, the compounds GTE and XM462 were metabolised. In the case of XM462, it was evidenced that this compound was hydrolysed and metabolised to the 1-glucosyl and 1-oxy derivatives, whereas in samples treated with GTE, the monomer and dimer of this compound were identified. Finally, the study of the effects of the proautophagic drugs on phospholipids of T98G cells evidenced an increase in some phospholipid species but also an interesting relative decrease of phospholipids containing polyunsaturated acyl groups. The latter results suggested an inhibitory capacity of the tested drugs of some fatty acid desaturases.

3.4. CONCLUSIONS

From the scientific research included in this Chapter, the following specific conclusions can be extracted:

Concerning the study of the effects of PFASs on the human placental choriocarcinoma JEG-3 cell line,

- Dose-response study of PFASs on JEG-3 cells evidences a strong correlation between the cytotoxicity of PFASs and the length of their fluorocarbon chain, being the longer ones the most cytotoxic and the shorter ones the less cytotoxic. Moreover, the uptake study of PFASs demonstrates a connection between the capacity of PFASs to enter the cells and the elongation of their fluorine carbon tail, being the longer PFAS the ones showing higher residues in JEG-3 cells after 24 h of exposure (PFDoA > PFOS ≫ PFNA N PFOA ~ PFHxA ≫≫ PFBA, PFBS and PFHxS, being the final three below detection limit).
- The evaluation of the capacity of PFASs to inhibit aromatase CYP19 activity performed in this Thesis demonstrates the high potential of PFOS, PFOA, PFBS and PFHxS to act as aromatase inhibitors in JEG-3 cells. Moreover, the capacity of PFBS and PFHxS to inhibit aromatase despite their low measured uptake evidences the ability of these two chemicals to produce endocrine disruption at low endogeneous cellular concentrations. Therefore, resulting from the findings of this Thesis, it is suggested to reconsider the idea that short-chain PFASs are good substitutes of long-chain PFAS, regarding effects on environment and human health.
- The study of the effects of the mixture of eight PFASs (*i.e.*, PFBA, PFBS, PFHxA, PFHxS, PFOA, PFOS, PFNA and PFDoA) on the lipidome of JEG-3 cells evidences an increase in the amount of membrane lipids (*i.e.*, lyso plasmalogen PC, plasmalogen PC and PC) after exposure to these chemicals. These results suggest the capacity of PFAS to interact with cellular membranes, possibly inducing the synthesis of PCs and plasmenyl-PCs as an autodefence mechanism of cells.

Concerning the study of the effects of five proautophagic drugs on the human glioblastoma T98G cell line,

- The study of the effects of five proautophagic drugs (*i.e.*, CCX, PXD, RV, GTE and XM462) on the lipidome of the glioblastoma cell line T98G evidences the capacity of these drugs to inhibit dihydroceramide desaturase 1. This effect is mainly noticeable in dihydroceramides, but also in other more complex dihydrosphingolipids such as dihydrosphingomielin, lactosyldihydroceramide or glucodihydroceramide.
- It is demonstrated that, resulting from exposure to T98G cells, the drugs GTE and XM462 are metabolised. In the case of XM462, it is proved that this compound is hydrolysed and metabolised to the 1-glucosyl and 1-oxy derivatives, whereas in samples treated with GTE, the monomer and dimer of this compound are identified.
- The study of the effects of the proautophagic drugs on the lipids of T98G cells proves an increase in some phospholipid species but also an interesting relative decrease of phospholipids containing polyunsaturated acyl groups. The latter results suggest an inhibitory capacity of the tested drugs of some fatty acid desaturases.